2019

Testing COULWAVE for use in modeling cross-shore sand transport and beach profile evolution

Patrick Michael Cooper
University of North Florida, patrickmcooper@gmail.com

TESTING COULWAVE FOR USE IN MODELING CROSS-SHORE SAND TRANSPORT AND BEACH PROFILE EVOLUTION

by

Patrick M. Cooper

A thesis submitted to the
School of Engineering
In partial fulfillment of the requirements for the degree of

Master of Science in Civil Engineering

UNIVERSITY OF NORTH FLORIDA

SCHOOL OF ENGINEERING

July 2019

The thesis "Testing COULWAVE for use in modeling cross-shore sand transport and beach profile evolution" submitted by Patrick Michael Cooper in partial fulfillment of the requirements for the degree of Master of Science in Civil Engineering is approved:

_____ _____

Dr. William R. Dally, Ph.D, P.E.
Thesis Advisor and Committee Chairperson

_____ _____

Dr. Cigdem Akan, Ph.D
Committee Member

_____ _____

Dr. Nick W. Hudyma, Ph.D, P.E.
Committee Member

Accepted for the School of Engineering:

_____ _____

Dr. Osama M. Jadaan, Ph.D
Director of the School of Engineering

Accepted for the College of Computing, Engineering, and Construction:

_____ _____

Dr. William F. Klostermeyer, Ph.D
Interim Dean of the College of Computing, Engineering, and Construction

Accepted for the University of North Florida:

_____ _____

Dr. John Kantner, Ph.D
Dean of the Graduate School

1 ACKNOWLEDGMENTS

I'd like to thank first and foremost Dr. Dally for his insight, teaching, and support throughout this process. Additionally, I am grateful for the patience and help of Dr. Akan and Dr. Hudyma for helping me complete this rigorous task. Special thanks to all of my fellow Taylor Engineering Research Institute (TERI) graduate students, without whom this experience would not have been nearly as fun. Ms. Hollis Klein deserves an extra special mention, it is with her guidance and support that the TERI program remains so successful. Finally, I want to thank my wife, Natalya, for supporting me in this endeavor.

2 TABLE OF CONTENTS

3 LIST OF FIGURES

4 LIST OF TABLES

5 ABSTRACT

Realistic, reliable, and effective modeling of cross-shore sediment transport is not present in the current literature. Building that model requires the accurate recreation of breaking wave processes in the nearshore. To develop that first step for an as-yet-to-be-designed model, multiple phase-resolving wave transformation algorithms are reviewed for in-depth investigation. The COULWAVE model is selected for robust testing. Testing of the COULWAVE model shows that, although capable of recreating realistic results, it does not adequately describe major wave characteristics in the surf zone, across a wide range of conditions, to warrant use in a future cross-shore sediment transport model.

1 Introduction and Background

Attaining a more complete knowledge of the physical processes that shape beaches and shorelines is essential to preserving and utilizing the valuable resources associated with the coastal zone. This is especially true as our coasts face the impact of potential hazards induced by global climate change, including increased storm intensity and a rise in eustatic sea level. These issues, coupled with encroaching coastal development and accelerating coastal erosion, are creating conditions of greatly increased risk. Although engineered measures such as beach nourishment and coastal protection structures have been utilized for decades to combat coastal erosion, due to an insufficient understanding and modeling capability of beach processes, these efforts have often not met expectations, and sometimes have had unintended consequences.

Underlying the general issue of coastal erosion is, of course, the physics of sediment transport induced by breaking waves and surf zone currents. Usually the movement of sand in the surf zone and nearshore is treated as two separate components: 1) alongshore transport, and 2) cross-shore transport. This is a simplistic approach to describing what is, in nature, a highly complex process that is not well understood. However, the simplification provides a more tractable means for describing the processes involved. Although both components of nearshore sediment transport warrant significant research effort, this investigation is limited to processes in the cross-shore direction. However, as will become evident, progress made in understanding and modeling the underlying physics of cross-shore transport processes can immediately be extended to the longshore direction.

1.1 Review of cross-shore sediment transport concepts

Movement of sediment in the cross-shore is generally the result of two opposing forces: 1) the 'disturbing force' induced by the motion of the water, which tends to lift and move sediment, and 2) the 'restoring force' of gravity which attempts to hold sand in place or return it to the bed. The primary hydrodynamic drivers responsible for the displacement and transport of sediment in the nearshore and surf zone are 1) oscillatory fluid motion induced by the waves, 2) turbulence generated by wave interaction with the seabed, as well as that generated by breaking, and 3) mean currents driven and shaped by mass, momentum, and energy transferred from the waves into the underlying water column. Firstly, as waves enter shallow water and undergo the process of shoaling, they become non-sinusoidal (i.e. 'nonlinear'), causing the oscillatory water particle motion to also become non-sinusoidal, with stronger onshore flows under the wave crest and weaker offshore flows under the wave trough. Because the tractive shear stress at the bed is nonlinear, in the mean this asymmetry in fluid motion tends to push sediment that remains close to the bed in the onshore direction. However, as turbulence near the bed increases, sediment is carried higher into the water column where the net displacement associated with the oscillatory motion tends to balance (i.e. equal zero). However, a mean offshore current ('undertow') exists between the bottom and the wave trough level that is a result of mean onshore mass transport generated in the wave crest due to wave nonlinearity (Stokes Drift) and the creation of the breaking wave roller. This onshore mass flux must be balanced by the offshore-directed undertow due to the physical barrier presented by the shoreline. Although somewhat mild, this current can now displace the sediment in the offshore direction before gravity pulls it back to the bed.

The three hydrodynamic processes, i.e. non-sinusoidal oscillatory motion, turbulence, and undertow, are highly dependent on the gross characteristics of the incident waves (i.e. height and period), and their interplay determines whether the bed locally erodes or accretes, as well as the overall evolution of the beach profile – e.g. erosion of the beach face and dune and formation of a bar and trough during storms, or onshore movement of the bar, infilling of the trough, and accretion at the beach face under recovery conditions. This is demonstrated in **Figure 1.1**, which presents the results of prototype-scale profile evolution tests conducted in a Large Wave Tank (LWT) where a specific condition is adjusted to demonstrate changes in the beach profile shape.

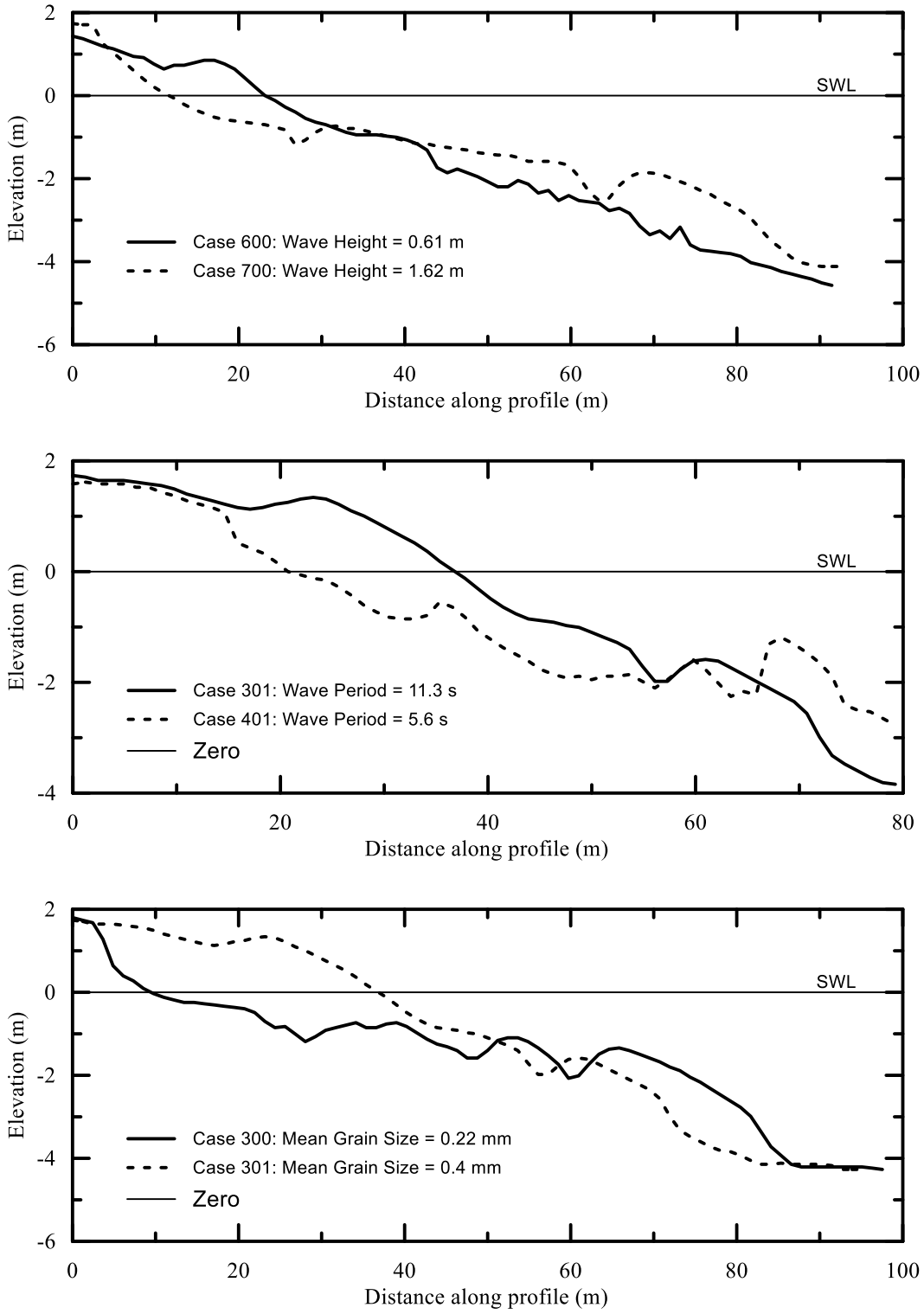

Figure 1.1: Three comparisons of beach profile shapes demonstrating shapes with one changed input variable from Kraus and Larson (1988).

1.2 Review and critique of physics-based beach profile evolution models

Although physics-based parameters that indicate whether a beach should erode or accrete have been developed and empirically calibrated in the past (see e.g. Gourlay and Meulen (1968); Dean, 1973; Kriebel, Dally, and Dean, 1987; Kraus and Larson, 1988; Dalrymple, 1992), they do not provide information as to the actual spatial shape and temporal behavior of the beach profile as it evolves. To this end a variety of models have been developed, all of which require numerical solution due to the general complexity of the problem. Dally (1980) and Dally and Dean (1984) proposed five criteria that a 'good' model for cross-shore transport and beach profile evolution should satisfy:

1) Generate profiles of both the normal and storm types depending on the wave conditions and sediment characteristics.
2) Predict the proper shape of these profiles; i.e. normal profiles should be monotonic and concave upwards, and the bar(s) of the storm profile should have the proper spacing and shape.
3) Correctly predict the rate of profile evolution.
4) Respond to changes in water level due to tides, storm surge, or long-term fluctuations.
5) Approach an equilibrium if all the relevant parameters are held constant.

The models presently used in coastal engineering practice can be loosely separated into two categories: 1) those based upon somewhat simple empirical or 'intuitive' sediment transport relationships, and 2) those founded upon more rigorous, hydrodynamics-based treatments of the underlying transport phenomena. The models based on intuitive transport relationships, e.g.

EDUNE (Kriebel and Dean, 1984) and SBEACH (Larson and Kraus, 1989) are somewhat lifelike in that results depend upon a prescribed mean grain size and initial beach profile, and that a time series for wave height, period, and water level are each required as input. EDUNE has been developed and calibrated to provide a reasonable representation of the spatial and temporal erosion of the beach face and dune during storms, but in so doing, creates only a monotonic profile and not a distinct bar/trough formation, and consequently does not meet the first two criteria. Although SBEACH was specifically developed to generate bar formations, it does not replicate the associated formation of the trough. For example, **Figure 1.2** is recreated from Larson and Kraus (1989; Figure 60). The plot shows the time series of the model-predicted profile evolution, and the final measured profile from a test case conducted in a large wave tank experiment by the U.S. Army Corps of Engineers (USACE). SBEACH described the amount of erosion of the beach face and the geometry of the primary bar reasonably well but failed to replicate the trough and the existence of the three secondary bars seen in the measured profile. In addition, EDUNE and SBEACH are not capable of representing onshore transport and beach recovery.

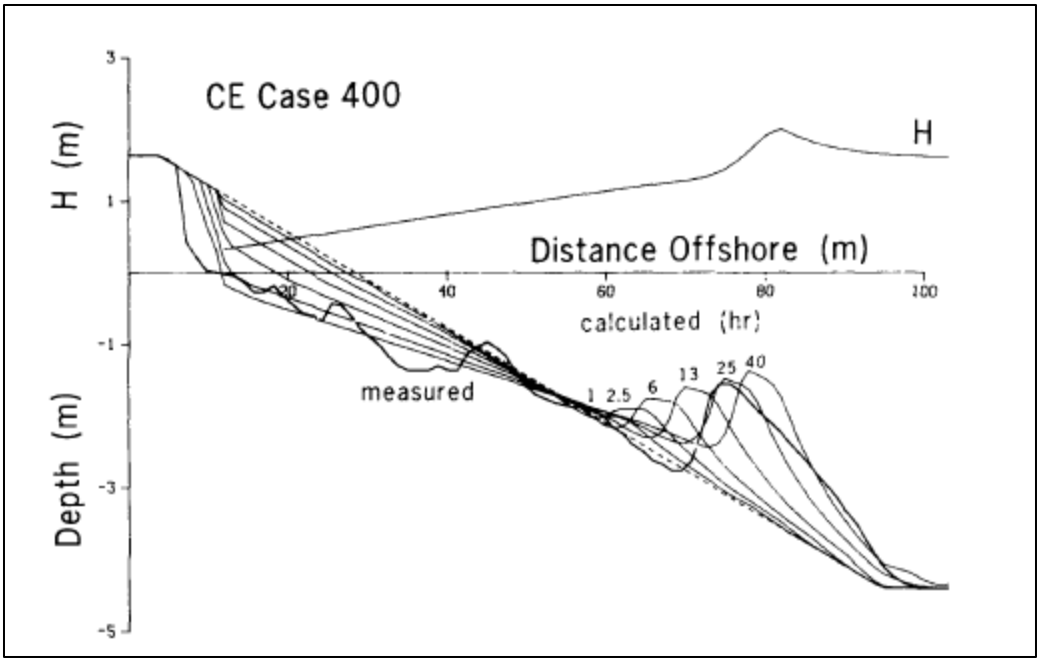

Figure 1.2: Results reproduced from Larson and Kraus (1989) of a measured beach profile from large wave tank experiments conducted by the U.S. Army Corps of Engineers along with simulated profiles from SBEACH at five (5) time intervals

Currently two of the most prominent cross-shore sediment transport and beach profile evolution models that are somewhat rigorously based on the underlying nearshore and surf zone hydrodynamics are CSHORE (Johnson et al. (2012)) and XBEACH (Roelvink et al. (2009)), and will be reviewed below. However, both models adopt/embrace several of the transport concepts first proposed by Dally and Dean (1984), in particular the role played by the undertow in carrying fully suspended sediment offshore. In fact, as will be shown, the model of Dally and Dean (1984) actually satisfies the five criteria listed above to a greater extent than both CSHORE and XBEACH. The major reason for this appears to be a difference in the model used to depict wave breaking adopted in both CSHORE and XBEACH and will be discussed subsequently.

Dally and Dean, 1984

Dally and Dean (1984) developed a model for suspended sediment transport and beach profile evolution that embraced, in some fashion, all three of the surf zone hydrodynamic processes discussed in the Introduction. Firstly, although assumed to be sinusoidal, the local oscillatory motion from wave action at the sea floor was utilized to compute the net displacement of sediment based upon its initial suspension elevation and its characteristic fall velocity, i.e. based upon the heuristic model of Dean (1973). Secondly, the mean return flow established as a counterbalance to the 'shear' induced by the gradient in the onshore momentum flux due to breaking provided the persistent offshore sediment flux as discussed above. Finally, a new model for (regular) wave transformation and breaking in the surf zone (see Dally (1980); Dally et al. (1985)) provided the means to estimate the turbulence in the water column. An exponentially shaped mean sediment concentration profile was adopted, with the degree of suspension determined by the ratio of the sediment fall velocity and the kinematic eddy viscosity, in turn estimated from both bed roughness and breaking-induced turbulence. The major problem encountered in the development of their model was in dealing with a sharp discontinuity in depth-integrated sediment flux that occurred at the breaker line. This discontinuity was treated in an intuitively based, ad hoc manner, which was a distinct shortcoming of the model. Nevertheless, results were at least qualitatively encouraging. **Figure 1.3** is from Dally and Dean (1984) and shows beach profile evolution generated by their model for three conditions. Cases (a) and (c) have the same input waves acting on two different sediments, whereas cases (b) and (c) have the same sediment but different incident wave heights. These comparisons demonstrate that larger grain sizes require more energy to become suspended and moved whereas larger waves provide more energy for sand suspension. Overall the model was shown to qualitatively satisfy the first four of the five criteria but could not approach a state of

dynamic equilibrium even when run for extended periods of time, due to stability problems. Most importantly, the model did produce both normal/accretive profiles as well as storm/erosive profiles that possessed distinct bar and trough formations – features which no other hydrodynamics-based model developed to date has been able to create.

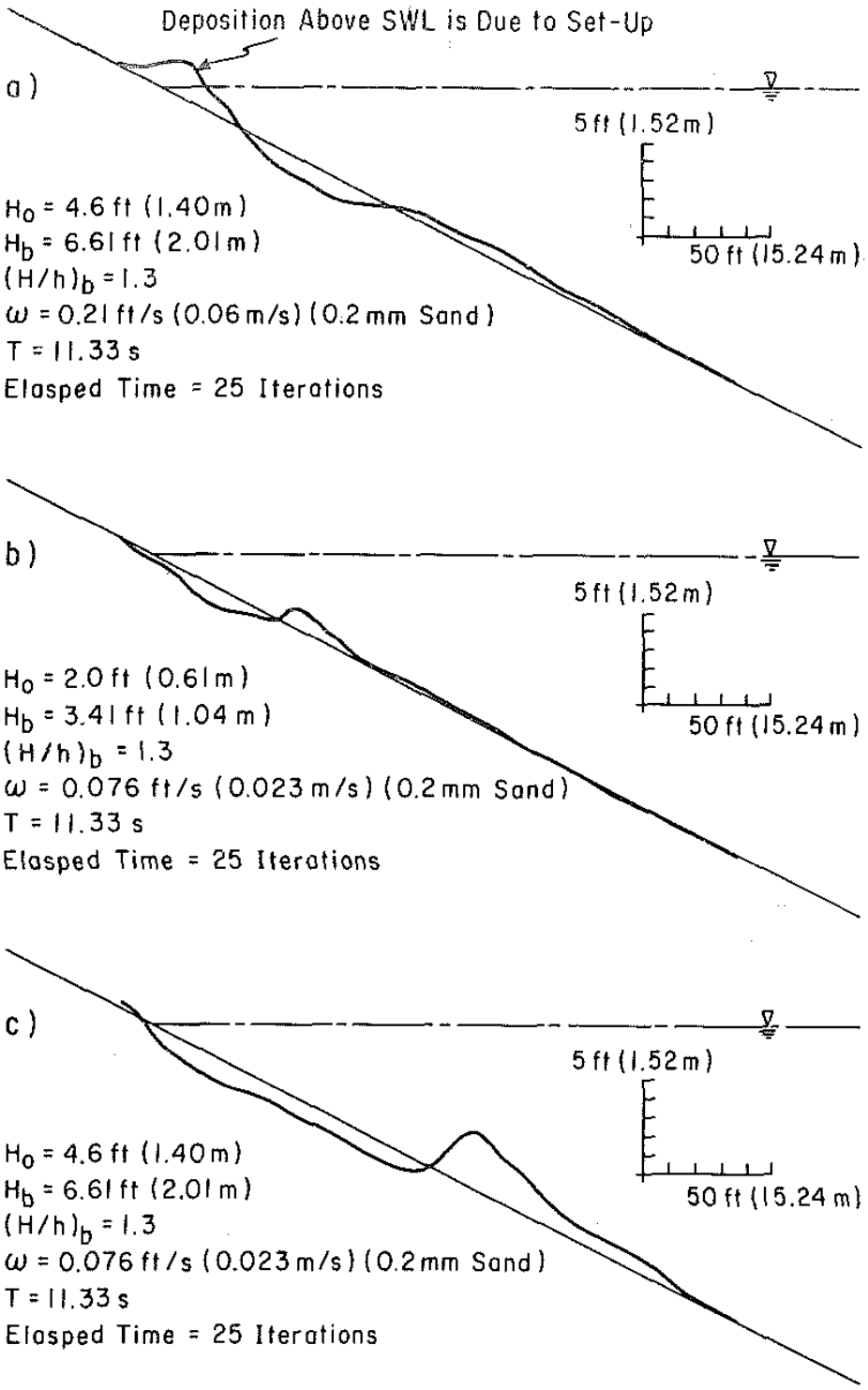

Figure 1.3: Results from Dally and Dean (1984) demonstrating the morphological change of the seabed from modeled results under different wave conditions and sediment characteristics.

CSHORE

Kobayashi and Johnson (1998) developed a model called CSHORE which, although originally used in the study of wave interaction with porous, rubble-mound structures, was eventually enhanced to address cross-shore transport and beach profile evolution (see Johnson et al. (2012)). Although adopting the undertow-driven transport feature of Dally and Dean (1984), a major (and apparently critical) flaw of CSHORE was that it was driven by the parametric breaking model for random waves proposed by Battjes and Janssen (1978), which provides only the transformation of the root-mean-squared wave height (H_{rms}), and adopts linear, sinusoidal wave theory. In result, transport predicted in the vicinity of the outer surf zone does not possess spatial gradients in transport that are strong enough to create distinct bar/trough formations and, because of this issue, CSHORE also always tends to smooth out any bars present in a measured profile used as an initial condition. Also, because of the use of the Battjes and Janssen (1978) parametric random wave model, CSHORE cannot be tested against the highly controlled large wave channel experiments conducted in the past because it is incapable of being driven by regular waves. **Figure 1.4** shows the result from one field-test case from Johnson et al. (2012) for the Halloween storm in 1991 in Ocean City, MD. Note that the measured pre-storm beach profile contains a distinct bar/trough formation, which becomes even more pronounced in the profile surveyed after the storm. However, the CSHORE-predicted result fails to replicate this behavior, and in fact smooths out the bar and creates a shelf-like deposit. It also fails to sufficiently erode the inner surf zone and beach face. Additional testing of CSHORE has also revealed an inability to properly recover the beach profile under accretive wave conditions which, as with SBEACH, is partly due to the focus of model calibration on erosive conditions. Of the five criteria for an acceptable cross-shore transport model, CSHORE appears to fall short, even qualitatively, in most measures.

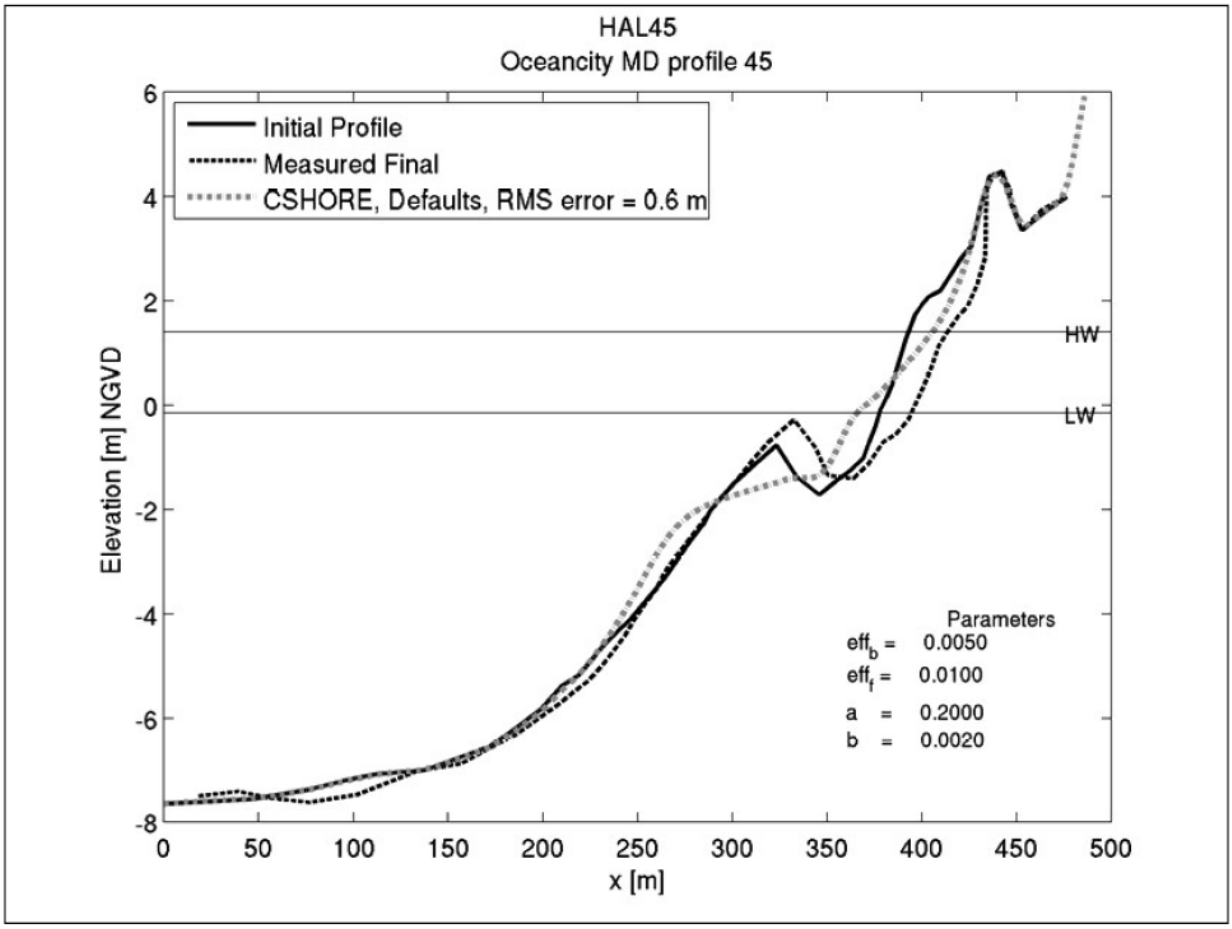

Figure 1.4: CSHORE results compared to measured profiles before and after the 1991 Halloween storm on the coast at Ocean City, Maryland.

XBEACH

A more recent effort in developing a model that describes storm impacts on sandy beaches is known as XBEACH, the foundation of which is described in Roelvink et al. (2009). The developers utilized innovative approaches for describing surf and swash motion, as well as the slumping processes of eroding dunes, which appear to have resulted in reliable predictions of dune erosion, overwash, and dune breaching under storm conditions.

XBEACH has been shown by Harter and Figlus (2017) to provide acceptable predictive results for erosion of the dune and beach face; however, like CSHORE, it does not effectively describe bar/trough formation in the outer surf zone during storms. As with CSHORE, XBEACH also adopts the parametric random breaking wave model of Battjes and Janssen (1978), which again indicates this is a key issue with shortcomings of the model. For example, in work done by Bolle et al. (2011) it was shown that XBEACH was unable to replicate a bar-trough formation after simulating storm conditions. **Figure 1.5** is taken from Bolle et al. (2011) showing the difference between measured storm effects and XBEACH results.

As with CSHORE, in addition to the inability to depict the bar/trough formation, XBEACH has not been shown to reproduce the accretional effects of recovery wave conditions. These findings indicate that XBEACH does not meet most of the five criteria of an acceptable cross-shore sediment model.

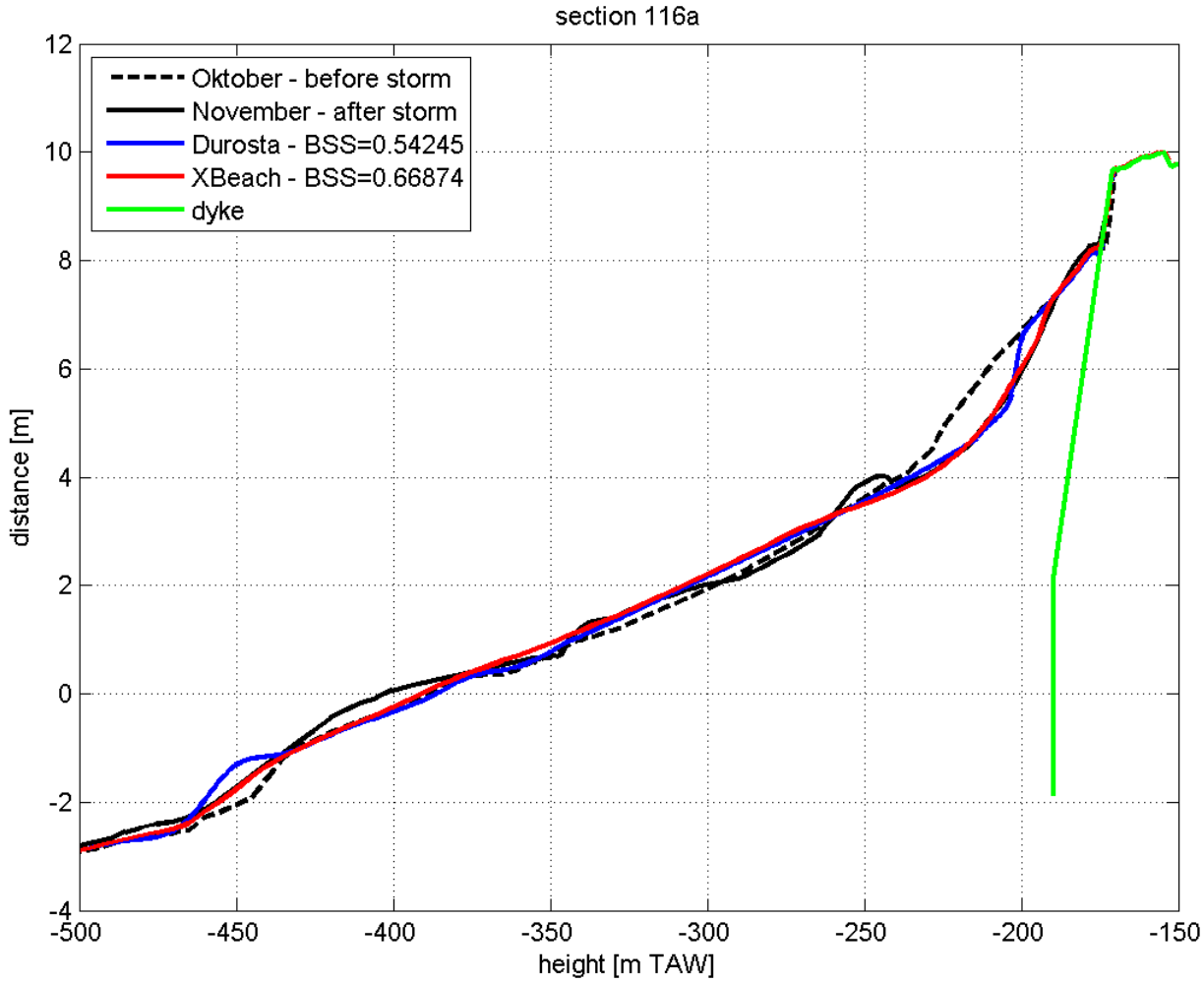

Figure 1.5: XBEACH results from Bolle et al. (2011) showing the pre-storm profile, post-storm profile, and XBEACH result which failed to capture the bar feature.

1.3 The apparent need for a phase-resolving wave transformation algorithm for driving models for cross-shore sediment transport and beach profile evolution

There are a multitude of approaches presented in the literature for modeling cross-shore wave transformation in the nearshore and breaking in the surf zone, ranging from shoaling computed from linear wave theory with breaking prescribed by the '0.78 criterion', to highly complex numerical models developed from Computational Fluid Dynamics. It appears from the review of the beach profile evolution models presented above, for a hydrodynamics-based cross-shore sediment transport model to be viable, the wave processes that must be reliably prescribed include shoaling, the determination of incipient breaking, breaker decay and formation of the wave roller, wave reforming, and run-up. Also, in order to portray onshore transport and beach recovery, the underlying non-linear/non-sinusoidal properties of the oscillatory water particle motion, particularly near the bed, must be included in some manner. In this regard, Dally and Brown (1995) demonstrated that in order to accurately model the cross-shore distribution of wave-induced setup and undertow, relatively sophisticated treatment of both the nonlinearity of the waves and the breaking wave roller are necessary. They adopted a phase-averaged approach that prescribes wave celerity and the mass, momentum, and energy fluxes of the organized wave motion using a routine that interpolated the Stream Function Tables of Dean (1972). They achieved excellent results for regular waves breaking on planar laboratory beaches, but prescription of the local wave height using the measured data was required. Even so, in attempting to represent the formation and behavior of bar/trough features in a profile evolution model, using this approach is questioned because Stream Function Theory assumes a horizontal bottom and assumes symmetric (albeit fully nonlinear) waves, whereas a steeply sloping bed and particularly a bar/trough formation is expected to have significant effects on the wave shape/behavior and associated fluid motion,

particularly at incipient breaking. Because bar/trough formations are typically of the same scale as the wave length, attempting to model their size and shape using a phase-averaged wave model is problematic, as seen in the results of Dally and Dean (1984) and SBEACH (which also utilizes the regular wave model of Dally (1980); Dally et al. (1985)). Because of these issues, use of a phase-resolving model for wave transformation across the nearshore and surf zone appears to be an important improvement in cross-shore sediment transport and profile evolution modeling.

2 Overview and suitability of available phase-resolving breaking wave models

The characteristics of the desired phase-resolving nearshore wave transformation model not only include the accurate representation of the processes discussed above, but the model must be suitable for incorporation into sediment transport algorithms contained in a beach profile evolution model that is intended for practical engineering use. This means the wave model must be relatively easy to use, provide the output (either directly or indirectly) that is required by the transport model, be reliable under a broad range of wave conditions and realistic profile shapes, and, perhaps as importantly, not require inordinate computational resources.

With these criteria, a search of the literature was conducted to identify those wave models that had already been proven reliable based upon comparison to measurements, particularly those taken under controlled conditions in laboratory wave channels. Consultation with researchers familiar with each model and prior experience aided the search and helped focus the effort on models that fit the desired criteria. The wave models identified fall into two broad categories: 1) those based on Computational Fluid Dynamics (CFD) and 2) those based on various forms of the Boussinesq equations. Three CFD models found to be potential candidates were OpenFOAM, IH Foam, and STAR CCM+. Three prominent Boussinesq type models were also identified: FUNWAVE, COULWAVE, and Celeris. The following sections describe the models within the two groups, illustrating how they are different, and how well each fits the criteria established above. Lastly, a single model is selected and the approach to its testing is described.

2.1 CFD models

One approach to describing fluid motion, including water waves, that has become popular is through Computational Fluid Dynamics (CFD). The CFD family of models solve basic governing equations for fluid motion at all locations within a gridded domain, subjected to prescribed boundary conditions. This method has been utilized in a wide range of applications, including gas dynamics and pipe flow. With recent advances in computing power and numerical methods, these tools have recently been adapted to model the complex behavior of waves in the nearshore, including breaking. Although generally not providing the required output directly, the CFD results can usually be post-processed accordingly.

OpenFOAM

OpenFOAM is based on the work of Weller et al. (1998) in which a new approach to building CFD programs was developed that relies on a library of C ++ codes, making the model more user friendly. From that work, with over two decades of open-source development, OpenFOAM has become a widely used platform for modeling complex fluid flows. A major strength of the OpenFOAM package is its broad user network, which has helped develop a wide array of pre-built packages that make OpenFOAM widely appealing. Because it is open-source, OpenFOAM also has the advantages of being transparent, customizable, and inexpensive. Although the OpenFOAM library of applications is extensive, coastal and nearshore wave problems are not its primary use.

Operation of OpenFOAM follows the same generic approach to developing computational solutions to fluid flow problems as described above. Establishing the proper domain is important, as the stability of the solution generally depends on quality of the mesh. For the treatment of

turbulence, OpenFOAM currently offers the user a choice between three approaches: 1) Reynolds Averaged Simulation (RAS), 2) Detached Eddy Simulation (DES), or 3) Large Eddy Simulation (LES). For addressing water wave problems, OpenFOAM currently offers five regular-wave theories for use as the required offshore boundary condition: 1) Cnoidal, 2) Stokes I, 3) Stokes II, 4) Stokes IV, and 5) Stream Function. OpenFOAM solves for the flow properties at each grid cell through the use of a Finite Volume approach, while allowing the user to choose from many numerical solution schemes. The setup and post-solution visualization and interpretation of results is generally performed using the OpenFOAM compatible Visual FOAM software.

IHFOAM

IHFOAM is a direct result of the weakness of OpenFOAM found in coastal structure applications. The solutions from IHFOAM are based on the Reynolds Averaged Navier-Stokes (RANS) equations and provide the velocity and pressure field within the domain as well as the turbulence magnitudes. Work done by Higuera et al. (2013) implemented wave generation and absorption principles into the OpenFOAM platform and showed that coastal-structure applications could now be addressed. Effectively, IHFOAM provides a simplified setup of the OpenFOAM set of options and introduces wave absorption, as well as a separate Graphical User Interface (GUI). Similarly, to OpenFOAM, IHFOAM allows for the user to select various turbulence modeling methods. The five regular wave theories available as offshore boundary conditions in IHFOAM are identical to those found in OpenFOAM. Additional phenomena needed for cross-shore sediment transport modeling such as the free surface elevation, run-up, and undertow can be computed via post-processing and described through the GUI.

STAR CCM+

STAR CCM+ is a high level, industry developed, CFD modeling suite. Distributed by the Siemens Corporation, STAR CCM+ is a robust platform which is primarily used in various industries to develop, test, and evaluate the results of products under various flow conditions, as well as heat transfer environments. The model is not open-source, requires a user's license, and incurs hourly operating costs. Fundamentally, the operation of STAR CCM + follows the same approach as OpenFOAM, where the user builds the domain, establishes boundary conditions and domain physics, and selects the solving methodology. The myriad of solution schemes in STAR CCM+ allow for a wide variety of applications and customization, including some specific approaches to solving wave problems. Advantages to adopting STAR CCM+ are the (proprietary) tools and advanced user interface that can make development of models efficient, with sufficient understanding and experience.

2.2 Boussinesq models

The remaining three models to be discussed represent over four decades of research surrounding phase-resolving nearshore breaking wave models, built upon the Boussinesq approximation (i.e. assuming that the pressure in the flow field is hydrostatic). The models operate on the underlying, depth-integrated equations for the conservation of mass and momentum for an inviscid and incompressible fluid. The fundamental Boussinesq approximation allows for the three-dimensional problem to be simplified to two dimensions by assuming that the vertical velocity varies linearly with depth. The work of Peregrine (1967), who applied the Boussinesq assumption to describe wave transformation, including shoaling, refraction, diffraction, and reflection, provided the earliest practical coastal application. As detailed by Brocchini (2013), Boussinesq

type models became increasingly popular as the simplified approach was easily solved as the use of computers for scientific calculations became widespread. The limitations imposed by the underlying fundamental Boussinesq approximation were reduced over the ensuing decades, allowing for extension into both deeper and shallower applications. Madsen et al. (1991) introduced additional terms to the momentum equation that allowed for higher order terms to be retained while not significantly increasing computational demand. Nwogu (1993) improved the application to deeper applications by describing the equations with a different reference velocity. Characterization of wave breaking was successfully introduced to Boussinesq models through the application of surface roller concept described by Svendsen (1984). These and other developments have resulted in Boussinesq models becoming the industry standard for a wide array of coastal applications, including basin design and nearshore hydrodynamics. Three of the current models, FUNWAVE, COULWAVE, and Celeris are described in more detail to justify the selection of the model used in this thesis.

FUNWAVE

FUNWAVE is a popular and well-supported wave model that has developed from initial work by Wei and Kirby (1995) and incorporates many of the modeling innovations presented in the literature through the years. By maintaining a network of developers/users, with support from the U.S. Army Corps of Engineers (USACE) Engineering Research and Development Center (ERDC), the FUNWAVE model has become one of the most widely used. A description of the improvements made to FUNWAVE since its initiation are described by Shi et al. (2012).

The numerical approach utilized in FUNWAVE is a hybrid Finite Volume/Finite Difference method. In this algorithm the finite difference approach is applied to the dispersive terms and the finite volume method to the Boussinesq equations. Breaking waves are described by the non-linear shallow water equations as it is assumed that for shallow water, dispersive terms become negligible and the Boussinesq approach can be substituted. This approach was first described by Tonelli and Petti (2009). Time integration in FUNWAVE is treated with an explicit, third-order Runge-Kutta method. The treatment of waves at the shoreline was originally performed with the 'slot method' which was described by Tao (1984). Recent updates described by Shi et al. (2012) replaced the slot method with a wetting-drying scheme that improves model stability.

COULWAVE

COULWAVE, like FUNWAVE, builds upon the long history of Boussinesq models. COULWAVE was first developed by Lynett and Liu (2004) for use in describing tsunami waves, and has been extended to many application that describe nearshore, wave-driven hydrodynamic processes. COULWAVE utilizes either a finite-difference or finite-volume solution algorithm, selected by the user, with both algorithms using a semi-implicit, fourth-order accurate Adams-Bashfort-Moulton predictor-corrector scheme for time integration. Wave breaking is modelled by an eddy-viscosity approach that is adapted from Kennedy et al. (2000). A unique feature of COULWAVE is the description of the water column with a multilayer approach, which allows the model to be applied in deeper water. In addition, shoreline interaction is described by a moving wet/dry boundary that linearly extrapolates the water level thereby allowing it to exist between grid points. This provides a more accurate description of the hydrodynamic process without requiring a higher-resolution domain and was later adopted by FUNWAVE.

Celeris

Work done by Tavakkol and Lynett (2017) established a novel approach to modeling nearshore wave conditions with their model Celeris, the last of the models reviewed for this work. Recognizing that the approach of Boussinesq models like FUNWAVE and COULWAVE requires significant parallel computing power to provide detailed results, the authors set out to develop a real-time method of describing coastal waves. Celeris provides these real-time results by utilizing the computational power of a Graphic Processing Unit (GPU), which not only makes the required computations but also provides an animated, graphical output. Celeris can be operated with off-the-shelf Windows machines and provides a powerful visual description of the wave field. The underlying approach in Celeris includes a hybrid finite difference/finite volume numerical scheme similar to FUNWAVE. Wave breaking is not directly treated in Celeris. Instead, energy dissipation is prescribed through a limiter in the underlying numerical description (i.e. numerical diffusion).

2.3 Selection of COULWAVE

Table 2.1 lists the six models with their major strengths and weaknesses, providing guidance for selecting one for further testing. As a group, the CFD models stand out as requiring excessive computational resources, particularly in anticipation of the additional load inflicted by the sediment transport computations and time-evolving boundary of the mobile bed. User training is also an important issue when seeking a practical engineering model. With further advancements in personal and small-cluster computing resources, and in becoming more user friendly, the CFD models may eventually become more suitable for this work; however, they will not be evaluated further herein.

Table 2.1: Comparison of the major strengths and weaknesses of the six nearshore wave transformation models evaluated for use in cross-shore sediment transport and beach profile evolution modeling.

Model	Strengths	Weaknesses
OpenFOAM (CFD)	• Versatile • Open source	• High operation demand • Complex operation • Limited wave data output
IH Foam (CFD)	• Open source • Focused on coastal applications.	• Limited wave data output • Complex operation • High operational demand
STAR CCM+ (CFD)	• Professional Support • Versatile	• Expensive • Limited wave data output • Elaborate setup • High operational demand
FUNWAVE	• Direct wave data output • Workshops available • Nearshore specific • Continuous updates	• Elaborate operation • Limited support
COULWAVE	• Direct wave data output • Nearshore specific	• Limited updates • Scarce support
Celeris	• Simple operation • Real-time output	• No support • Limited wave data output

Although similar in basis, the Boussinesq type models have differences that will determine which one is selected and how it will be tested further. Major differences between COULWAVE and FUNWAVE include 1) the numerical treatment of the temporal solution, 2) the determination of the water elevation at the shoreline, and 3) the user interface. The approach to time integration represents a novel difference between the two models and both have been shown to accurately describe experimental results in various publications. However, to create detailed results, the use

of robust parallel processing is required by both models. This substantial computational demand imposes nearly the same limitation as the CFD approaches.

The treatment of the water level at the shoreline represents one of the major differences between FUNWAVE and COULWAVE. The novel approach in COULWAVE may be key to describing follow-on sediment motion, specifically beach face recovery processes under accretive wave conditions. The operation of each model, including the user interface, may be a minor discriminator between the two, yet the complexity of FUNWAVE could represent a major hurdle during the comprehensive testing over a wide variety of wave channel configurations and wave conditions. In terms of ease of operation, Celeris stands out as a clear favorite. Its ease in setup and operation with a stand-alone machine is an extremely attractive feature; however, the output of Celeris is not easily converted into the underlying hydrodynamic properties of interest.

Based on these key aspects and differences between the six models, COULWAVE will be tested further as a hopefully suitable phase-resolved wave model for a future cross-shore sediment model. To maintain the focus on simplicity and ease of application, and inspired by the approach of Celeris, the COULWAVE model will be operated and tested on a stand-alone machine without utilizing parallel processing. This approach will establish the reliability of COULWAVE results while requiring limited computational resources.

3 Background and description of COULWAVE

Lynett et al. (2002) provides a brief description of the development of basic Boussinesq-type wave models before introducing a new approach which is the basis for the COULWAVE model. The Cornell University Long and Intermediate Wave (COULWAVE) modeling software builds on other models of its type while implementing improvements in the description of wave runup and computational solutions. The COULWAVE model also incorporates the ability to describe multiple depth layers, presented in Lynett and Liu (2004). This feature extends the effectiveness of the model to deeper relative depths; however, in this work the single-layer approach is utilized. Further description of the numerical scheme used for solving the model is provided by Kim, et al. (2009). Operation and application of the model is described in Lynett et al. (2008). In the following sections the governing equations for COULWAVE and the wave breaking approach are presented in detail, to provide background that will aid in the present investigation.

3.1 Governing equations

The fundamental two-dimensional equations that drive the COULWAVE model follow the form laid out by Liu (1994) and are described in Lynett et al. (2002). These highly nonlinear, weakly dispersive wave equations are ultimately used to solve for (1) the free surface displacement (ζ) and (2) the two components of horizontal water particle velocity (u_α, v_α) within the model domain. In dimensional form the equations are:

$$\zeta_t + M = 0,$$

$$\boldsymbol{u_{\alpha t}} + \boldsymbol{F} = 0$$

where the conservation of mass (M) is defined as:

$$M = \nabla \cdot [(h+\zeta)\boldsymbol{u_\alpha}] - \nabla \cdot \left\{(h+\zeta) \times \left[\left(\frac{1}{6}(\zeta^2 - \zeta h + h^2) - \frac{1}{2}z_\alpha^2\right)\nabla(\nabla \cdot \boldsymbol{u_\alpha}) + \left[\frac{1}{2}(\zeta - h) - z_\alpha\right]\nabla[\nabla \cdot (h\boldsymbol{u_\alpha})]\right]\right\}$$

and the conservation of momentum (F) is given by

$$F = \boldsymbol{u_\alpha} \cdot \nabla \boldsymbol{u_\alpha} + g\nabla\zeta$$

$$+\left\{\frac{1}{2}z_\alpha^2\nabla(\nabla \cdot \boldsymbol{u_{\alpha t}}) + z_\alpha\nabla[\nabla \cdot (h\boldsymbol{u_{\alpha t}})]\right\}$$

$$+\left\{[\nabla \cdot (h\boldsymbol{u_\alpha})]\nabla[\nabla \cdot (h\boldsymbol{u_\alpha})] - \nabla\left[\zeta\left(\nabla \cdot (h\boldsymbol{u_\alpha})\right)\right] + (\boldsymbol{u_\alpha} \cdot \nabla z_\alpha)\nabla[\nabla \cdot (h\boldsymbol{u_\alpha})]\right\}$$

$$+\left\{z_\alpha\nabla\left[\boldsymbol{u_\alpha} \cdot \nabla\left(\nabla \cdot (h\boldsymbol{u_\alpha})\right)\right] + z_\alpha(\boldsymbol{u_\alpha} \cdot \nabla z_\alpha)\nabla(\nabla \cdot \boldsymbol{u_\alpha}) + \frac{z_\alpha^2}{2}\nabla[\boldsymbol{u_\alpha} \cdot \nabla](\nabla \cdot \boldsymbol{u_\alpha})\right\}$$

$$+\nabla\left\{-\frac{\zeta^2}{2}\nabla \cdot \boldsymbol{u_{\alpha t}} - \zeta\boldsymbol{u_\alpha} \cdot \nabla[\nabla \cdot (h\boldsymbol{u_\alpha})] + \zeta[\nabla \cdot (h\boldsymbol{u_\alpha})]\nabla \cdot \boldsymbol{u_\alpha}\right\}$$

$$+\nabla\left\{\frac{\zeta^2}{2}[(\nabla \cdot \boldsymbol{u_\alpha})^2 - \boldsymbol{u_\alpha} \cdot \boldsymbol{\nabla}(\nabla \cdot \boldsymbol{u_\alpha})]\right\}$$

where $\boldsymbol{\zeta}$ is the free surface elevation, h is the local water depth and $\boldsymbol{u_\alpha} = (u_\alpha, v_\alpha)$ is the reference horizontal velocity. Following the methodology laid out by Nwogu (1993) the velocity ($\boldsymbol{u_\alpha}$) is evaluated at an elevation of $z_\alpha = -0.531h$ to produce an optimum agreement between the governing equations and the linear-wave dispersion relationship.

To account for bottom friction and wave breaking two parameters, $\boldsymbol{R_f}$ and $\boldsymbol{R_b}$ are introduced. The bottom friction is described as:

$$R_f = \frac{f}{h+\zeta}\boldsymbol{u_\alpha}|\boldsymbol{u_\alpha}|$$

where *f* is the bottom friction coefficient. The breaking parameter is described in detail in the following section.

Although these equations represent a physical description of the propagation of waves, they cannot be solved in closed form and a numerical solution is necessary. The conservative form of the equations adopted in COULWAVE allows for the efficient application of a discretization method and are given by:

$$\frac{\partial H}{\partial t} + \frac{\partial HU_\alpha}{\partial x} + \frac{\partial HV_\alpha}{\partial y} + D^c = 0$$

$$\frac{\partial HU_\alpha}{\partial t} + \frac{\partial HU_\alpha^2}{\partial x} + \frac{\partial HU_\alpha V_\alpha}{\partial y} + gH\frac{\partial \zeta}{\partial x} + HD^y + U_\alpha D^c = 0$$

$$\frac{\partial HV_\alpha}{\partial t} + \frac{\partial HU_\alpha V_\alpha}{\partial x} + \frac{\partial HV_\alpha^2}{\partial y} + gH\frac{\partial \zeta}{\partial y} + HD^x + V_\alpha D^c = 0$$

where $H = \zeta + h$ represents the total instantaneous water depth, U_α and V_α are the horizontal components of velocity, D^c represents the second order terms for the continuity equation, while D^x and D^y are the second order terms for the depth-integrated x and y horizontal momentum equations, respectively.

As described in Kim et al. (2009) and Lynett et al. (2008), the numerical scheme applies a third-order Adams-Bashforth predictor and fourth-order Adams-Moulton corrector scheme for time integration. For determining the interface values within the finite volume domain, a fourth-order compact MUSCL TVD scheme that is described by Yamamoto and Daiguji (1993) is used.

3.2 Wave breaking algorithm

Early Boussinesq numerical models accounted for wave breaking by supplementing the governing equations with a third equation that represented creation and evolution of the roller (Schäffer et al. 1993). However, this numerical method relies on an evaluation of the water surface where the smoothness represents where breaking occurs. This method is limited by the parameters of the model grid and time step, which would, in turn, require greater computational resources to describe accurately. For this reason, the COULWAVE model relies on an ad hoc addition of transfer terms to the momentum equations, which represent the transfer of momentum from the organized motion to the turbulent motion of the breaking wave roller. This ad hoc treatment contains several coefficients that must be calibrated using suitable experimental data.

Work by Kennedy et al. (2000) is the foundation of the COULWAVE breaking wave algorithm. An additional dissipative term, $\boldsymbol{R}_b = R_{bx}\boldsymbol{i} + R_{bz}\boldsymbol{k}$, is added to the momentum equation that is solved in the model. The x- and z-direction components are defined as:

$$R_{bx} = \frac{1}{H}\{[\nu(Hu_1)_x]_x + \frac{1}{2}[v(Hu_1)_z + \nu(Hv_1)_x]_z\}$$

$$R_{bz} = \frac{1}{H}\{[\nu(Hu_1)_z]_z + \frac{1}{2}[\nu(Hu_1)_x + \nu(Hv_1)_z]_x\}$$

where H is the total water depth and ν is the eddy viscosity, u is the horizontal velocity, and v is the vertical velocity in the x-direction. The eddy viscosity is defined by:

$$\nu = BH\zeta_t$$

where B is a variable used to ensure the transition from a non-breaking state to a breaking state is smooth. The approach for defining B, described by (Kennedy et al., 2000) is:

$$B = \begin{cases} \delta,\ \zeta_t \geq 2\zeta_t^b \\ \delta\left(\zeta_t/\zeta_t^b - 1\right),\ \zeta_t^b \leq \zeta_t \leq 2\zeta_t^b \\ 0,\ \zeta_t \geq \zeta_t^b \end{cases}$$

The term δ is an amplification factor and ζ_t^b controls when breaking is initiated or stopped. ζ_t^b is determined by:

$$\zeta_t^b = \begin{cases} \zeta_t^{(F)}, t - t_o \geq T^b \\ \zeta_t^{(I)} + \dfrac{t - t_0}{T^b}\left(\zeta_t^{(F)} - \zeta_t^{(I)}\right), 0 \leq t - t_o < T^b \end{cases}$$

where the initiation of breaking occurs when the threshold, $\zeta_t^{(I)}$, is exceeded. Breaking continues if the minimum (final) threshold, $\zeta_t^{(F)}$, is not exceeded, t is the local time, t_o represents the start of breaking, and T^b is a transition time. As acknowledged by Kennedy et al. (2000), this approach is not directly supported by physical principles but has demonstrated the ability to recreate experimental results for a limited number of laboratory experiments.

From here the methodology from Kennedy et al. (2000) is adapted for use in the COULWAVE model, where the free surface is calculated to the maximum extent possible, by implementing $\zeta_t^{(I)} = \sqrt{gH}$ instead of $\zeta_t^{(I)} = 0.65\sqrt{gh}$. The replacement is necessary as values of h above the still water level are negative. As a result of the change, the four parameters ($\delta, \zeta_t^{(I)}, \zeta_t^{(F)}, T^b$) must be re-evaluated from those found by Kennedy et al. (2000) to determine best fit values.

However, COULWAVE has not been rigorously validated for a wide range of bed slopes and profile configurations. This reality will likely be a factor in the ultimate findings of this investigation. If COULWAVE is unable to operate over complex bathymetries for a wide range of wave characteristics, a model that utilizes a different numerical method may be appropriate.

3.3 Previous calibration

For the COULWAVE model the four free parameters that control breaking have been set by Lynett et al. (2002) through a trial-and-error iterative process that compares model results to the experimental data from Hansen and Svendsen (1979). The experimental data used consist of five regular wave tests on a single planar slope of 1:34.25. The specifics of the tests are listed in **Table 3.1**. The Iribarren number is used as an indicator of breaker type based on the recommendations of Battjes (1974) and is calculated using the incident wave height that is generated by the model.

Table 3.1: Test cases from Hansen and Svendsen (1979) used for establishing COULWAVE breaking wave parameter.

Test	Iribarren Number	Incident Height H_i	Period (s)	Wave Steepness	Breaker Type
031041	0.59	4.3	3.33	0.0070	Plunging
041041	0.46	3.9	2.5	0.0086	Spilling
051041	0.38	3.6	2.0	0.0102	Spilling
061041	0.24	6.7	1.67	0.0234	Spilling
A10112	0.14	6.7	1.0	0.0467	Spilling

With the four breaking parameters selected based on a single slope condition, it may be that the COULWAVE model is limited in its applicability to other beach slopes and/or complex beach profiles. Investigation of this potential limitation is the main emphasis of this thesis.

4 Corroborative testing of COULWAVE

4.1 Attempts to reproduce the calibration tests of Lynett et al. (2008)

As described, the overall approach is to test COULWAVE while operating on a single, stand-alone processor and determine whether COULWAVE is efficient and reliable for use in a cross-shore sediment transport model. Establishing proper operation of COULWAVE is the first step in that investigation. To ensure the model is being operated correctly, a direct comparison of the Hansen and Svendsen (1979) laboratory data and the breaking wave calibration results from Lynett et al. (2008) is first performed. The results of these test runs will also help establish how well the model performs while using a single processor. Lacking the original data and model results in raw format, values were obtained by digitizing the plots provided in Lynett et al. (2008). The results include both the wave height and mean water level elevations along the wave flume. The model was set up with incoming waves generated in 0.36 m of water and shoaled on a 1:34.25 slope. Representative input settings from the first test are provided in **Appendix A**.

Figure 4.1 through **Figure 4.5** show the results from the corroborative tests in comparison to the original calibration tests. The figures represent the data inside the surfzone, plots with all the data are provided in **Appendix B**. In each case both the wave heights (upper panel) and the mean free surface (lower panel) are compared. The expectation was not for the results produced from this investigation to perfectly match the calibration tests when COULWAVE was developed. The literature does not provide the specific model parameters that were used, and the number of factors that determine the results could not all be matched perfectly. In fact, with the use of limited computer resources, the application of the model in this work is decidedly different. Even with

these differences, the results show qualitatively good agreement and provide confidence that the COULWAVE model is operating correctly.

Figure 4.1 shows the results for test case 031041. Comparison of the corroborative test to the original calibration results, prior to the wave breaking, is the most inconsistent result of all five cases. However, inside of the break point, the wave height results do follow the trend of the experimental results although not as well as the original Lynett test. Unfortunately, after a lengthy investigation of possible causes of the discrepancy, no resolution was found.

The mean free surface comparison in **Figure 4.1** actually shows good comparison between the flume experiment, Lynett's Test, and the present test. The remaining four cases, shown in **Figure 4.2** through **Figure 4.5**, display better agreement between calibration results and the corroborative test. In test case 041041 (**Figure 4.2**) the mean water surface elevation of the corroborative test has a positive offset outside the breaking zone. **Figure 4.3** shows the comparison of test case 051041, in which the corroborative test results appear to predict the height and location of incipient breaking better than the original calibration results. The results in **Figure 4.4** follow the overall trend with good agreement; however, there appear to be undulations in the mean water surface elevation in the corroborative results. This anomaly is likely attributed to reflected wave energy in the new model case. **Figure 4.5** appears to demonstrate the best results for the corroborative COULWAVE test, relative to the original test. Like test case 05104, the wave heights match more closely with the measured data at incipient breaking.

This qualitative comparison indicates that the corroborative tests produced acceptable results compared with those found in the original COULWAVE calibration tests and the laboratory data. Before testing of the COULWAVE model against data on varying geometries of planar beaches and ultimately complex bathymetries can proceed, the results of the corroborative tests will be quantitatively compared to the original data from Hansen and Svendsen (1979).

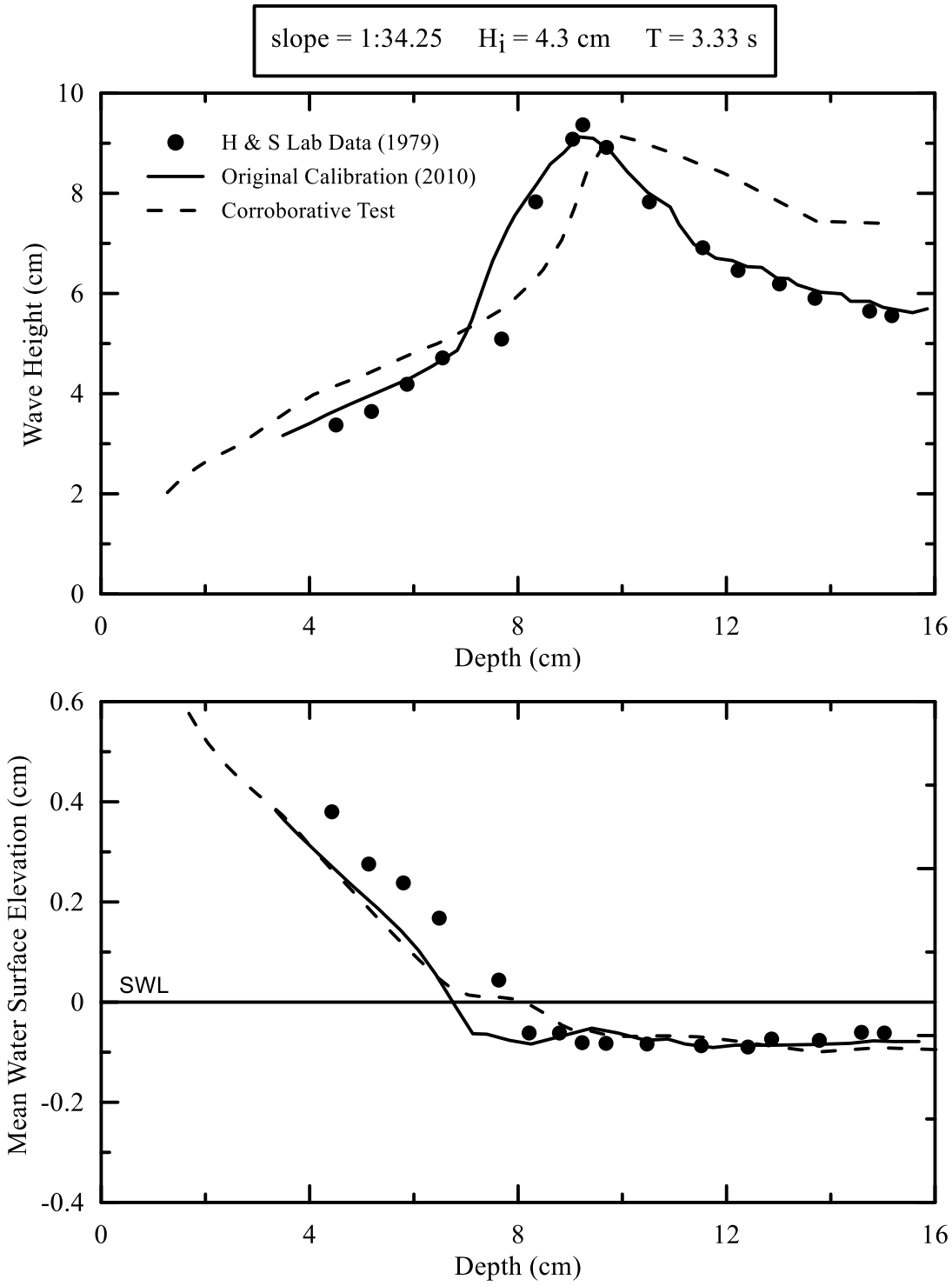

Figure 4.1: Comparison of Hansen and Svendsen (1979) measured wave data for case 031041 with predicted results from Lynett et al. (2008) and current results for this investigation.

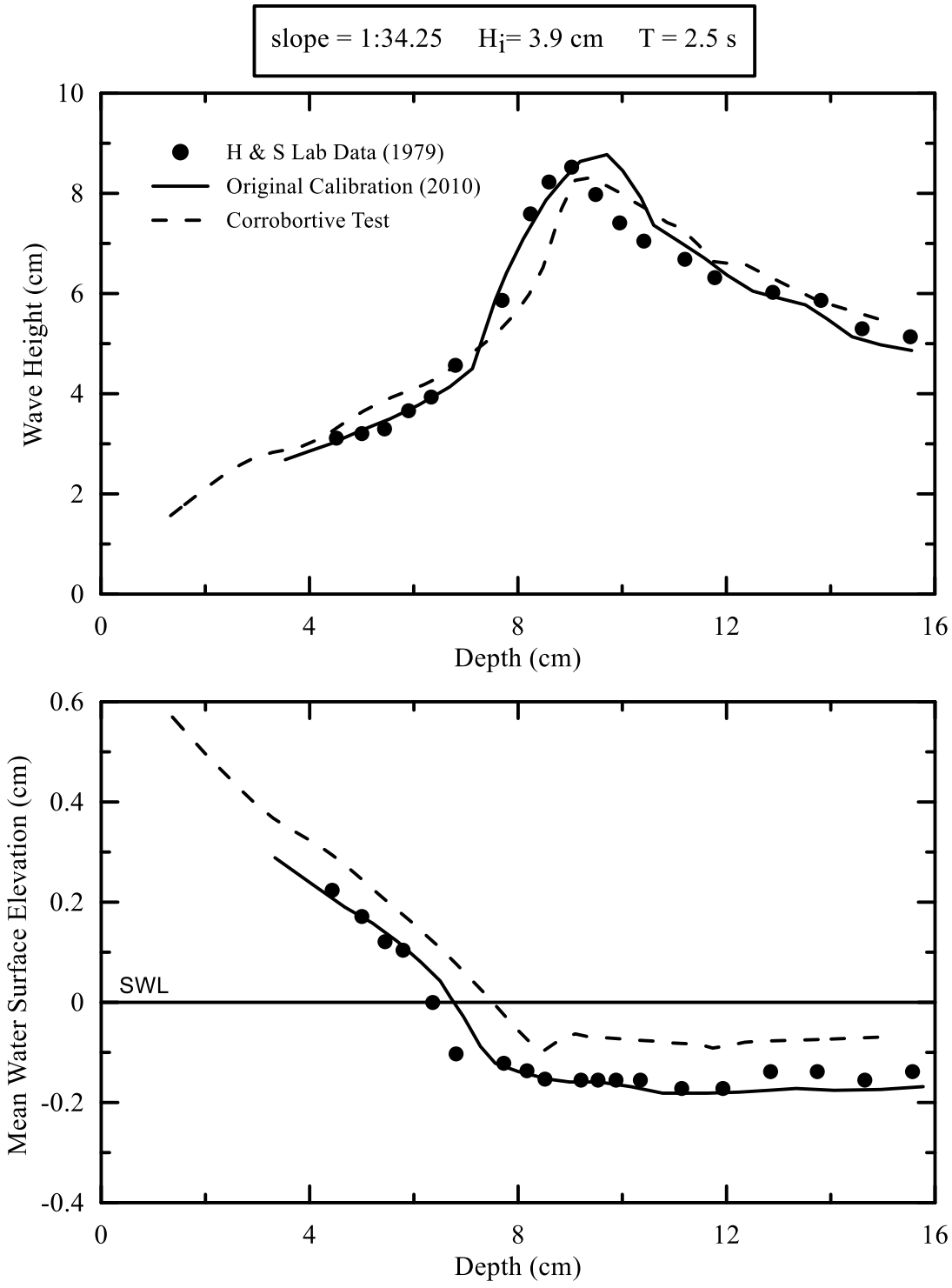

Figure 4.2: Comparison of Hansen and Svendsen (1979) measured wave data for case 041041 with predicted results from Lynett et al. (2008) and current results for this investigation.

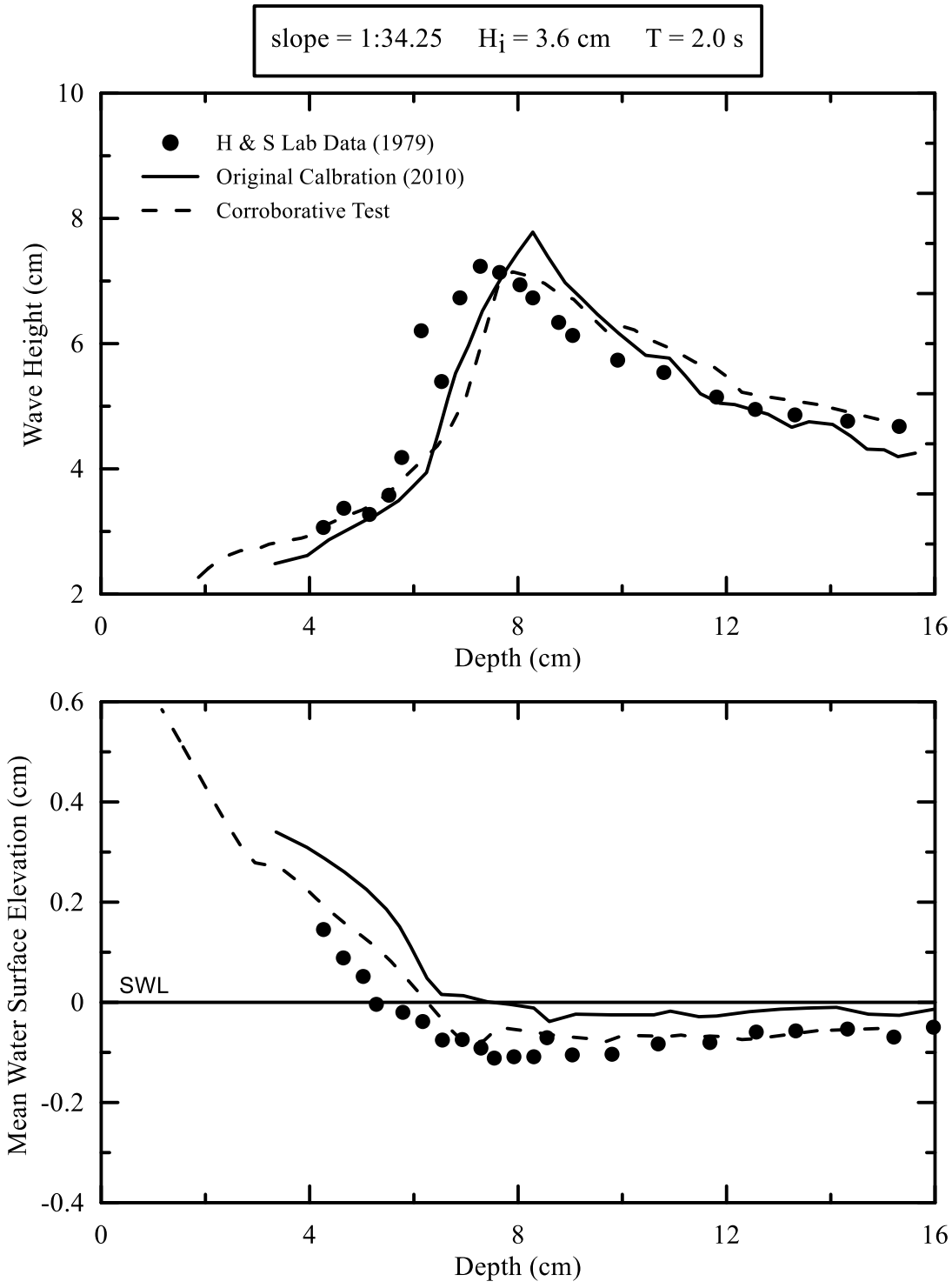

Figure 4.3: Comparison of Hansen and Svendsen (1979) measured wave data for case 051041 with predicted results from Lynett et al. (2008) and current results from this investigation.

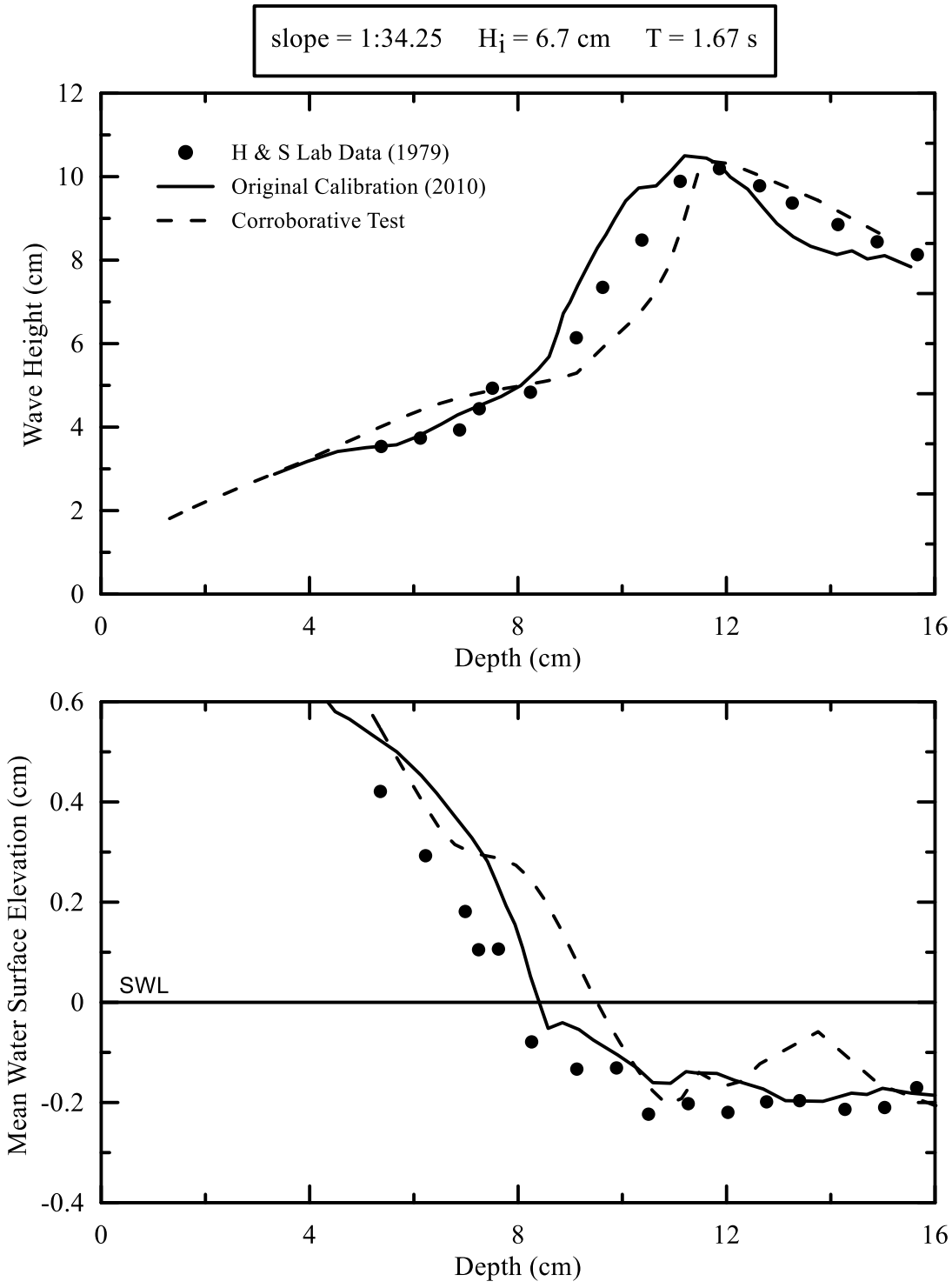

Figure 4.4: Comparison of Hansen and Svendsen (1979) measured wave data for case 061071 with predicted results from Lynett et al. (2008) and current results from this investigation.

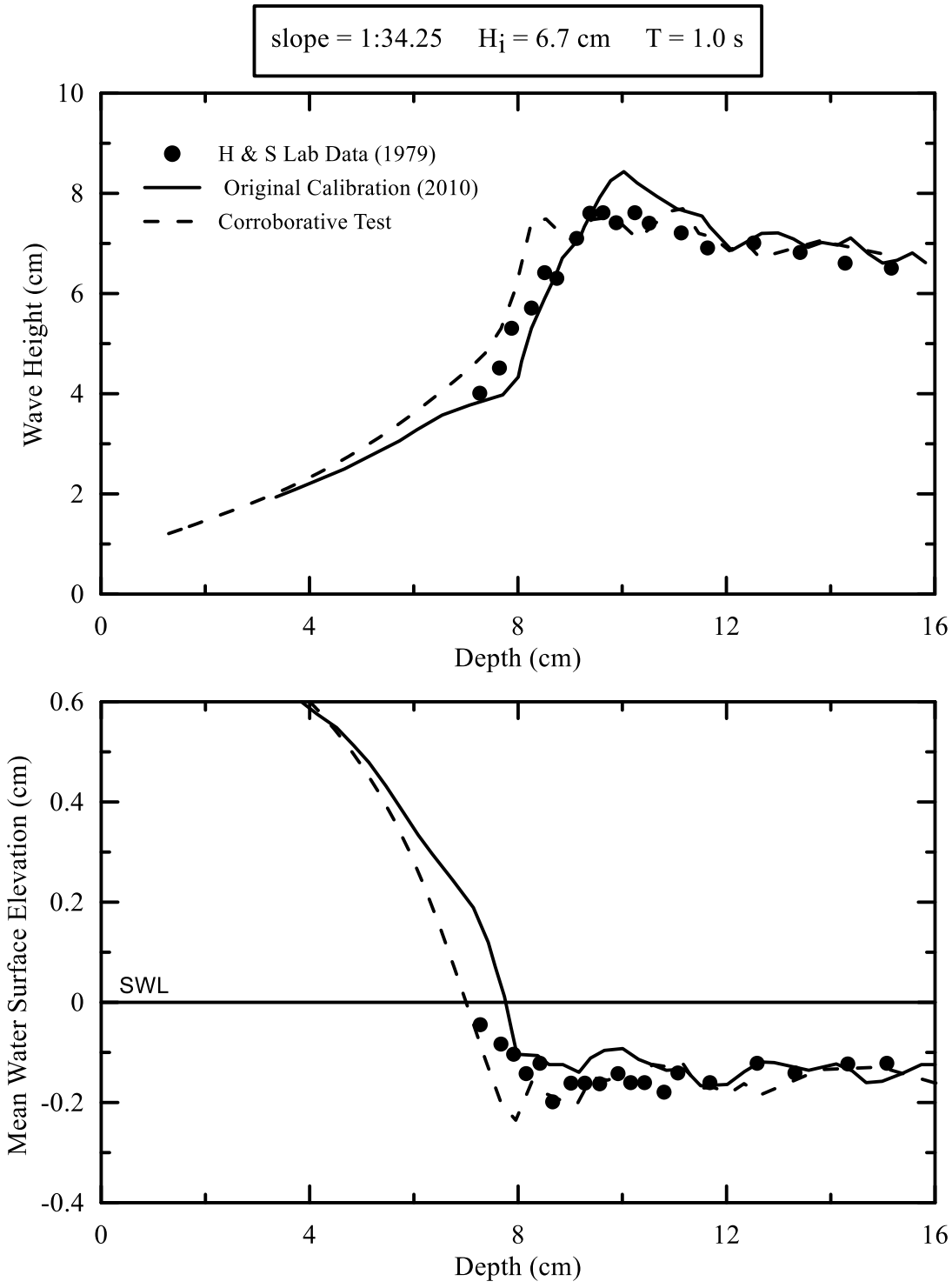

Figure 4.5: Comparison of Hansen and Svendsen (1979) measured wave data for case A10112 with predicted results from Lynett et al. (2008) and current results from this investigation.

4.2 Assessment and discussion

As a quantitative baseline assessment of COULWAVE's breaking algorithm as calibrated, the wave height data are used to compute error metrics. The laboratory data of Hansen and Svendsen (1979) (measured wave heights) and the model results (predicted wave heights) are compared shoreward of the break point, defined by the highest wave height achieved in the model. The error metrics to be computed include the bias (*bi*), root mean square error (*rmse*), scatter index (*si*), and the modified index of agreement (*mia*) between the two data sets. These are defined as:

$$bi = \frac{1}{N}\sum_{i=1}^{N}(P_i - M_i)$$

$$rmse = \left[\frac{1}{N}\sum_{i=1}^{N}(P_i - M_i)^2\right]^{1/2}$$

$$si = \frac{rmse}{\sqrt{|\overline{PM}|}}$$

$$mia = 1 - \frac{\sum_{i=1}^{N}|M_i - P_i|}{\sum_{i=1}^{N}(|P_i - \bar{M}| + |M_i - \bar{M}|)}$$

where N is the number of data points, P_i is the model-predicted value, M_i is the corresponding measured value, and $\bar{P}$ and $\bar{M}$ are the mean values of the respective parameters. Results from this analysis for all five test cases are presented in **Table 4.1**. The modified index of agreement is a measure of how a model's predictions are error free. *mia* values range from 0 to 1, with 1 representing perfect agreement. This form of the index agreement was shown by Legates and McCabe (1999) to be more appropriate than other forms used in the past.

Table 4.1: Comparative statistical parameter for predicted (COULWAVE) versus measured (wave tank) wave heights.

Test	N	Bias (cm)	RMS error (cm)	Scatter index	Mod. index agreement
031041	8	-0.13	1.0	0.17	0.73
041041	10	-0.18	0.73	0.14	0.82
051041	9	-0.39	0.67	0.15	0.83
061041	11	-0.23	0.88	0.15	0.81
A10112	5	0.97	1.05	0.19	0.91
Average*	-	**0.008**	**0.86**	**0.16**	**0.74**

The results in **Table 4.1** show that the overall agreement is reasonable, but with case 031041 (i.e. the sole plunging breaker case) showing the most error. Generally, the bias shows a negative trend with case A10112 the sole outlier, which also has the highest wave steepness and lowest Iribarren Number. The RMS error shows closer agreement among the group, yet case A10112 and 031041 demonstrate larger errors. The scatter index shows near consistent results. Through the modified index of agreement, the inconsistency in case 031041 is demonstrated; however, the overall agreement is very good.

Along with the statistics above, **Figure 4.6** shows the comparison of the five data sets in graphical form, in which each of the five wave cases is represented by a different symbol. This plot demonstrates the close agreement between the measured and predicted wave heights. Based on these findings from the corroborative tests, further investigation with COULWAVE is warranted.

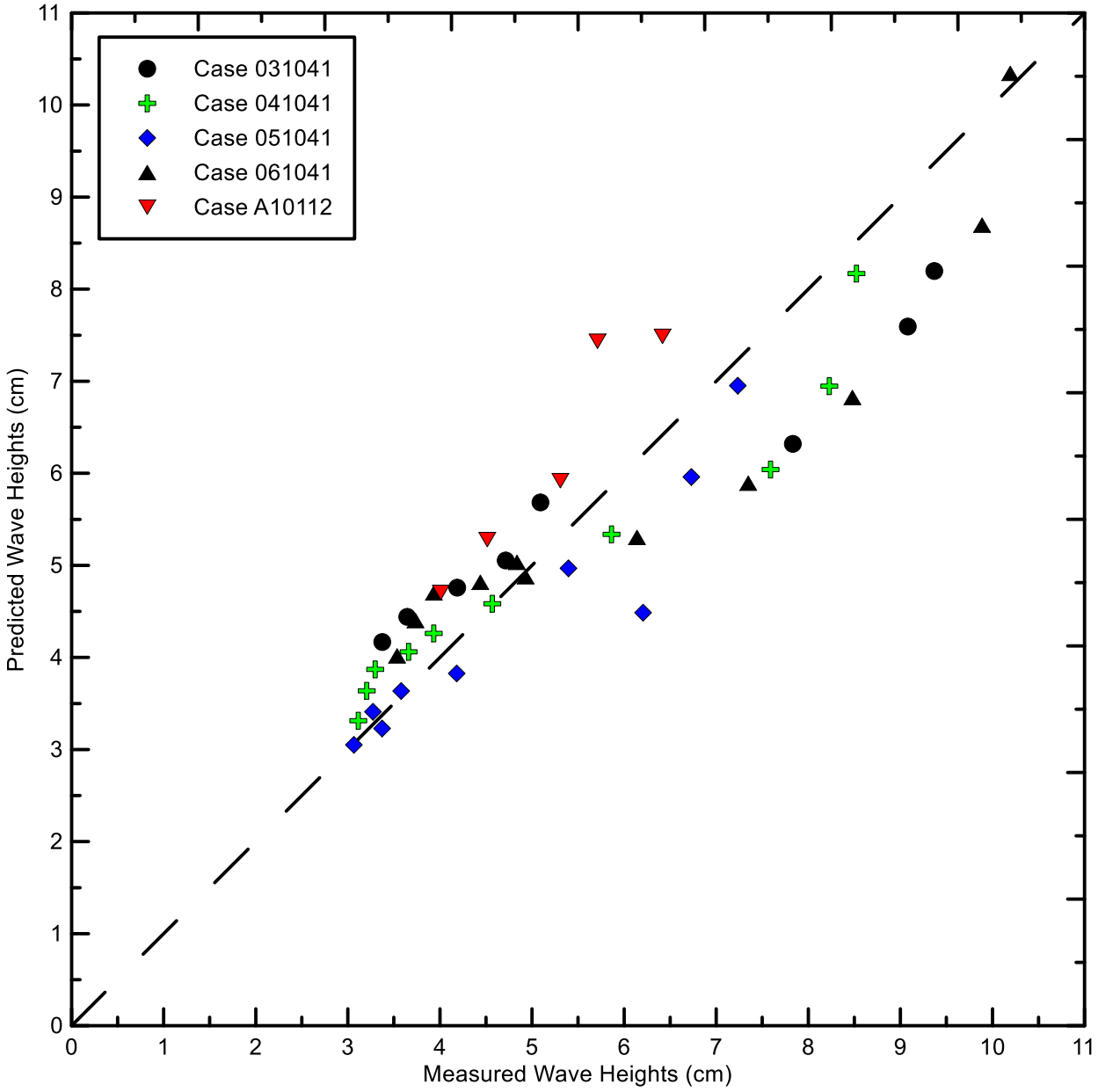

Figure 4.6: Measured v. predicted wave heights plotted to show effectiveness of the current COULWAVE model study to recreate laboratory data.

5 Testing COULWAVE for a range of planar beach slopes

Having established that the use of COULWAVE for pursuing the objectives of this thesis is acceptable relative to the calibration and laboratory data, this chapter will begin to test the model beyond the 1:34.25 slope of Hansen and Svendsen (1979) used in its original calibration. This will be done by testing the model against nine additional laboratory tests with a variety of planar beach slopes. As with the corroborative tests, a statistical assessment will be conducted of the agreement between observed and modeled wave height inside the breaking point.

5.1 Available laboratory data

Before conducting an extensive search for additional laboratory data, three criteria for acceptable data were established. Most importantly, either the data had to be available in raw form from the literature or obtainable directly from a reliable source. When the raw experimental data was not provided in tabular from, values were extracted by digital means from graphs presented in the various works. The second criterion to be met was that the experimental set-up was provided in enough detail to be recreated in the model. This included the channel dimensions, bottom geometry, water level(s), and input wave conditions. Finally, the waves generated in the experiments had to satisfy the conditions for which the Boussinesq equations within COULWAVE are valid.

An extensive review of the literature provided various options. The first two criteria were the most apparent discriminators. Verifying the proper shallow water wave heights required additional scrutiny. In general, the measurements collected were in small scale laboratory setups; therefore,

the required depth to wavelength ratio was within the bounds for the COULWAVE model. A thorough search of the literature produced nine data sets that satisfied these conditions, and fortunately were found to encompass a wide variety of incident wave conditions and beach slopes, allowing for a more comprehensive test of COULWAVE. **Table 5.1** provides a list of the related data sets and their test conditions. In addition to one additional test on the 1:34.25 slope of Hansen and Svendsen is now a range in slopes from 1:20 to 1:65. The range in wave steepness is 0.015 to 0.044 and the Iribarren Number ranges from 0.08 to 0.58. However, only one test produced a breaker of the plunging type.

Table 5.1: Data sources and test conditions selected for COULWAVE testing.

Test	Iribarren Number	Slope	Height (cm)	Period (s)	Wave Steepness	Breaker Type
Okayasu et al. (1988)	0.58	1:20	5.60	2.00	0.015	Plunging
Smith and Kraus (1990), 10000	0.34	1:30	9.10	2.49	0.020	Spilling
Okayasu et al. (1986)	0.33	1:20	8.15	1.5	0.032	Spilling
Hansen and Svendsen (1984)	0.21	1:34.25	12.00	2.00	0.034	Spilling
Smith and Kraus (1990), 8000	0.20	1:30	13.7	1.74	0.044	Spilling
Stive and Wind (1986)	0.14	1:40	15.9	1.79	0.037	Spilling
Horikawa and Kuo (1966), Case #7	0.10	1:65	10.0	1.60	0.028	Spilling
Horikawa and Kuo (1966), Case #5	0.09	1:65	12.8	1.60	0.036	Spilling
Horikawa and Kuo (1966), Case #4	0.08	1:65	15.2	1.60	0.043	Spilling

5.2 Results and error analysis

Figure 5.1 through **Figure 5.9** show the results for each of the cases presented in **Table 5.1**. The measurements presented are generally limited to the surfzone (i.e. from inside the breakpoint) and are subjected to quantitative error analysis. Across the nine tests there is a varying amount of agreement between the modeled and measured results. The most important features are the height of incipient breaking, the location of the initiation of breaking, and the general agreement of the wave decay as the wave propagates to the shoreline. In regard to the mean water level, general agreement in the applicable cases provides another indication as to the veracity of the modeled results.

A feature prevalent in the model results, particularly **Figure 5.4**, is the presence of reflected wave energy seaward of the break point. Recreating the effects of energy reflection from a given boundary is complex. Not only are the results in the test cases much different than what would be expected in a natural beach condition, the modeling provides another result. COULWAVE is unique in its approach to describing the energy changes along the beach face by utilizing a moving boundary algorithm that is described in Lynett et al. (2002).

Another feature of the following results that is an important component of the qualitative discussion is the determination of where breaking is generated based on the defined coefficients within COULWAVE. This factor is demonstrated in the following graphs where the peak wave height, as well as the location of that peak value, differs between the modeled and predicted results.

Modeled results in **Figure 5.1** demonstrates very good agreement of the incipient break point and wave height decay into the shoreline with the Okayasu et al. (1988) data. This case represents the sole plunging breaker case. The mean water surface agreement outside the breakpoint does not agree well, the modeled set-down appears to exceed the laboratory data. **Figure 5.2** shows good agreement of the modeled wave height to data from Case 10000 of Smith and Kraus (1990), especially near incipient breaking. Yet, the modeled results inside the break point consistently overestimate the wave height. The set-up in this case is also consistently over-estimated. The Okayasu et al. (1986) data in **Figure 5.3** provide the most points for comparison; however, the COULWAVE model fails to capture the major features. The modeled height and location of incipient breaking do not follow the data and the mean water surface overestimates both the set-down and set-up. The reflected wave energy in the modeled domain is observed clearly in **Figure 5.4** where both the wave height and set-down are grossly inaccurate outside the breakpoint. This is likely caused by a node developed from the reflected energy. The second case from Smith and Kraus (1990), Case 8000 in **Figure 5.5**, again demonstrates poor agreement between the modeled and measured water surface outside the break point. The excellent agreement of wave heights in Case 10000 is not recreated in this case; however, the general trend is captured by the COULWAVE model. For **Figure 5.6**, the comparison of the COULWAVE wave heights to Stive and Wind (1986) data shows excellent agreement. The mean water surface in this case continues to show a mismatch, specifically with the modeled set-up overshooting the measured data. The last three cases all come from lab data of Horikawa and Kuo (1966) and consist of only wave height comparisons. The modeled results tend to initiate breaking prematurely but the wave height decay follows the trend in the measured data.

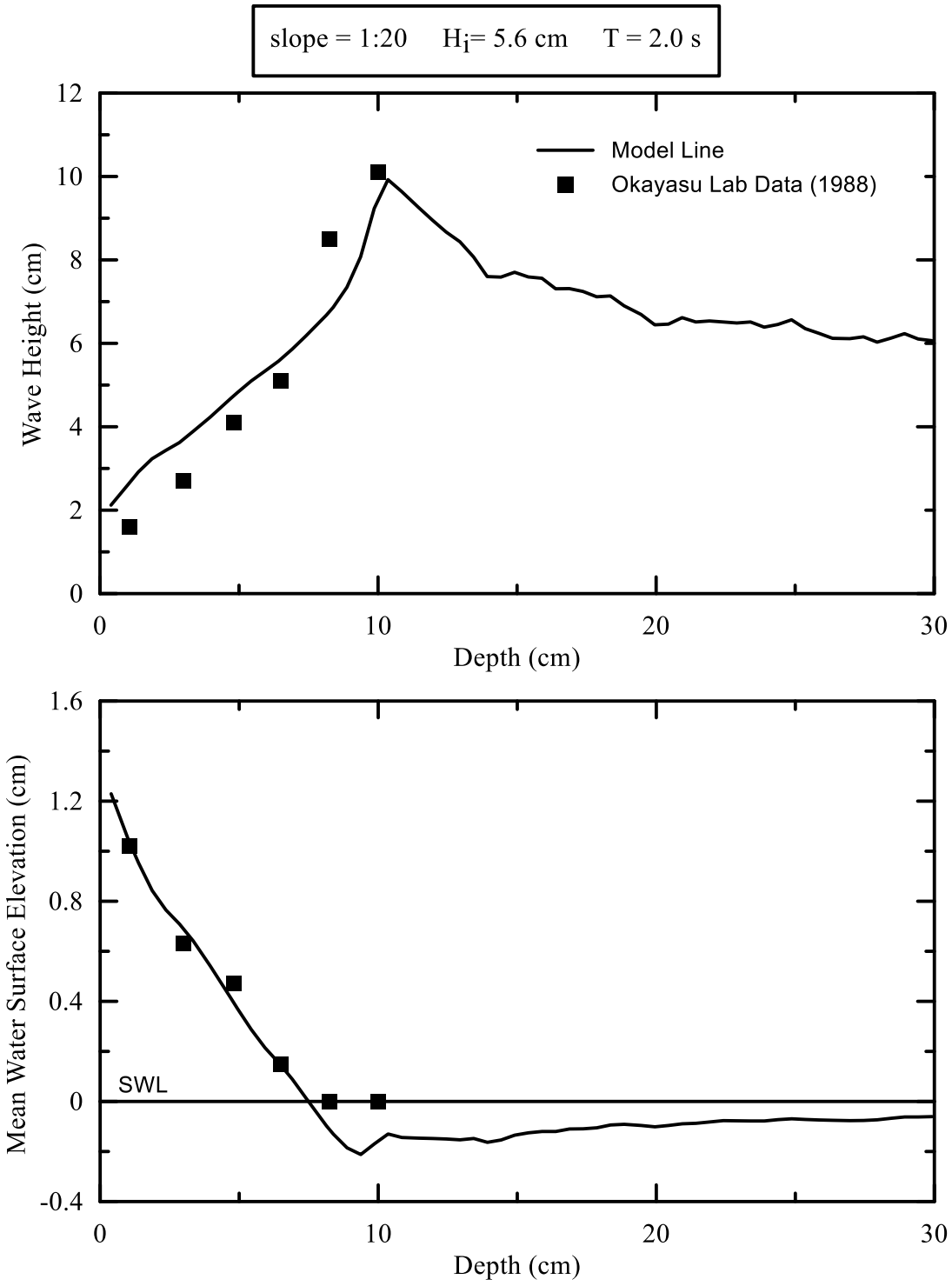

Figure 5.1: Comparison of measured lab data from Okayasu (1988) to modeled COULWAVE results.

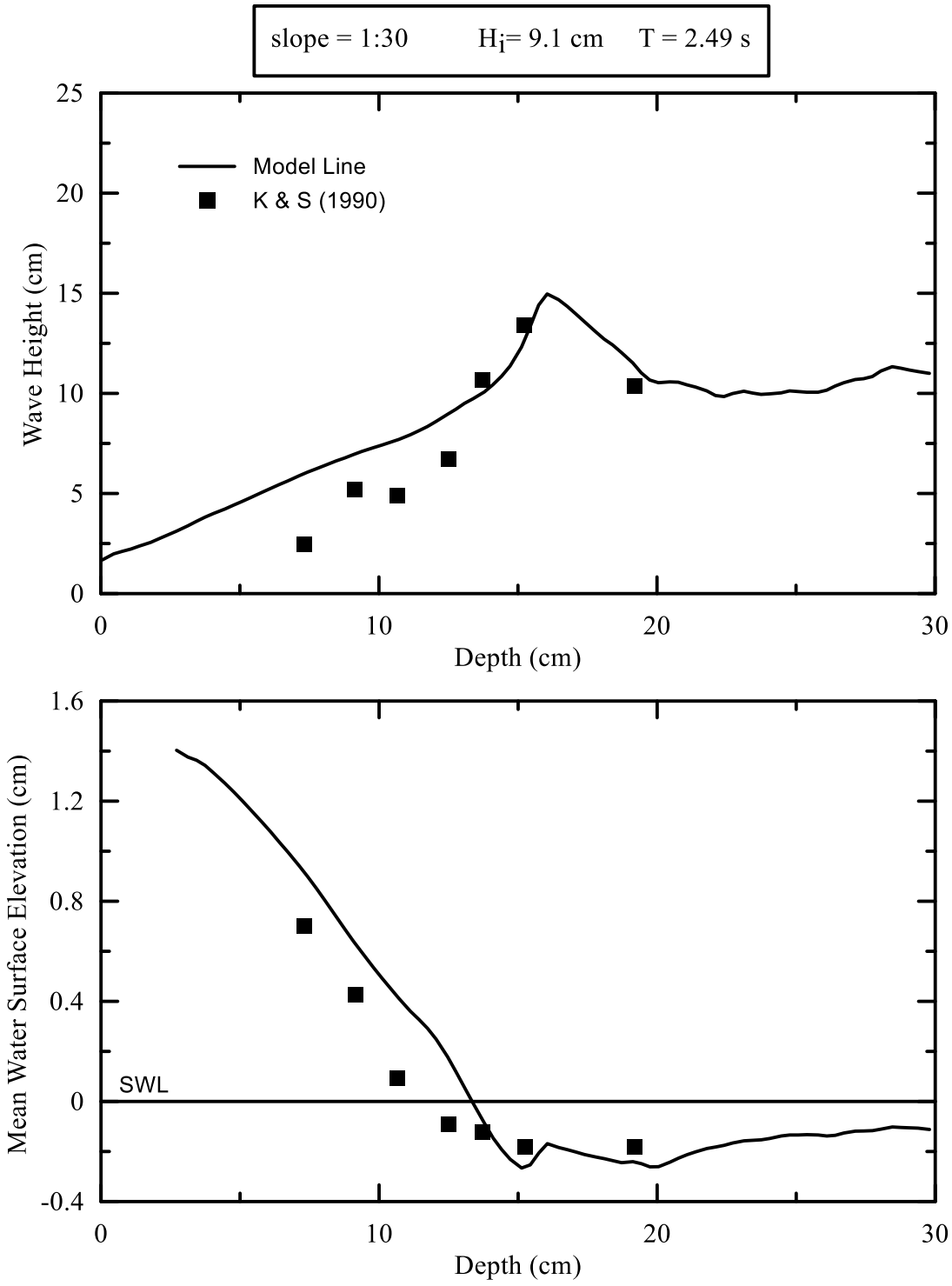

Figure 5.2: Comparison of measured lab data from Smith and Krause (1990) case #10000 to modeled COULWAVE results.

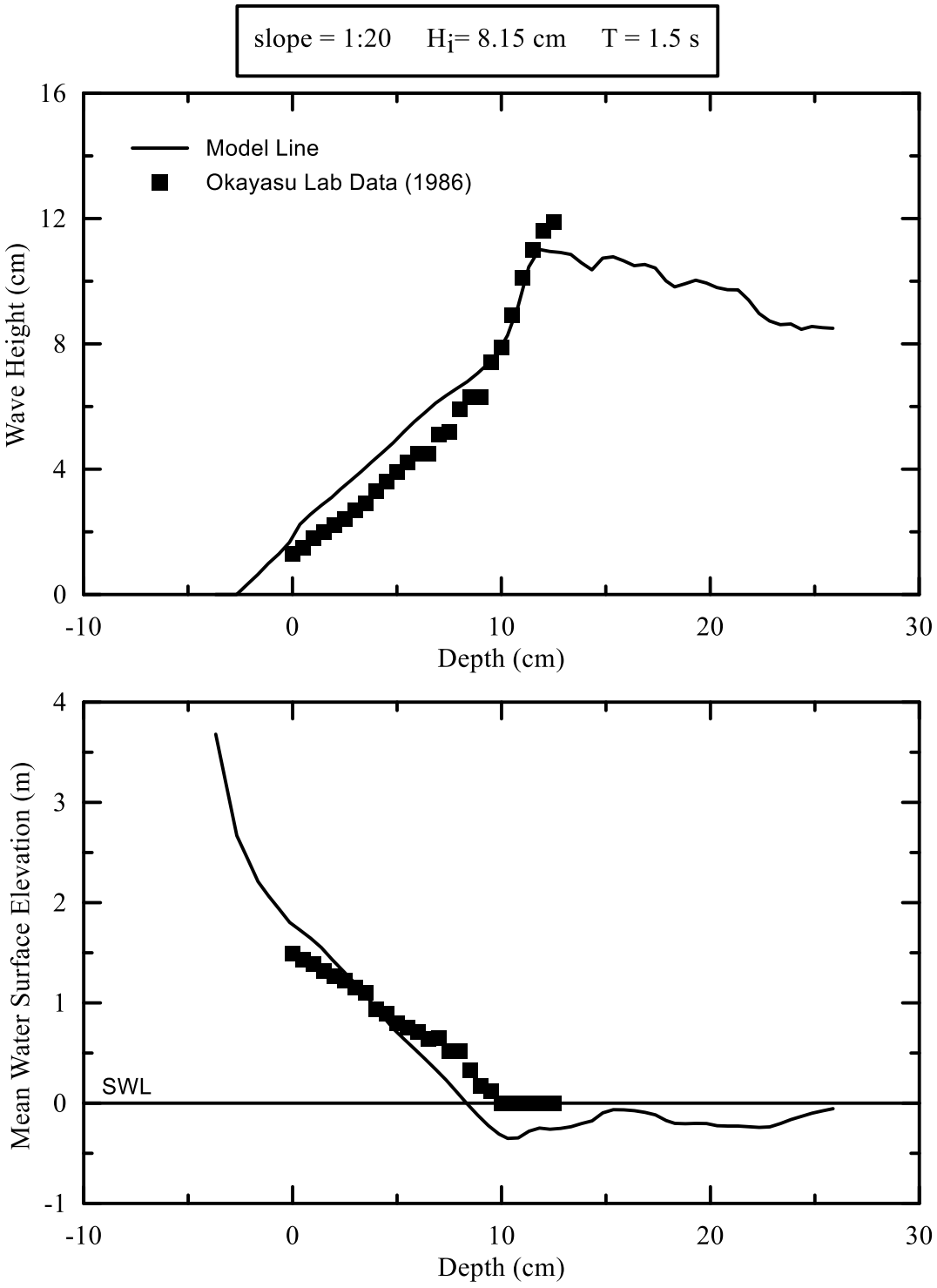

Figure 5.3: Comparison of measured lab data from Okayasu (1986) to modeled COULWAVE results.

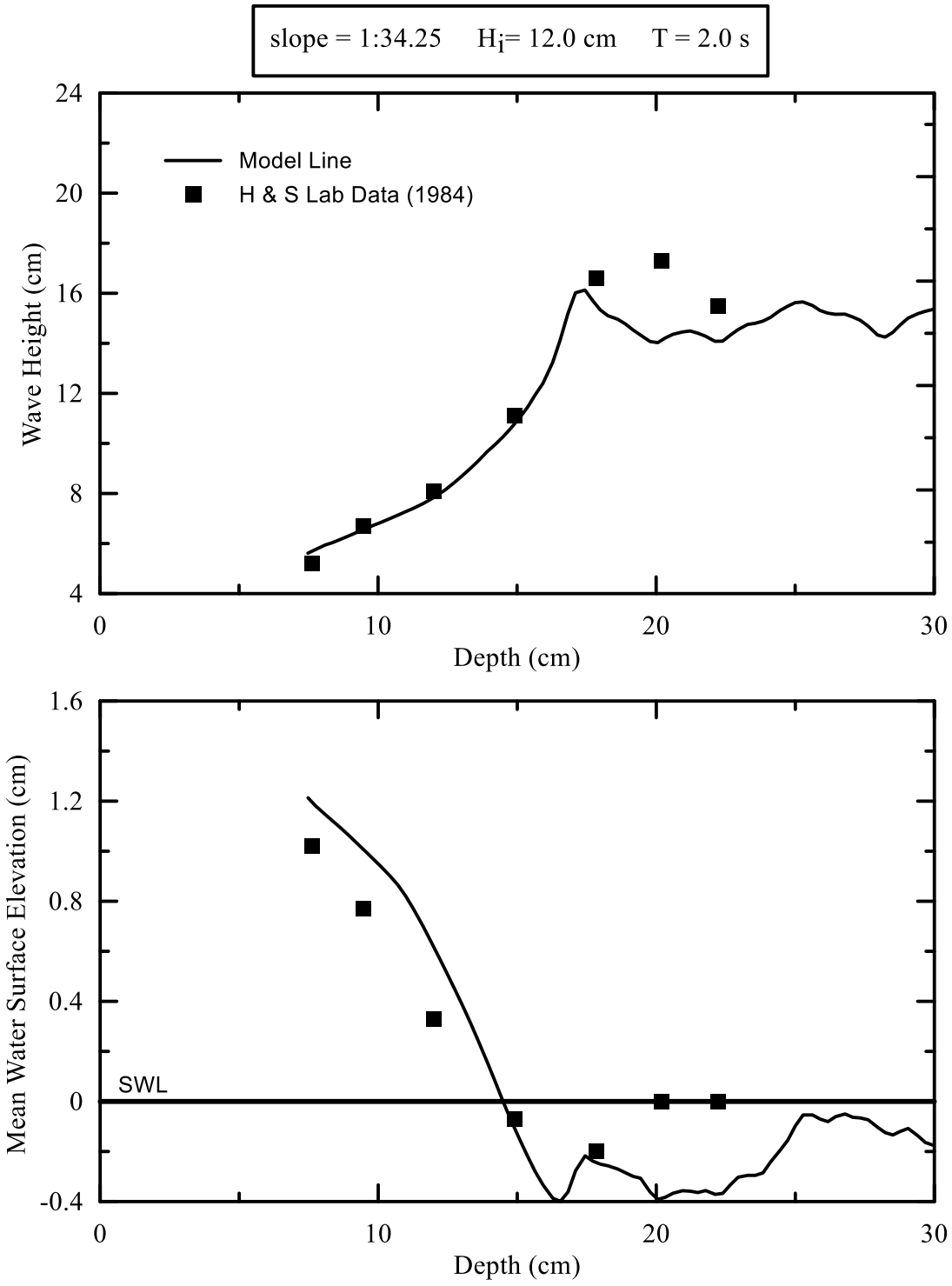

Figure 5.4: Comparison of measured lab data from Hansen and Svendsen (1984) to modeled COULWAVE results.

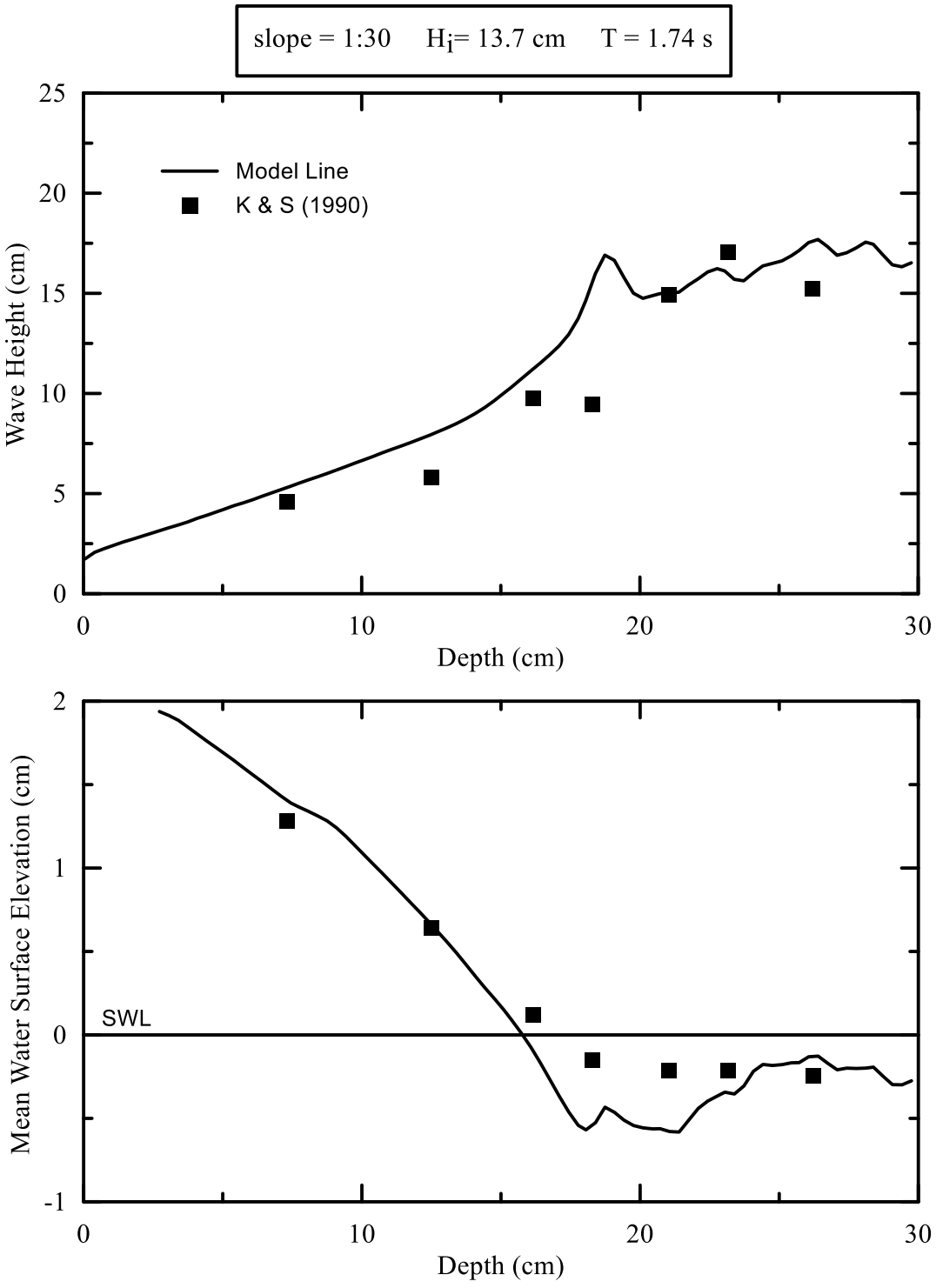

Figure 5.5: Comparison of measured lab data from Smith and Kraus (1990) case #8000 to modeled COULWAVE results.

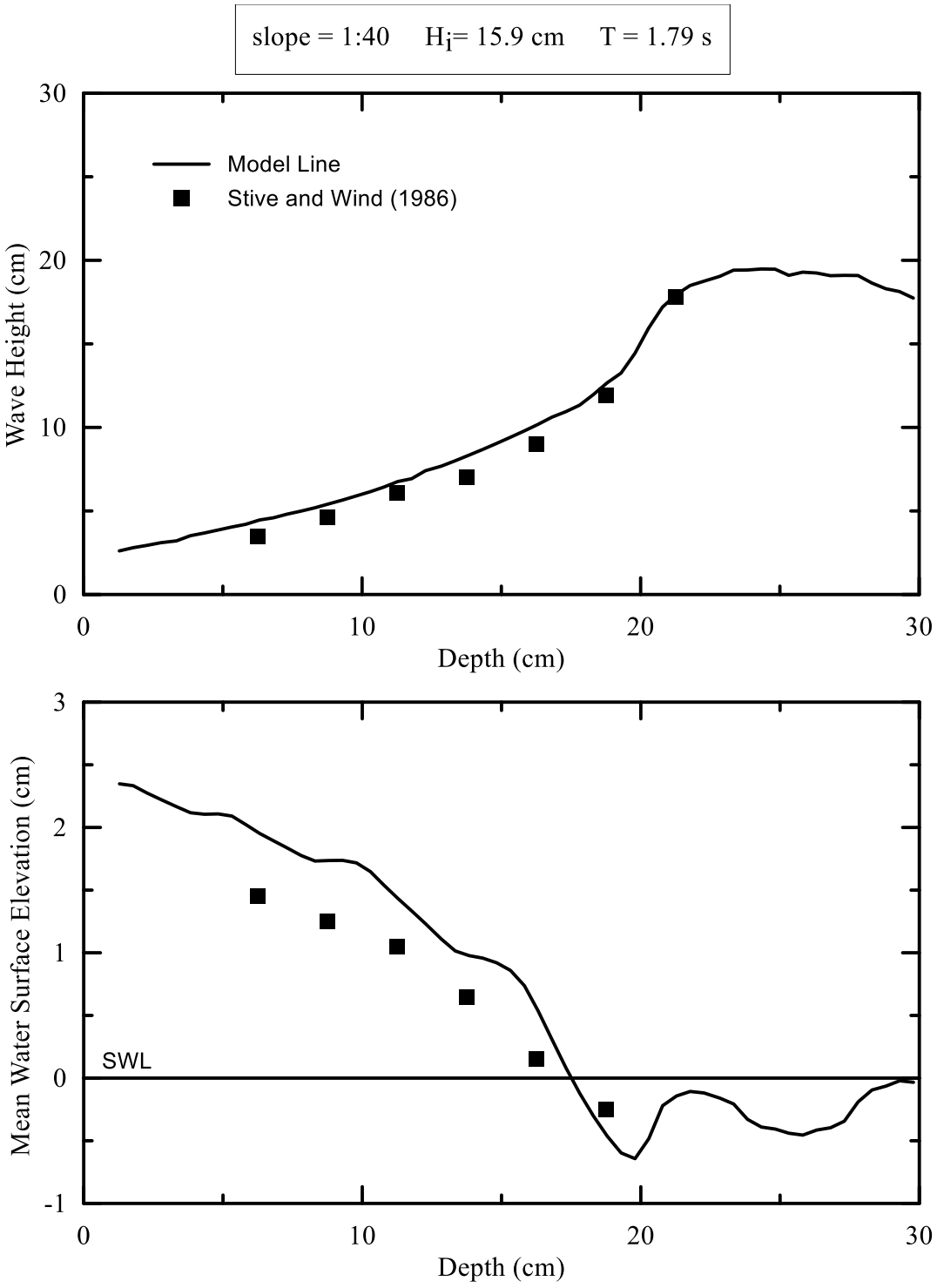

Figure 5.6: Comparison of measured lab data from Stive and Wind (1986) to modeled COULWAVE results.

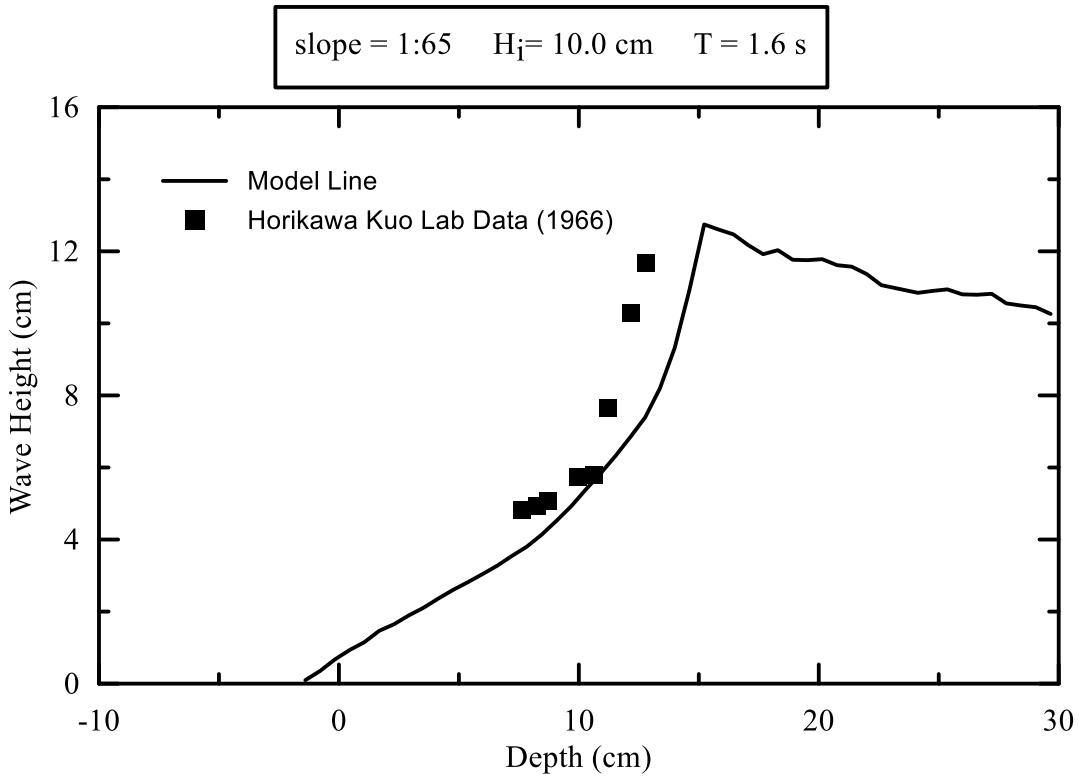

Figure 5.7: Comparison of measured lab data from Horikawa and Kuo (1966) case #7 to modeled COULWAVE results.

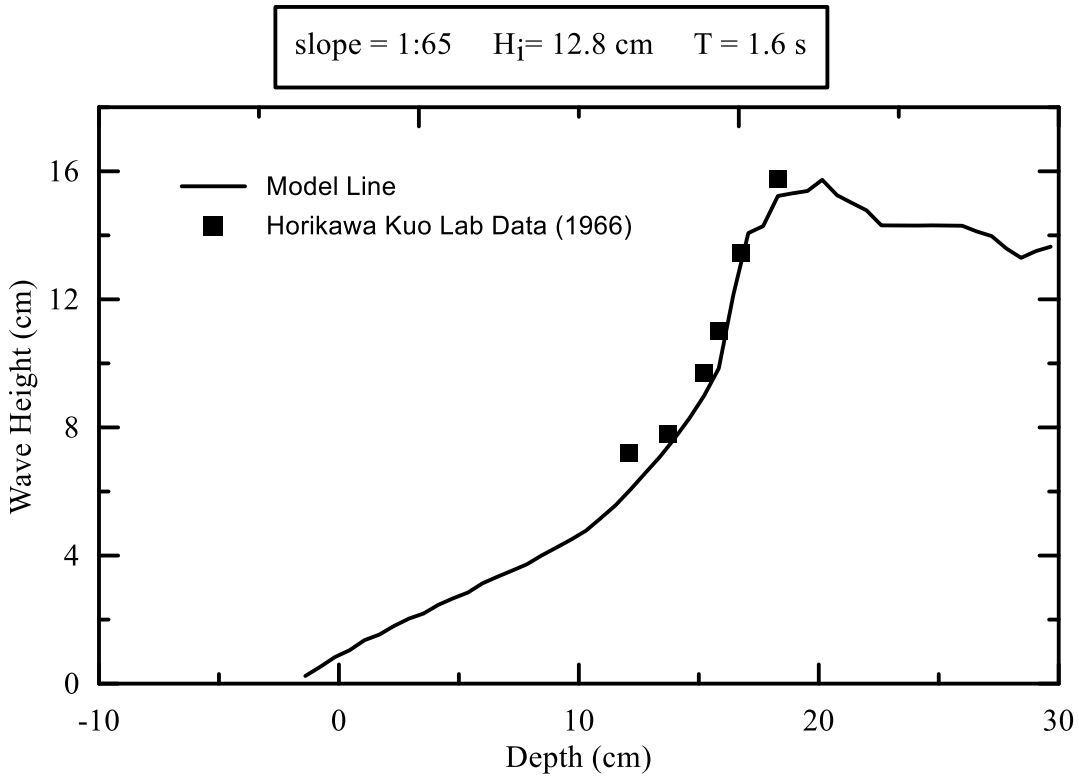

Figure 5.8: Comparison of measured lab data from Horikawa and Kuo (1966) case #5 to modeled COULWAVE results.

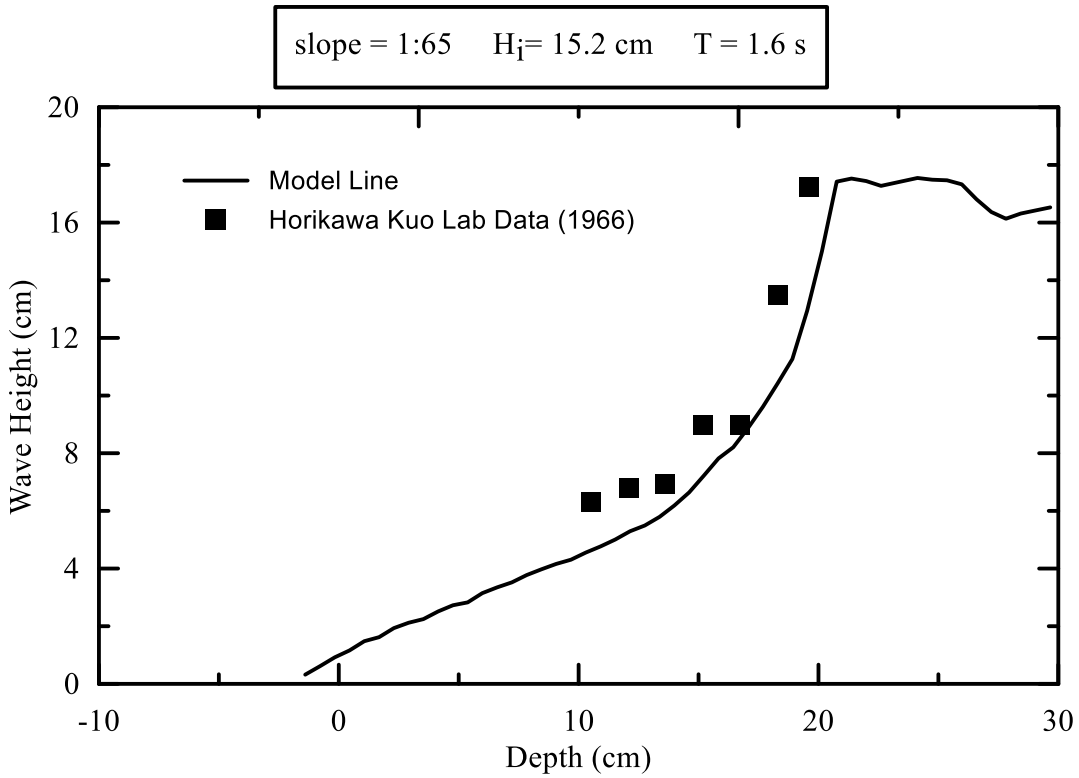

Figure 5.9: Comparison of measured lab data from Horikawa and Kuo (1966) case #4 to modeled COULWAVE results.

Results of statistical error analysis of the nine test cases, following the method described in Chapter 4, is presented in **Table 5.2**. These statistics show that the overall agreement is reasonable with some cases showing more variance between the measured and modeled results. The trends are not as consistent compared to the results in Chapter 4; specifically, the bias in these nine cases varies widely. Multiple test cases show an *rmse* greater than 2.0; however, there is not a consistent pattern as to which cases show these discrepancies. Tests with varying slopes and Iribarren Numbers have both good and poor agreement. The scatter index also varies widely. In Chapter 4 the five cases had scatter indexes that fell between 0.14 to 0.19, a very close range compared to the range of 0.06 to 0.39. The Hansen and Svendsen (1984) test case, which utilized the same slope as the corroborative tests, has the best agreement based on both the scatter index and the *mia*. This may indicate that COULWAVE is best utilized on planar slopes that are consistent with that used in establishing the breaker criteria.

Along with the statistics in **Table 5.2**, the measured and predicted results were plotted in **Figure 5.10**. This plot shows the generally good agreement between the measured and predicted values but also shows that there is more variability compared to the five examples from Chapter 4.

Table 5.2: Comparative statistical parameters for predicted (COULWAVE) versus measured (wave tank) wave heights for nine varying bed slope conditions.

Test	N	Bias (cm)	RMS error (cm)	Scatter index	Mod. index of agreement	Comments
Okayasu et al. (1988)	6	0.14	1.02	0.19	0.79	Plunging case with good agreement.
Smith and Kraus (1990), 10000	4	2.63	3.36	0.39	0.55	Similar slope to corroborative tests but with poor agreement.
Okayasu et al. (1986)	25	0.69	0.89	0.17	0.82	Agreement consistent with corroborative tests.
Hansen and Svendsen (1984)	5	-0.26	0.56	0.06	0.93	Same slope as corroborative tests and consistent *bias* measure.
Stive and Wind (1986)	7	0.81	0.88	0.10	0.89	1:40 slope with very good agreement.
Smith and Kraus (1990), 8000	6	1.51	2.24	0.28	0.62	Poor agreement with no consistent reasoning.
Horikawa and Kuo (1966), #7	8	-1.59	2.10	0.34	0.59	Shallowest slope with very poor agreement.
Horikawa and Kuo (1966), #5	6	-0.72	0.79	0.08	0.87	Excellent agreement with nearly exact parameters as previous case.
Horikawa and Kuo (1966), #4	7	-1.93	2.23	0.25	0.69	Consistent negative bias in all three Horikawa and Kuo (1966) cases.
Average		**0.14**	**1.56**	**0.21**	**0.75**	

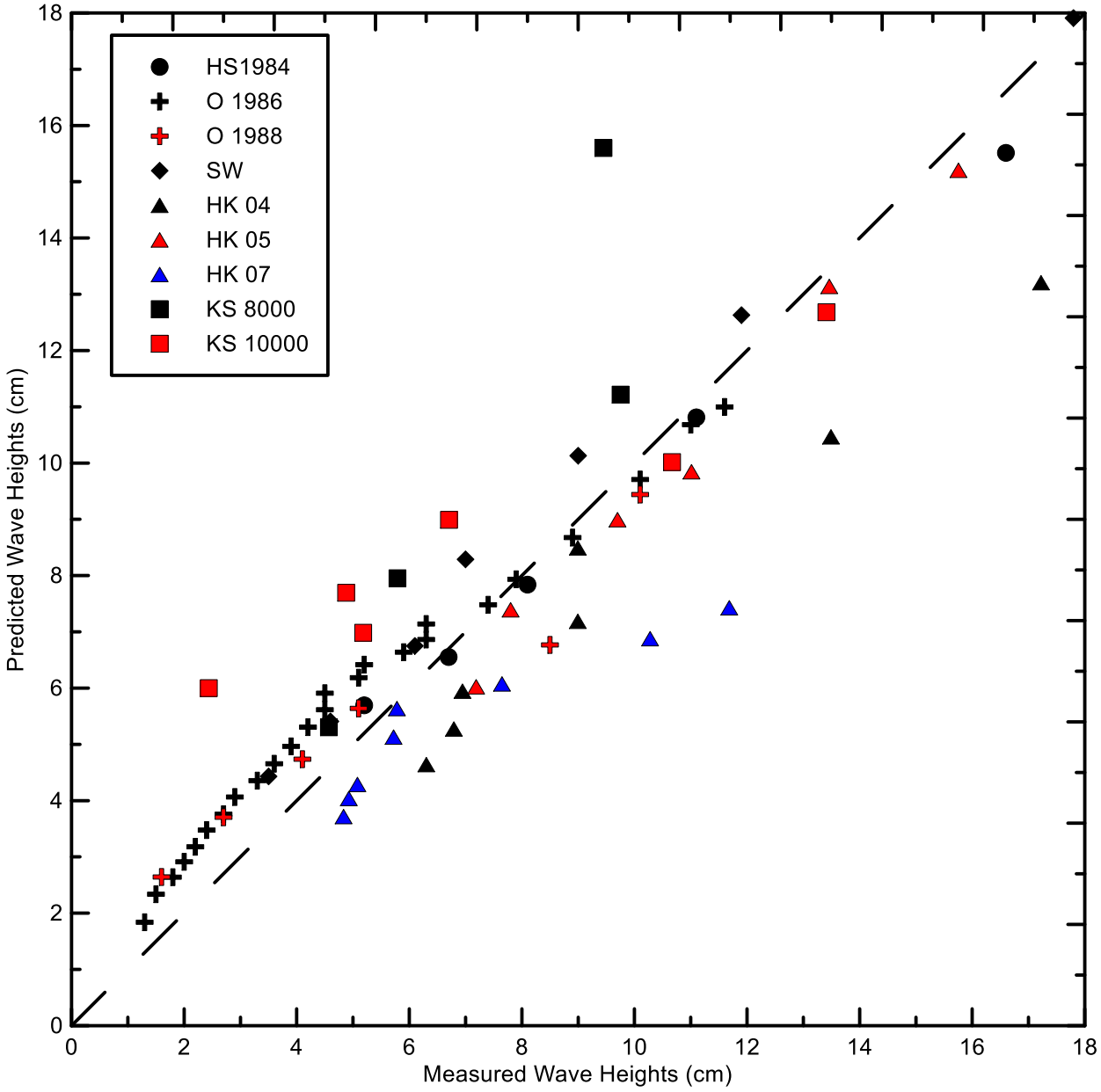

Figure 5.10: Measured v. predicted wave heights plotted to show effectiveness of the current COULWAVE model to study to recreate laboratory data from varying planar slopes.

5.3 Discussion and conclusions for planar beach slopes

These nine cases, with varying beach slope conditions, provide no definitive indication that the COULWAVE model is robust enough to accurately depict conditions outside of a 1:34.25 slope. Although there are some cases that show good comparison, the trend is not definitive or consistent, as it was with the five cases from Chapter 4. With these inconclusive results, the next steps of evaluating the COULWAVE model, on artificial bars, with a higher spatial and temporal resolution, and finally on barred profiles, will be conducted with a critical view of the resulting agreement and for any indications of other factors that are affecting the results.

6 Testing of COULWAVE on artificial bars

Because this study is motivated by the greater issue of modeling cross-shore sediment transport and beach profile evolution, it is of course beneficial to test the ability of COULWAVE to model wave breaking and reforming across bar/trough formations. However, it appears that suitable data from controlled laboratory experiments are available from only a limited number of sources. One sure source is that of Smith and Kraus (1990), who studied wave breaking across rigid, artificial bars constructed in a small-scale wave channel.

6.1 Overview of Smith and Kraus (1990)

An in-depth investigation of breaking wave features over bars and reef-like structures was conducted at the Coastal Engineering Research Center (CERC) and published in 1990. The experiment was conducted in a wave channel using submerged, triangular-shaped obstacles of various geometries to represent nearshore bars. In total 180 monochromatic wave cases were run, six of which used a planar 1:30 slope, with two of those tests already utilized in Chapter 4. Here, 23 test cases of varying bar shapes, drawn from two test subgroups, were modeled using COULWAVE. **Table 6.1** and **Table 6.2** present the original test number, Iribarren Number, incident wave height, wave period, wave steepness, and bar geometry in terms of two angles, alpha and beta that are defined in **Figure 6.1**. COULWAVE was configured and run for each of these test cases.

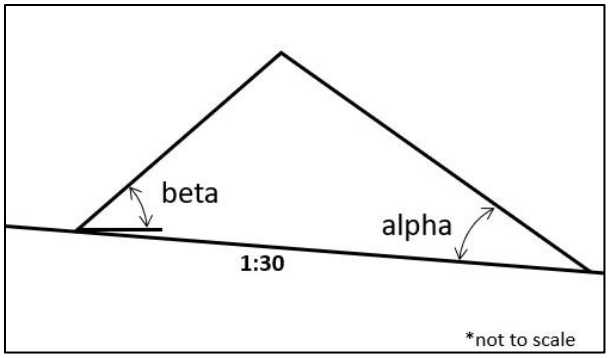

Figure 6.1: Description of bar geometry based on angles alpha and beta on the planar 1:30 test slope.

Table 6.1: Laboratory cases from 8000 series of Smith and Kraus (1990) study of wave breaking over artificial bars used for comparison to COULWAVE modeled results.

Test	Iribarren Number	Height (cm)	Period (s)	Wave Steepness	Breaker Type	Alpha	Beta
8110	0.19	14.02	1.74	0.030	Spilling	5.6	0
8210	0.19	14.63	1.74	0.032	Spilling	5.3	20
8220	0.19	15.24	1.74	0.034	Spilling	10.5	20
8240	0.18	15.54	1.74	0.034	Spilling	23.6	20
8310	0.19	14.63	1.74	0.032	Spilling	5.0	30
8320	0.19	15.24	1.74	0.034	Spilling	11.0	30
8330	0.19	15.24	1.74	0.034	Spilling	16.5	30
8340	0.19	15.24	1.74	0.034	Spilling	22.1	30
8420	0.19	15.24	1.74	0.034	Spilling	11.2	40
8430	0.19	15.24	1.74	0.034	Spilling	16.5	40
8440	0.19	15.24	1.74	0.034	Spilling	20.6	40

Table 6.2: Laboratory cases from 10000 series of Smith and Kraus (1990) study of wave breaking over artificial bars used for comparison to COULWAVE modeled results.

Test	Iribarren Number	Height (cm)	Period (s)	Wave Steepness	Breaker Type	Alpha	Beta
10110	0.32	10.36	2.49	0.010	Spilling	5.4	0
10120	0.36	8.23	2.48	0.008	Spilling	9.2	0
10130	0.36	8.23	2.49	0.008	Spilling	12.9	0
10210	0.34	9.14	2.49	0.009	Spilling	5.6	20
10220	0.34	9.14	2.49	0.009	Spilling	11.9	20
10230	0.36	8.23	2.49	0.008	Spilling	17.4	20
10310	0.36	8.53	2.49	0.008	Spilling	5.0	30
10320	0.35	8.84	2.49	0.008	Spilling	12.3	30
10330	0.36	8.23	2.49	0.008	Spilling	15.7	30
10410	0.36	8.23	2.49	0.008	Spilling	5.2	40
10420	0.37	7.92	2.49	0.008	Spilling	9.8	40
10430	0.36	8.23	2.49	0.008	Spilling	15.7	40

6.2 Results and error analysis

The plotted results from all 23 cases can be found in **Appendix C**. Here, four examples are presented to demonstrate the variability between the two test series and the different bar configurations. **Figure 6.2** shows the results of test 8110, for which the bar angles were 5.6^{o} and 0^{o} for alpha and beta, respectively. **Figure 6.3** shows the results from test case 10110 for which the bar configurations were similar, but the input wave conditions were different. **Figure 6.2** shows favorable agreement for both wave height decay and mean water level, whereas in **Figure 6.3** the maximum wave height and location of incipient breaking display the same trends as previous results, in which wave reflection in the model may be affecting the results.

To illustrate the effect of bar geometry, two more test cases are presented in **Figure 6.4** and **Figure 6.5** in which alpha is 15^{o} and beta is 40^{o} (i.e. a 'sharp' bar). In **Figure 6.5**, the COULWAVE results for wave height display notable disparity from the data on the seaward side of the bar, but improve significantly inside the surf zone. In regard to set-up, the modeled results appear quite favorable. In **Figure 6.6** the modeled wave height performs reasonably well as the wave approaches incipient breaking, but does not replicate the rapid decay in height during initial breaking. Once again, however, the agreement of the modeled set-up with the data is somewhat reasonable.

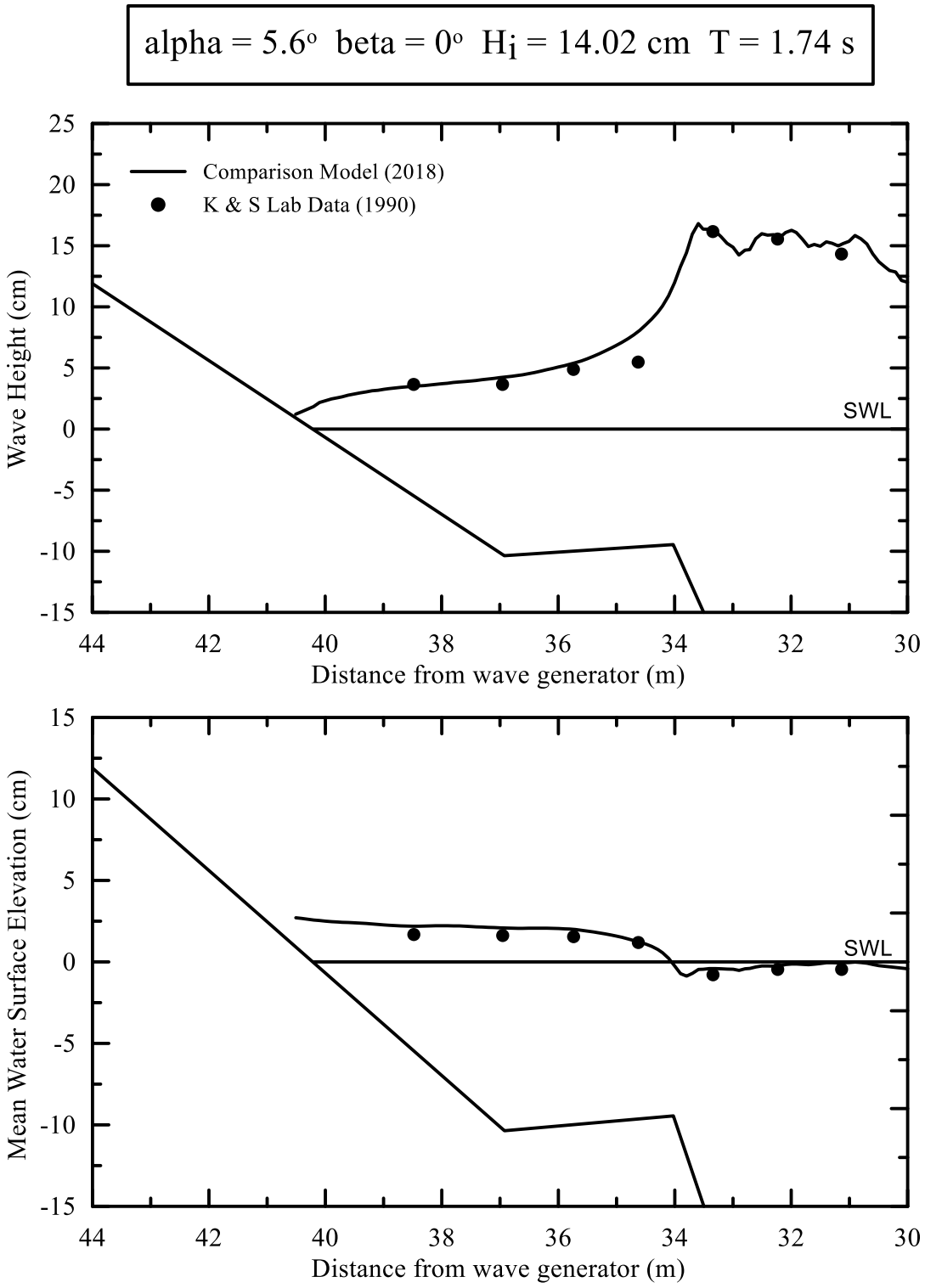

Figure 6.2: Comparison of measured lab data from Kraus and Smith (1990) test 8110 to modeled COULWAVE results.

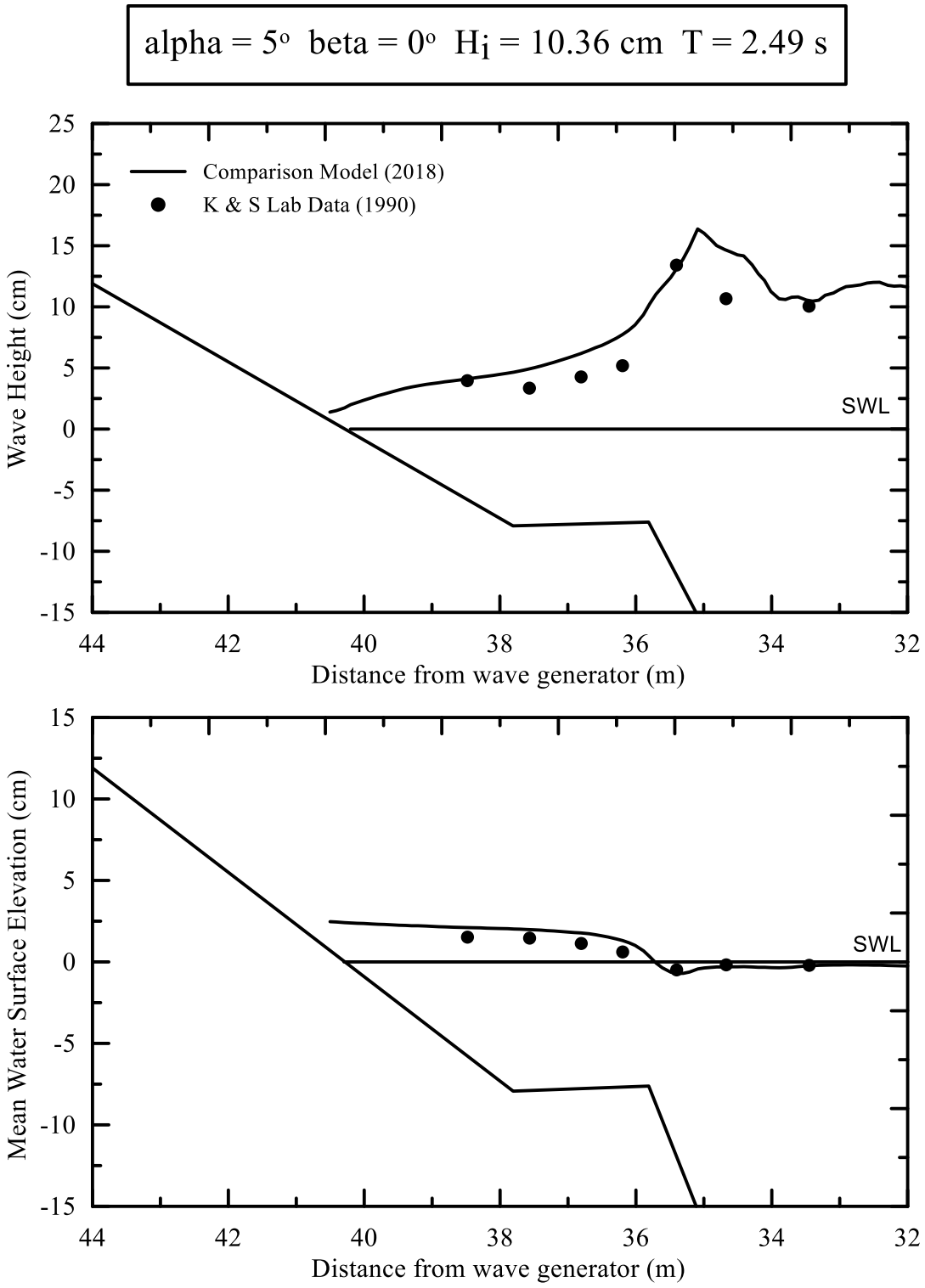

Figure 6.3: Comparison of measured lab data from Kraus and Smith (1990) test 10110 to modeled COULWAVE results.

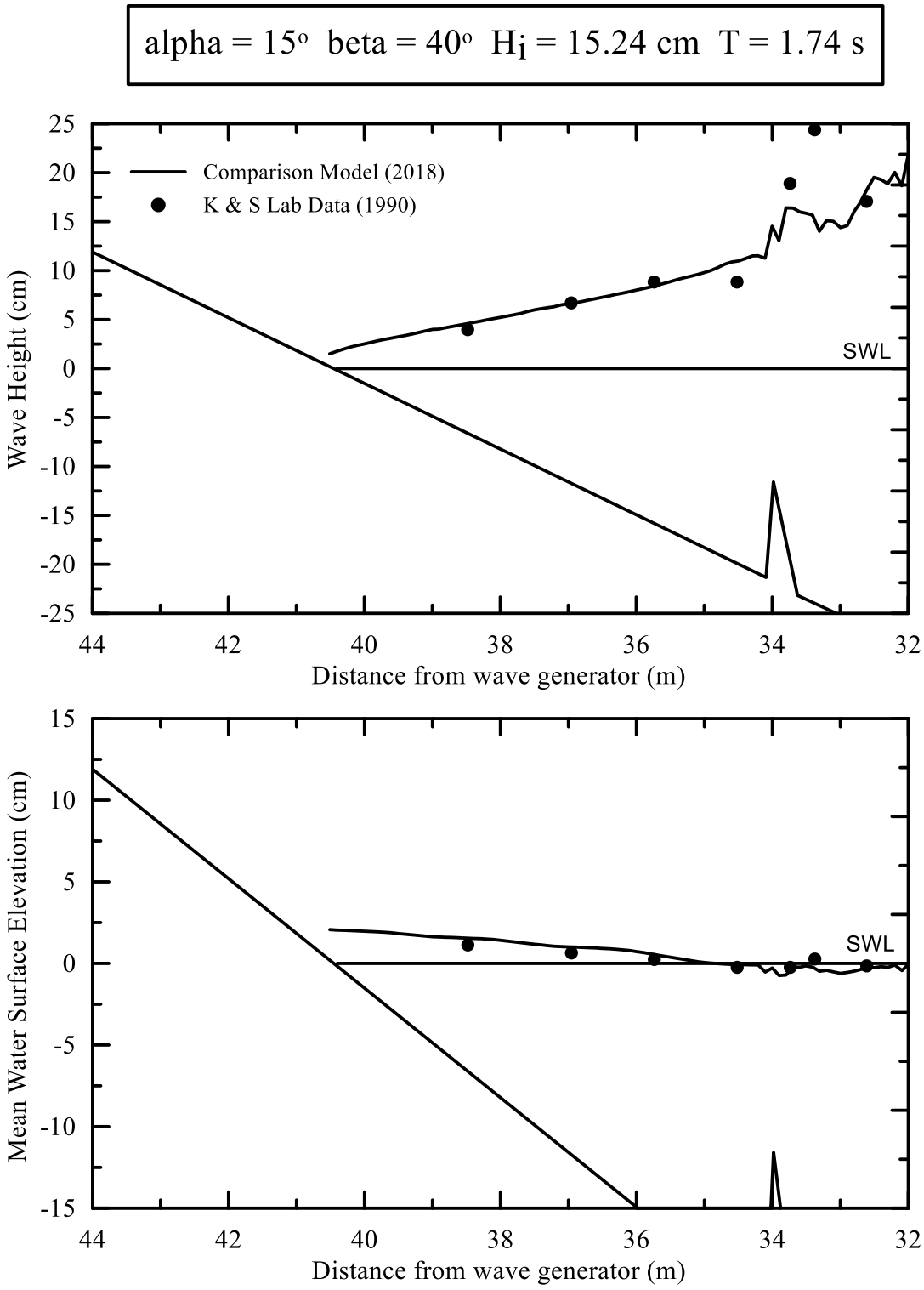

Figure 6.4: Comparison of measured lab data from Kraus and Smith (1990) test 8430 to modeled COULWAVE results.

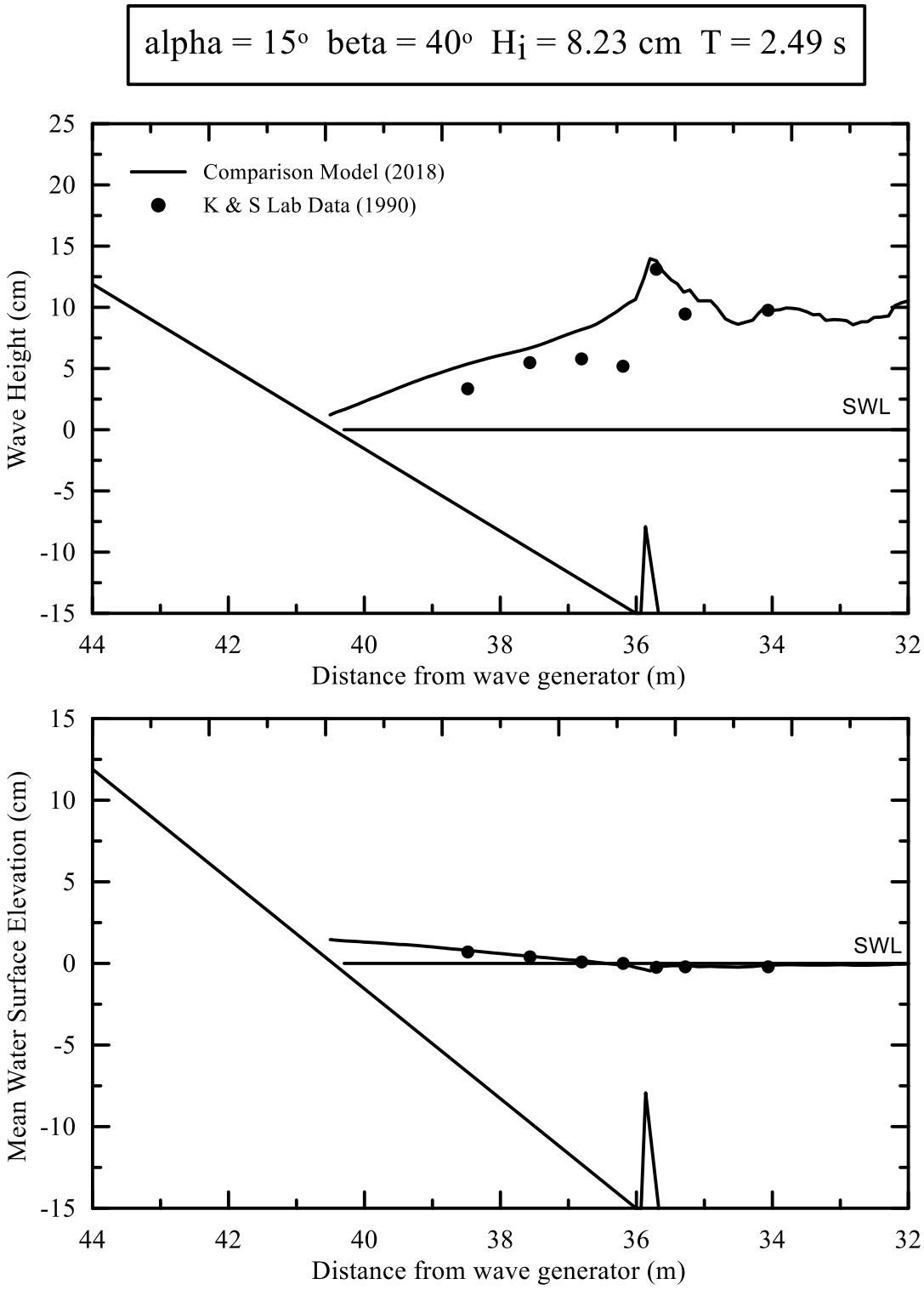

Figure 6.5: Comparison of measured lab data from Kraus and Smith (1990) test 10430 to modeled COULWAVE results.

The computed error statistics for the two groups of tests are presented in **Table 6.3** and **Table 6.4**. These results give a mixed indication of the abilities of COULWAVE, with a wide variability within each group. For the 8000 series, the average modified index of agreement is better than that from the nine planar beach test cases in Chapter 5, and surprisingly better than the planar cases taken from Smith and Kraus (1990). Yet, for the 10000 series, the average error statistics show a worse fit, with error statistics similar to those for the planar test cases.

Figure 6.6 and **Figure 6.7** present scatter plots of measured versus predicted wave heights for the 8000 and 10000 series cases, respectively. For the 8000 series it is seen that COULWAVE significantly overpredicted wave heights at incipient breaking for five test cases (8330, 8440, 8420, 8430, and 8440) as was seen for the planar case 8000 in Chapter 5. However, wave height in the inner surf zone is predicted reasonably well. **Figure 6.7** shows a different trend where, except for test 10230, incipient breaking is predicted well by COULWAVE, whereas the rate of decay in the surf zone is underpredicted.

Table 6.3: Comparative statistical parameters for predicted (COULWAVE) versus measured (wave tank) wave heights for 8000 series artificial bar cases.

Test	N	BI (cm)	RMSE (cm)	SI	MIA	Comments
8110	5	0.71	1.17	0.17	0.89	Wave height and mean surface elevation agree well.
8210	6	0.48	2.05	0.19	0.83	Setup overshoots data, wave heights modeled well.
8220	6	-0.05	0.84	0.08	0.98	Wave height immediately post breaking modeled well.
8240	6	0.07	0.43	0.04	0.99	Wave height immediately post breaking modeled well.
8310	6	-0.11	1.16	0.11	0.95	Wave decay trend follow data with some variability.
8320	6	-0.29	1.23	0.12	0.80	Incipient breaking height and location not modeled well.
8330	6	0.91	1.45	0.15	0.85	Maximum wave height underpredicted in model.
8340	6	1.18	1.43	0.15	0.80	Maximum wave height underpredicted in model.
8420	6	0.48	1.88	0.20	0.82	Maximum wave height underpredicted in model.
8430	6	-0.03	1.38	0.15	0.84	Maximum wave height underpredicted in model.
8440	6	0.48	1.37	0.14	0.86	Maximum wave height underpredicted in model.
Average		**0.35**	**1.31**	**0.13**	**0.87**	

Table 6.4: Comparative statistical parameters for predicted (COULWAVE) versus measured (wave tank) wave heights for 10000 series artificial bar cases.

Test	N	BI (cm)	RMSE (cm)	SI	MIA	Comments
10110	5	1.18	1.60	0.24	0.76	Poor modeled location of incipient breaking.
10120	5	1.73	1.79	0.28	0.68	Wave height consistently modeled over measured data.
10130	5	2.08	2.32	0.36	0.62	Wave height consistently modeled over measured data.
10210	5	1.77	2.05	0.28	0.62	Wave height consistently modeled over measured data.
10220	5	2.71	2.92	0.40	0.52	Wave height consistently modeled over measured data.
10230	6	0.23	0.91	0.11	0.63	Wave height consistently modeled over measured data.
10310	5	1.12	1.39	0.19	0.74	Incipient breaking modeled well along with wave decay.
10320	5	2.06	2.16	0.28	0.60	Incipient breaking captured, surf zone heights overshoot.
10330	5	2.00	2.35	0.31	0.59	Inconsistent agreement in surfzone, max height captured.
10410	5	0.14	2.74	0.41	0.63	Inconsistent agreement in surfzone, max height captured.
10420	5	1.61	2.00	0.27	0.65	Inconsistent agreement in surfzone, max height captured.
10430	5	2.23	2.66	0.35	0.85	Inconsistent agreement in surfzone, max height captured.
Average		**1.57**	**2.07**	**0.29**	**0.63**	

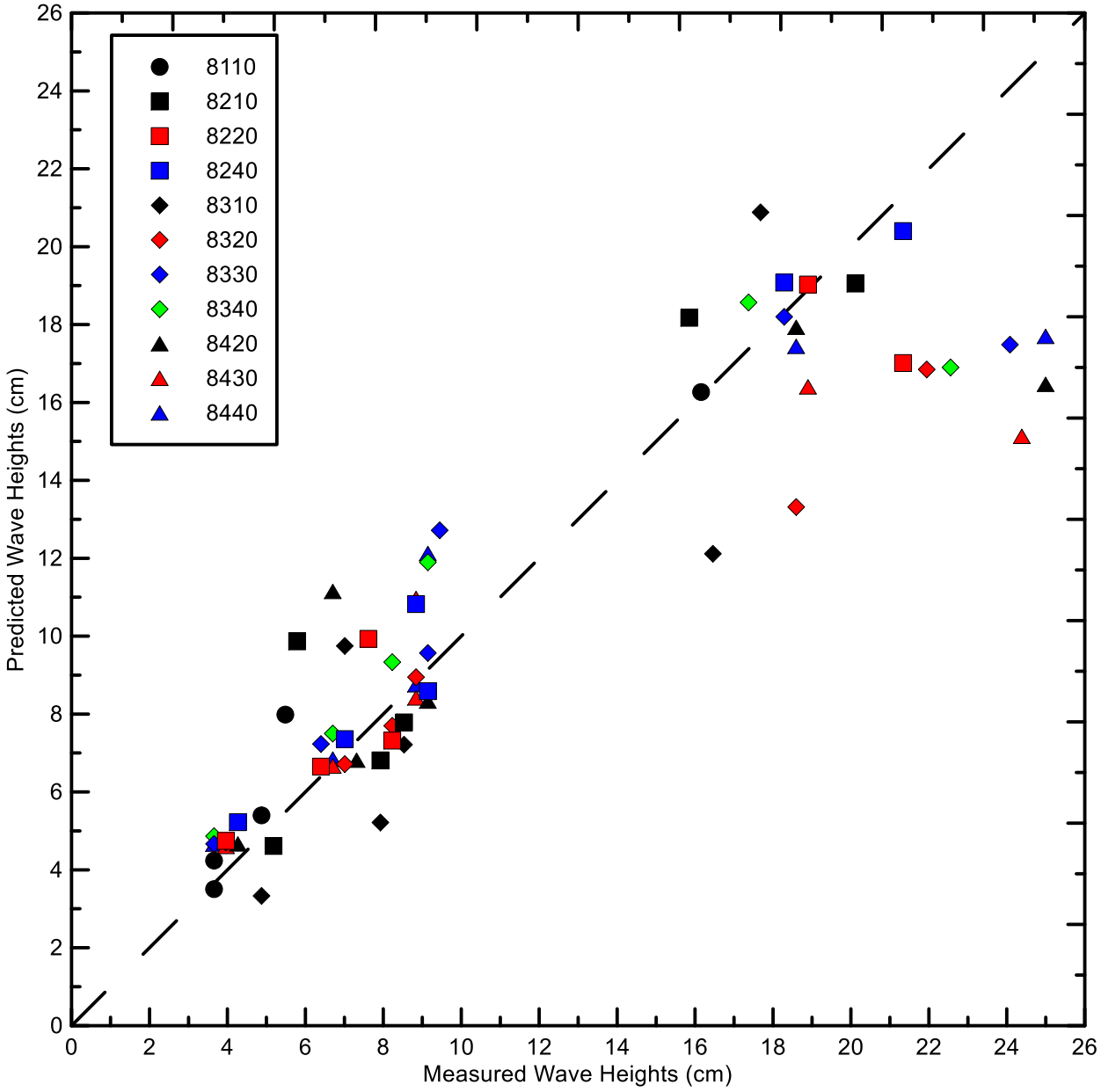

Figure 6.6: Measured v. predicted wave heights plotted to show effectiveness of the current COULWAVE model to recreate laboratory data of the 8000 series artificial-bar cases.

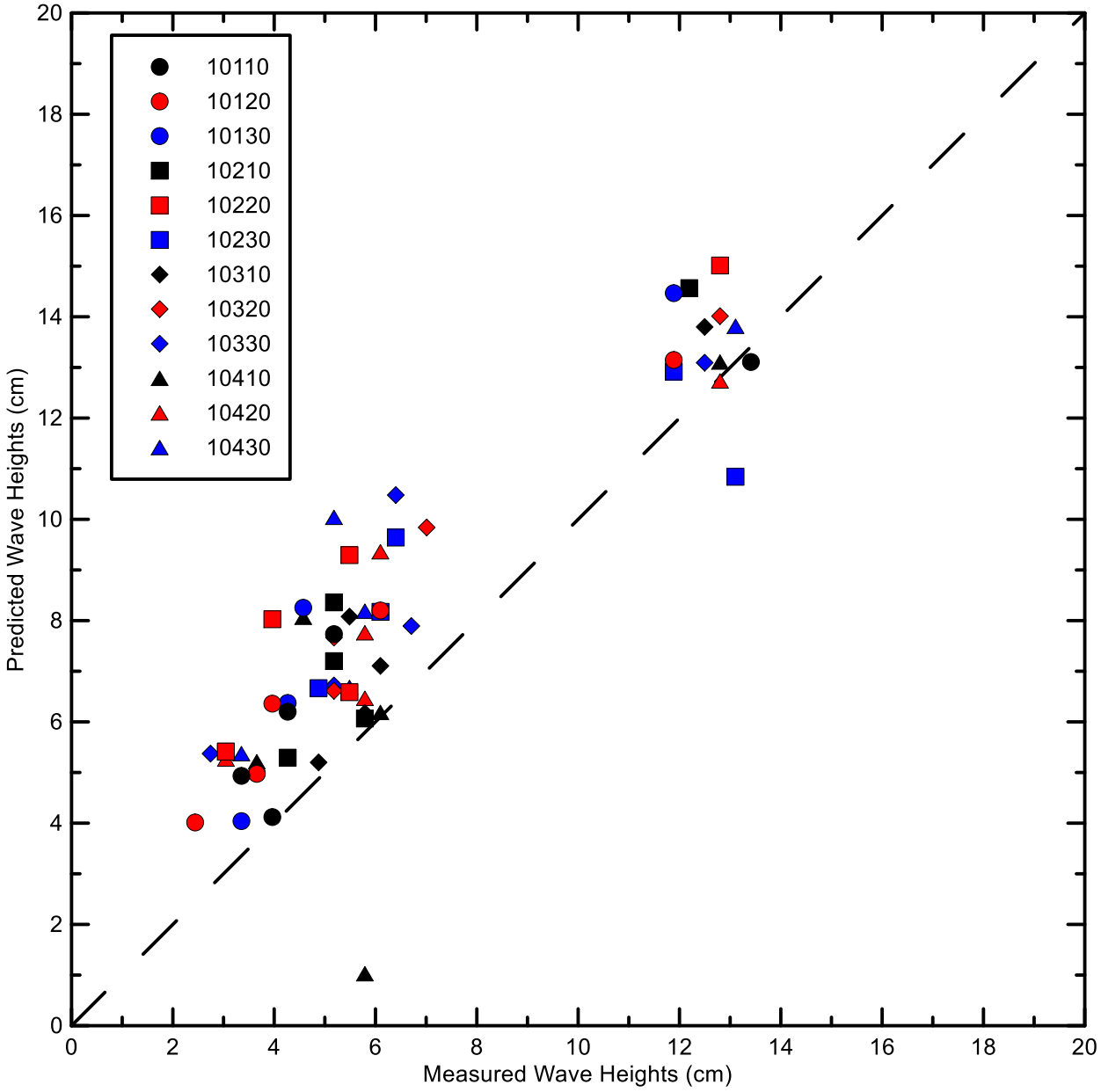

Figure 6.7: Measured v. predicted wave heights plotted to show effectiveness of the current COULWAVE model to recreate laboratory data of the 10000 series artificial-bar cases.

6.3 Summary and Conclusions for Artificial Bars

The results from the 23 test cases do not instill confidence in the ability of COULWAVE to consistently replicate wave-breaking over artificial bars. Some individual cases show excellent agreement, whereas others display significant disparity. With a limited range of input conditions these tests did not clarify what conditions created the varied results in Chapter 5.

7 Varying Spatial and Temporal Resolutions in COULWAVE

To this point the operation of COULWAVE in comparison to the variety of wave channel data has been conducted utilizing a 'minimal-computation' approach. The goal was to determine how effective COULWAVE could be operated for replicating breaking wave conditions, without intense computing resources. With the somewhat inconsistent performance observed in the results thus far, checking to see if results can be improved by increasing the temporal and/or spatial resolution of the model is worthwhile.

7.1 Methodology

Within the COULWAVE model there are two methods to manipulate the spatial and temporal resolution. The number of grid points per wavelength is a user-defined setting that will increase or decrease the spatial resolution. All previous tests have used a value of 150, which was chosen based on the default setting. Additionally, the user can prescribe a Courant number which establishes the necessary time step of the model. The Courant number is given by:

$$C = \frac{u\Delta t}{\Delta x}$$

where u represents the characteristic water velocity, Δt is the time step, and Δx is the grid spacing within the model. Generally, changes to the Courant number are used to ensure the COULWAVE model is stable and converges to a solution as described in Lynett et al. (2008). Again, adopting the default settings, all previous tests were conducted with a Courant number of 0.35.

To investigate whether changes to the spatial and temporal resolution would improve modeled results of measured data, three previous cases were selected: Horikawa and Kuo (1966) #7, and cases 8310 and 10220 from Smith and Kraus (1990). These cases were chosen for two reasons. Firstly, they each had the poorest agreement among their groups. Secondly, the three cases yielded opposing results relative to the measured data. That is, in the Horikawa and Kuo case and test 8310, the COULWAVE model underpredicted the wave heights in the surf zone, whereas the modeled results in test 10220 overpredicted the wave heights.

The preferred means of testing at higher spatial and temporal resolution is to increase the spatial resolution (decreasing Δx) while maintaining the Courant number, which would require that the temporal resolution become higher (smaller Δt). However, the COULWAVE model did not consistently maintain numerical stability for significant increases in the number of points per wavelength on all three tests. In fact, the greatest increase in spatial resolution that would successfully run on all three examples was only 160 points per wavelength. To help understand the trends and impacts of the spatial resolution, tests with lower values were also run. Figure **7.1** shows the four results for the Horikawa and Kuo (1966) test case. The test with the lowest resolution does not capture major features of the breaking wave. Specifically, the shoaling of the wave and the maximum wave height attained are not well-represented. The test with a spatial resolution of 75 points per wavelength does considerably better in representing the major features of a wave and has the best statistical comparison to the measured wave. The plot indicates that there is not a significant difference between the default setting (150 points per wavelength) and the highest spatial resolution run (160 points per wavelength).

Table 7.1: List of variable resolution runs for three test cases with fixed Courant number (0.35).

Trial	Points per Wavelength	App. Run Time	N	BI (cm)	RMSE (cm)	SI	MIA
Horikawa and Kuo (1966) #7	25	40 sec	8	-0.86	0.87	0.15	0.64
Horikawa and Kuo (1966) #7	75	4 min	8	0.09	0.20	0.03	0.94
Horikawa and Kuo (1966) #7	150	16 min	8	-1.59	2.10	0.34	0.59
Horikawa and Kuo (1966) #7	160	20 min	8	-1.58	2.09	0.34	0.59
8310	25	30 sec	5	-0.19	0.98	0.10	0.96
8310	75	3 min	5	-0.02	0.78	0.08	0.97
8310	150	6 min	5	-0.11	1.16	0.11	0.95
8310	160	8 min	5	-0.10	1.20	0.12	0.70
10220	25	10 sec	5	3.17	3.95	0.52	0.39
10220	75	70 sec	5	3.00	3.29	0.44	0.49
10220	150	4 min	5	2.71	2.92	0.40	0.52
10220	160	5 min	5	0.53	1.29	0.17	0.52

7.2 Discussion for Higher Spatial and Temporal Resolution Tests

Figure 7.1 shows the four results for the Horikawa and Kuo (1966) test case. The test with the lowest resolution does not capture major features of the breaking wave. Specifically, the shoaling of the wave and the maximum wave height attained are not well-represented. The test with a spatial resolution of 75 points per wavelength does considerably better in representing the major features of a wave and has the best statistical comparison to the measured wave. The plot indicates that there is not a significant difference between the default setting (150 points per wavelength) and the highest spatial resolution run (160 points per wavelength).

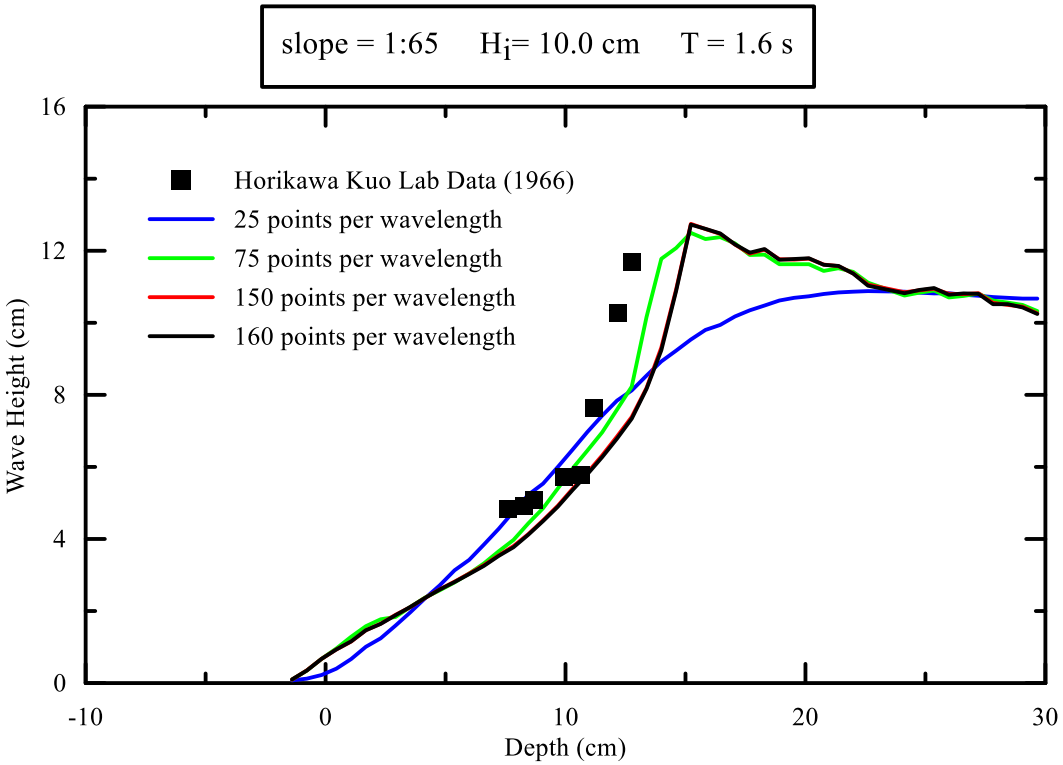

Figure 7.1: Comparison of the measured lab data from Horikawa and Kuo (1966) to the COULWAVE runs of varying spatial and temporal resolution.

The results of varying the model resolution for the Smith and Kraus (1990) test 8310 measured are shown in **Figure 7.2**. The lowest resolution results again failed to capture the highest wave height but did follow the general trend of the wave decay captured by the models with higher resolution. The model run with 75 points per wavelength appears to replicate the measured data the best and in fact has the highest *mia* of all four tests. Based on the statistical analysis the highest resolution run appears to correlate the worst. However, unlike the four Horikawa and Kuo tests, these all have similar statistical agreement.

Figure 7.3 shows the results of varying the spatial and temporal resolution for the Smith and Kraus (1990) test 10220. Again, the lowest resolution test fails to capture the shoaling behavior and major features, but after an increase to 75 points per wavelength the agreement with the measured data improves. The two highest resolution models have very similar graphical and statistical results.

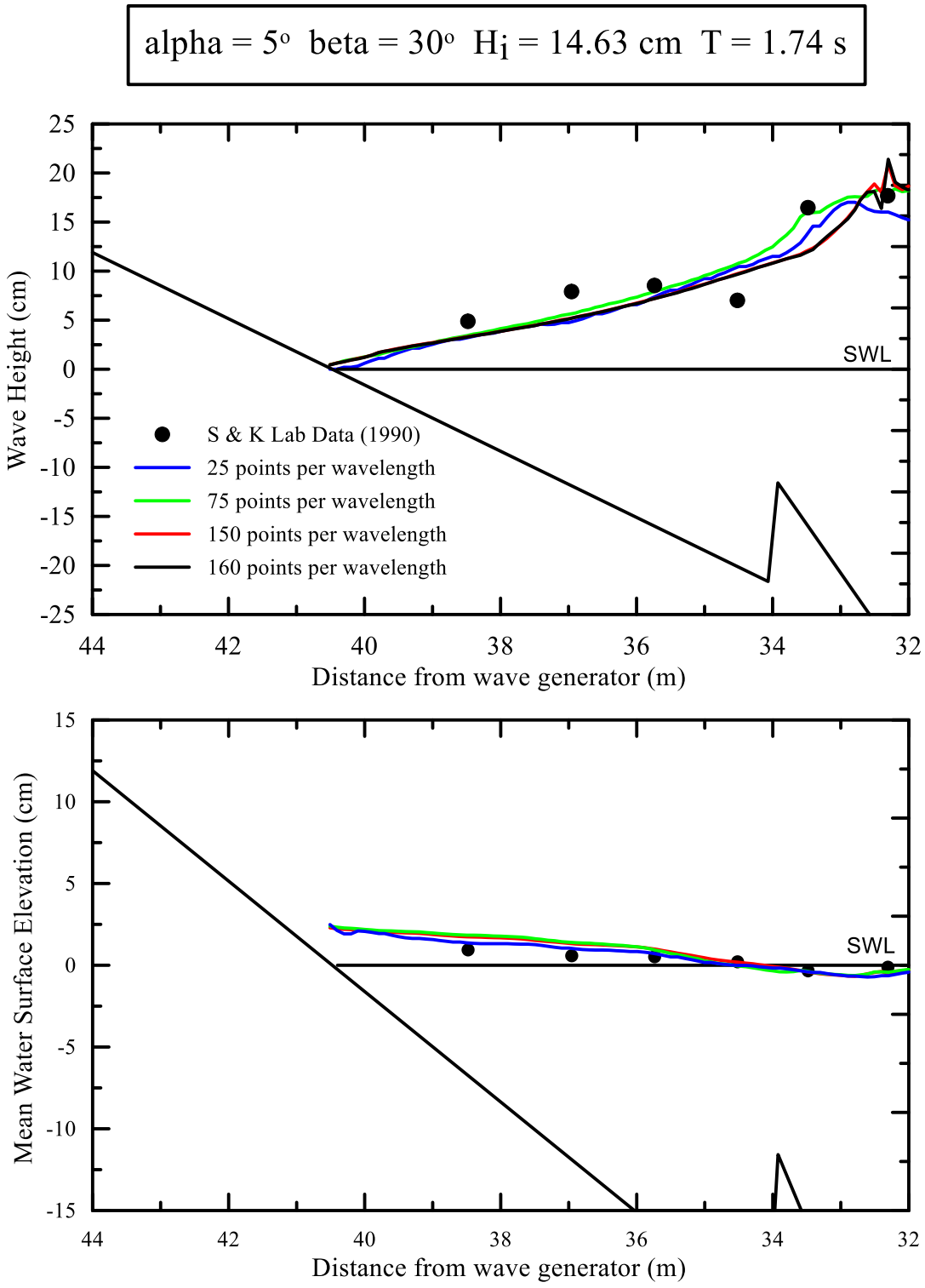

Figure 7.2: Comparison of the measured lab data from Smith and Kraus (1990), test case 8310, to the COULWAVE runs of varying spatial and temporal resolution.

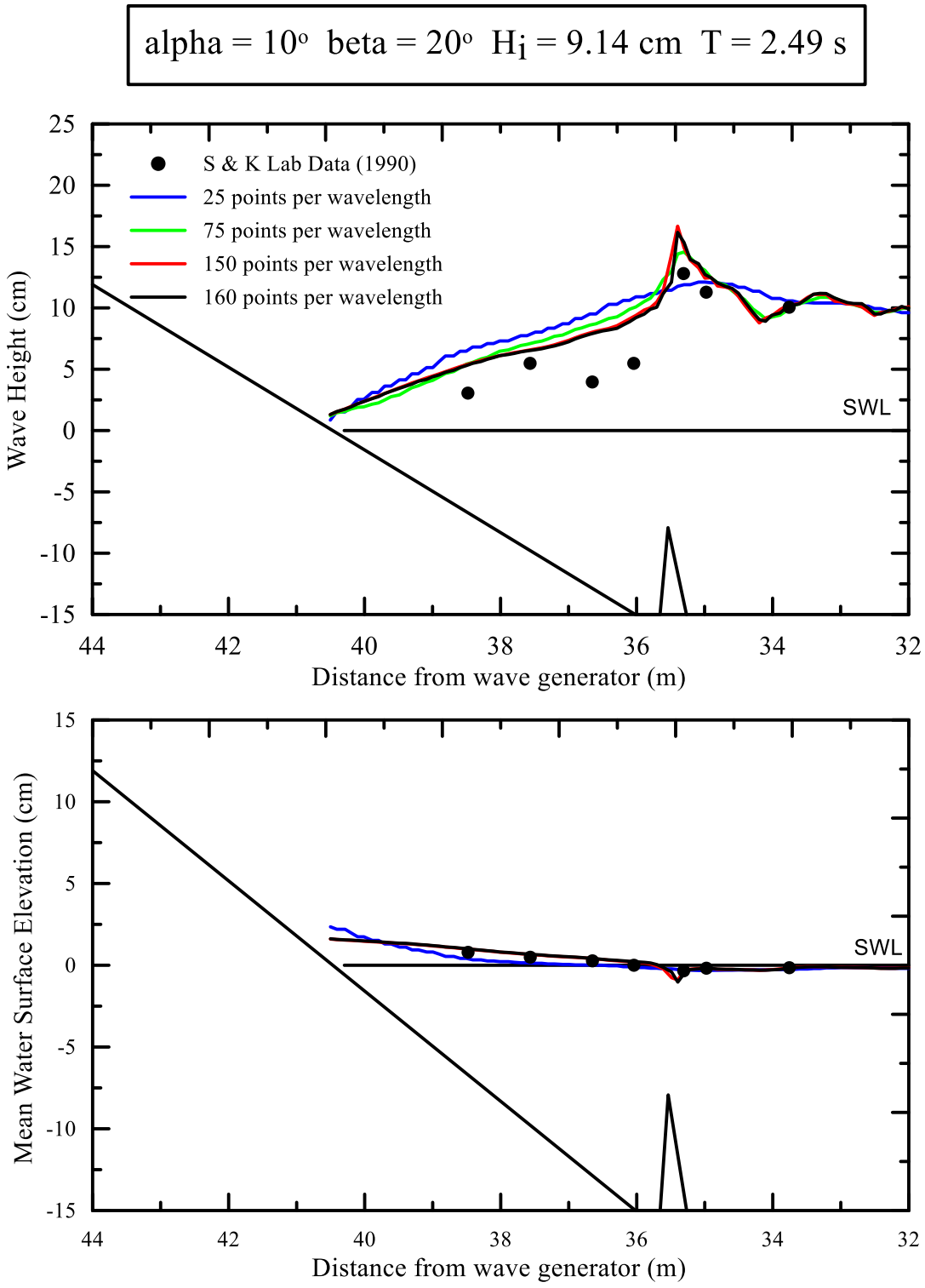

Figure 7.3: Comparison of the measured lab data from Smith and Kraus (1990), test case 10220, to the COULWAVE runs of varying spatial and temporal resolution.

7.3 Tests with Reduced Courant Number

Another series of tests were conducted in which the number of points per wavelength was fixed at 150, and the Courant number was reduced. This permits the evaluation of impacts associated with reducing the time step. **Table 7.2** lists the three model run conditions, the approximate runtime, and the resultant statistical parameters for the three chosen examples.

Table 7.2: Tests of lower Courant number with static points per wavelength with comparative statistical parameters for predicted versus measured wave heights.

Trial	Courant Number	App. Run Time (min)	N	BI (cm)	RMSE (cm)	SI	MIA
Horikawa and Kuo (1966) #7	0.35	25	8	-1.59	2.10	0.34	0.59
Horikawa and Kuo (1966) #7	0.05	138	8	-1.45	2.00	0.32	0.61
Horikawa and Kuo (1966) #7	0.01	690	8	-0.99	1.62	0.25	0.69
8310	0.35	20	5	-1.43	2.75	0.33	0.58
8310	0.05	60	5	-1.31	2.54	0.31	0.61
8310	0.01	330	5	0.16	2.15	0.14	0.77
10220	0.35	7	5	2.71	2.92	0.40	0.52
10220	0.05	30	5	2.97	3.22	0.43	0.49
10220	0.01	150	5	3.77	4.08	0.52	0.41

Figure 7.4 shows the Horikawa and Kuo (1966) data and the original model results to those COULWAVE results obtained by reducing the Courant number. The general trend shows that as the Courant number decreases, the modeled break point moves slightly towards the shoreline. For the Horikawa and Kuo (1966) case notable improvement in the error statistics becomes significant only when the Courant number is reduced to 0.01, but at great computational expense.

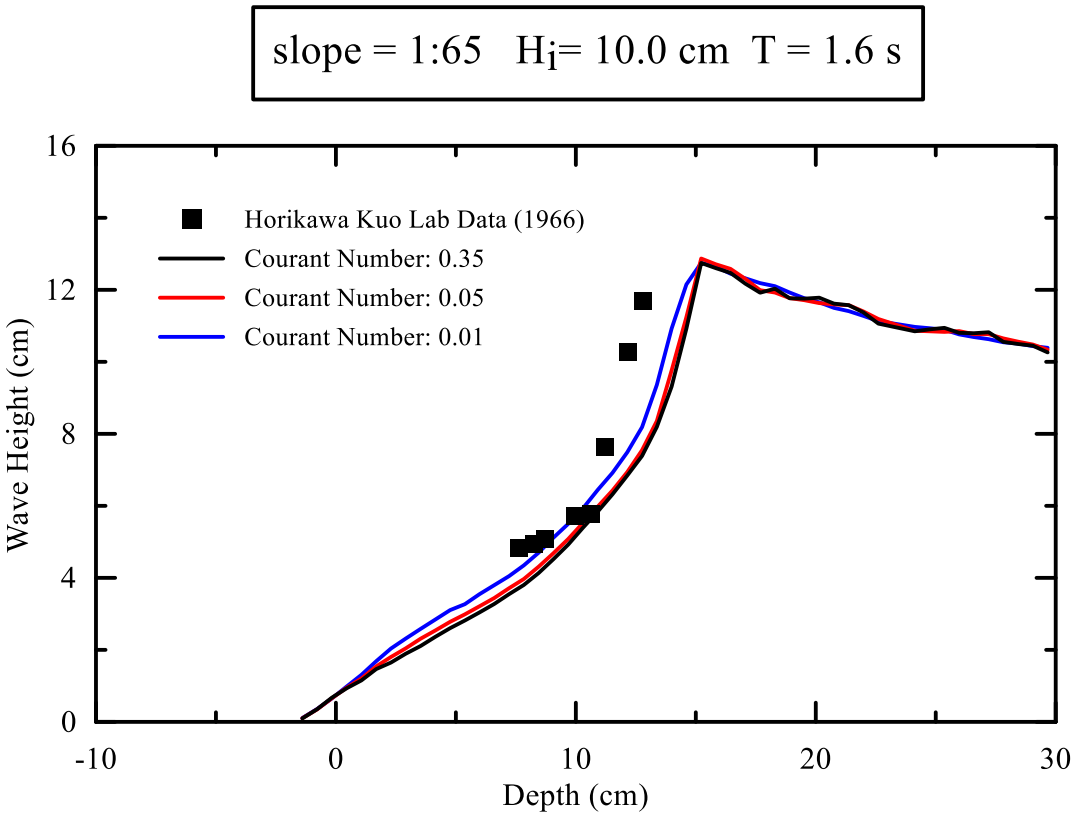

Figure 7.4: Comparison of model results when Courant number is reduced for Horikawa and Kuo (1966) laboratory data.

Figure 7.5 shows the model results for test case 8310 (artificial bar). The reduction in Courant number again had the general effect of moving the break point shoreward and maintaining a slightly higher height as the wave decays into the shoreline, but only for $C = 0.01$. For this case, evidence of incipient breaking was improved, but subsequent wave decay was not. This single feature appears to be mostly responsible for the improvement of error statistics present in **Table 7.2**. Overall the summary statistics indicate a significant improvement utilizing the lower Courant number.

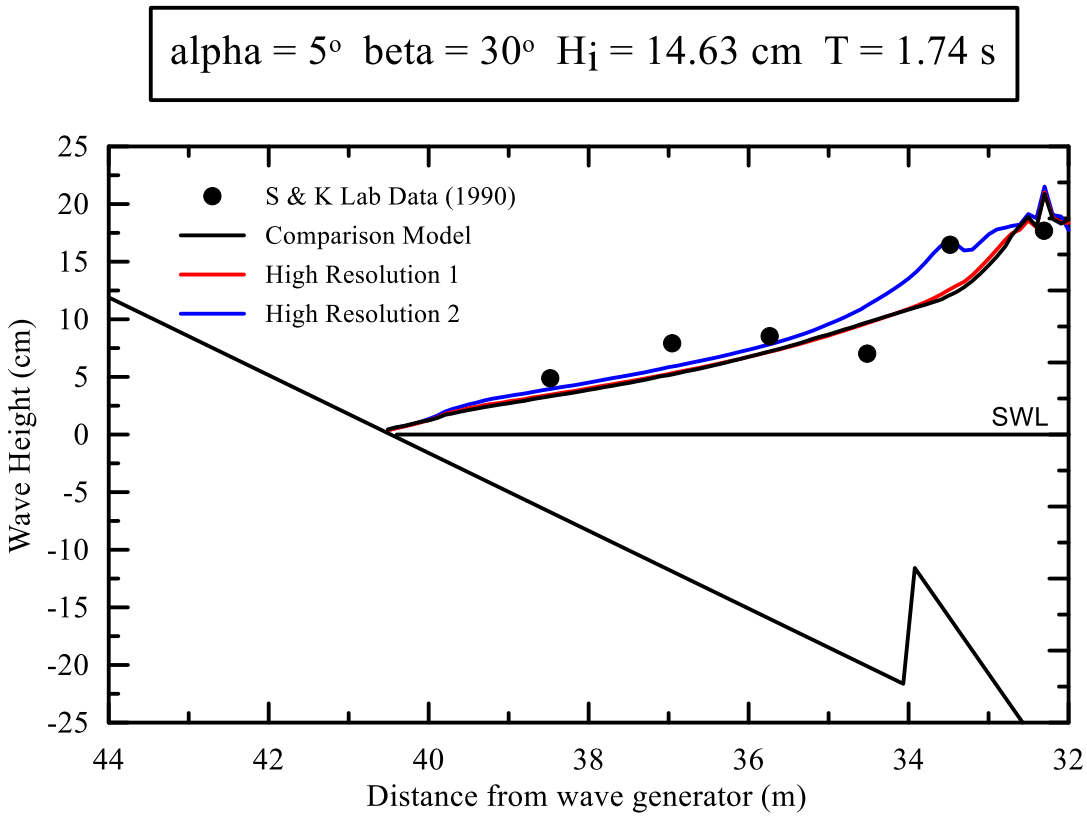

Figure 7.5: Comparison of model results when Courant number is reduced for Smith and Kraus (1990), test case 8310.

Figure 7.6 presents the results for the Courant number tests for case 10220. The original modeled results differed from Horikawa and Kuo (1966) and Smith and Kraus (1990) cases as the model had overpredicted the measured wave heights at almost every location. The result shows slightly delayed onset of breaking and higher wave heights in the surf zone. In this case the model became less accurate, as demonstrated by the error statistics presented in **Table 7.2**.

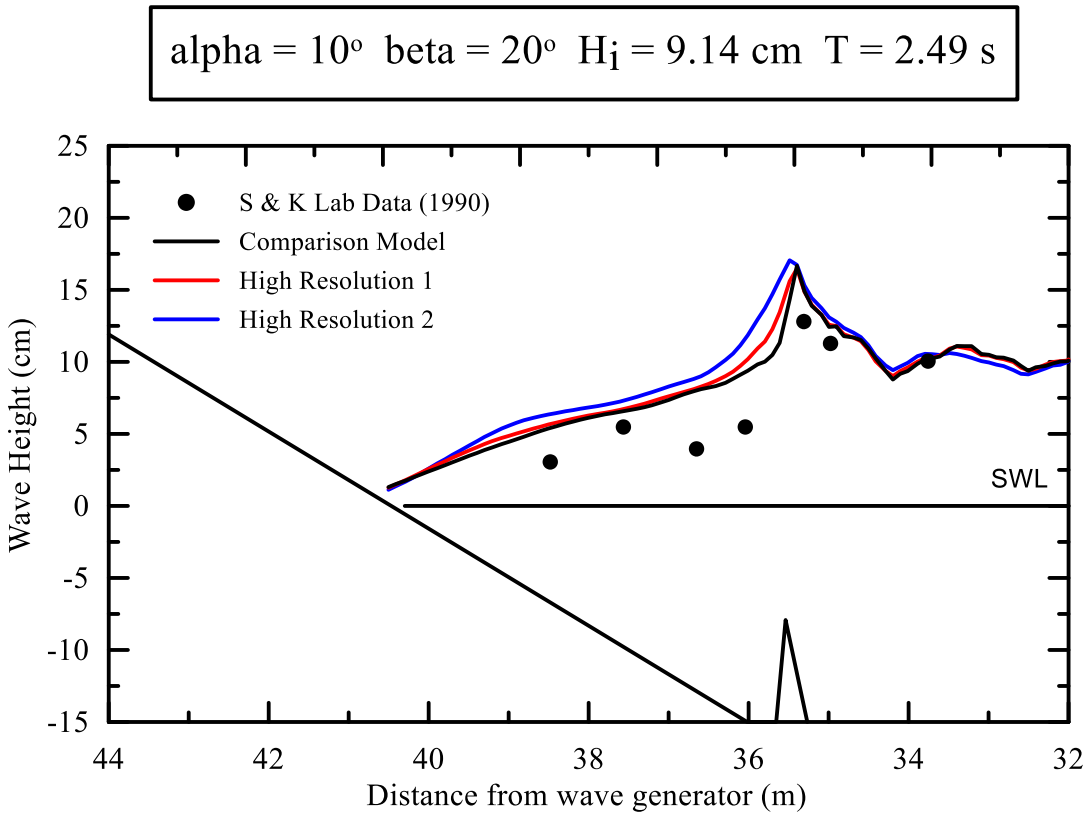

Figure 7.6: Comparison of model results when Courant number is reduced for Smith and Kraus (1990), test case 10220.

7.4 Conclusions for Varying-Resolution Tests

Results in which the spatial resolution was modified imply that there is a 'best' threshold for achieving reasonable results with the COULWAVE model. Although computing time can be drastically reduced with tests set with 25 points per wavelength, this configuration does not provide enough information for driving a cross-shore sediment model. It appears that to obtain the most accurate results with minimal computation expense, the spatial resolution should be nominally 75 points per wavelength. Running the model at higher spatial resolution (e.g., the default of 150 points per wavelength) does not appear to provide significantly better results, particularly given the increased computation time.

The second investigation demonstrated that increases in temporal resolution, by reducing the Courant number, result in better prediction of incipient breaking, but highlight the apparent need to increase the rate of wave decay in the breaking algorithm. However, this approach does not guarantee that the model will be more accurate, as there are test conditions where the model already overestimated the wave height. A review of all test cases shows that COULWAVE predominantly overestimated the wave height in the region of wave decay; therefore, the increased temporal resolution would likely create less accurate results for many cases.

The investigations into the temporal and spatial resolution provide another indication that the COULWAVE model may be limited in its ability to replicate wave breaking for conditions that vary significantly from those to which it was originally calibrated.

8 Testing COULWAVE on Mobile Beds with Realistic Bars

The investigation of COULWAVE's abilities thus far has been limited to small-scale laboratory experiments with fixed beds. These fixed-bed tests are useful in demonstrating model performance over a wide range of test conditions; however, this investigation is motivated by the need for an improved cross-shore sediment transport model. Therefore, it is most relevant to test COULWAVE against data gathered at large scales, on mobile beds, and with natural profile features. Two data sets will be utilized for this comparison. Firstly, beach profiles generated in a Large Wave Tank by Saville (1957) and described by Kraus and Larson (1988), will show how COULWAVE functions on more realistic beach profiles. However, waves were not measured during the Saville tests. Secondly, results from SUPERTANK described by Kraus et al. (1993) will be utilized, which do include wave data.

8.1 Exercising COULWAVE on Profiles with Multiple Bars

An extensive record of moveable bed wave testing was conducted by Saville (1957) and later published by Kraus and Larson (1988). The experiments were completed at the Beach Erosion Board's Large Wave Tank which was 635 ft long, 15 ft wide, and 20 ft deep. The data included beach profile surveys and incident wave characteristics measured during two sets of experiments performed in 1956-1957 and 1962. The tests were done at a large scale, consistent with wave heights and periods representative of field conditions. The tests were primarily focused on quantifying the change in the bed configuration, and consequently there is limited information on wave transformation and breaking. Nonetheless, these realistic bed conditions provide another

means of testing COULWAVE to determine, at least qualitatively, how well the model performs on realistic barred profiles.

Each of the test cases was run for multiple hours, some as few as 30 and others as much as 100 hours, during which the bed conditions could change naturally under the wave forcing. The beach profile from test case 400 (after 40 hours of wave excitation) is simply used to examine how well COULWAVE functions qualitatively. **Figure 8.1** provides the input conditions for the test and presents the results. The model setup followed the same default settings as previous tests with 75 points per wavelength and a Courant number of 0.35. The run-time was approximately 7 minutes. Overall, the findings are encouraging. The wave height follows what would be expected as the wave breaks over the first bar, reforms briefly in the adjacent trough, and then breaks again as the water depth decreases towards the second bar.

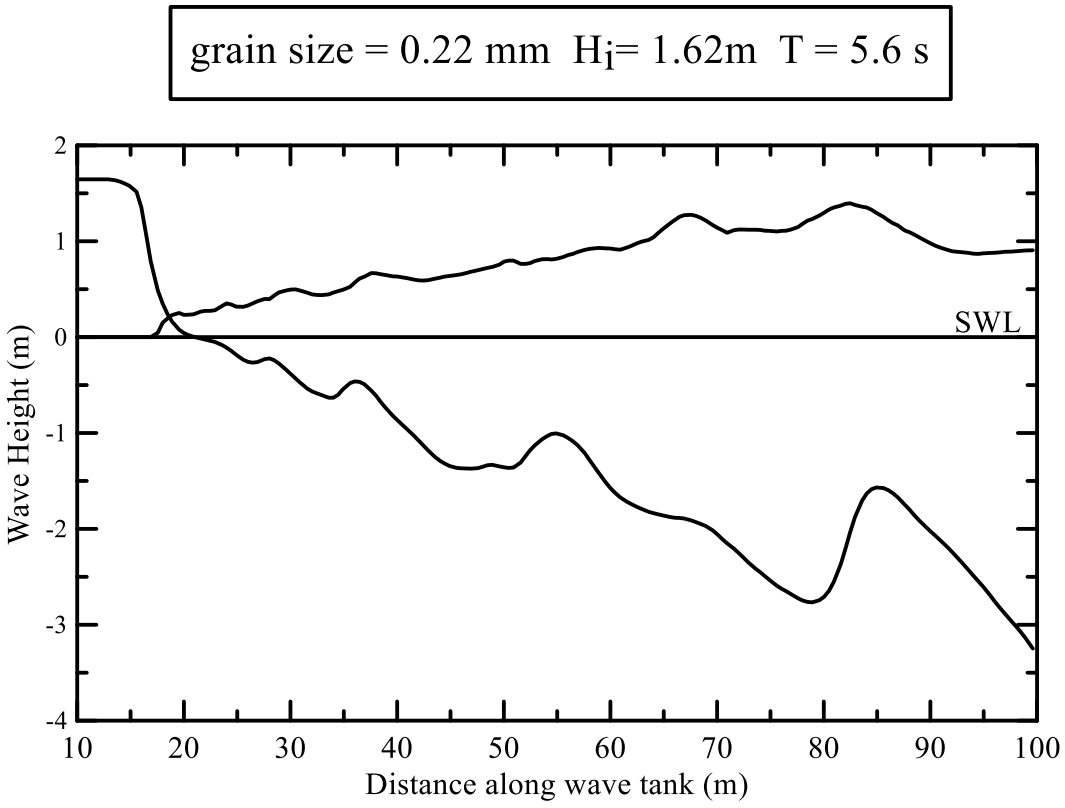

Figure 8.1: Modeled COULWAVE wave height over the barred profile of test case 400 from Kraus and Smith (1988).

8.2 Supertank Test ST_G0

The previous results demonstrate that the COULWAVE model can qualitatively create wave conditions that would be expected on a multi-barred profile. To more rigorously investigate the models effectiveness on 'natural bars', data from Kraus et al. (1993) are used, which do include direct measurements of wave transformation across the profile. The Supertank data was collected at Oregon State University's Wave Research Facility. The wave channel was 342 ft long, 12 ft wide, and 18 ft deep, close to half the length of the tank used by Saville (1957). The complete Supertank project includes 20 different tests, each of which included multiple wave runs, with a total of 129 hours of wave action. Data collection along the tank included wave and current measurements and beach profile surveys.

To be as consistent with the other COULWAVE tests conducted thus far, the test designated 'ST_G0: Erosion toward equilibrium, monochromatic waves' is utilized. The test includes wave runs of different durations, all with $T = 3.0\,s$ and $H_i = 0.8\,m$. Time series of water surface elevation were measured at 26 stations along the channel with 16 resistance wave gauges positioned in the mid surf zone and 10 capacitance wave gauges within the surf zone, from which the wave height and mean surface elevation were determined. The time series results are provided in Kraus et al. (1993). COULWAVE is then tested using the same methodology as the previous fixed-bed tests for four of the ST_G0 runs. **Figure 8.2** presents the comparison of the wave height and mean water surface for wave case 0415. The agreement of the modeled wave height with measurements is generally good with the approximate incipient break point outside of the bar captured by COULWAVE. However, the model appears to remove too much energy during the initial phase of breaking.

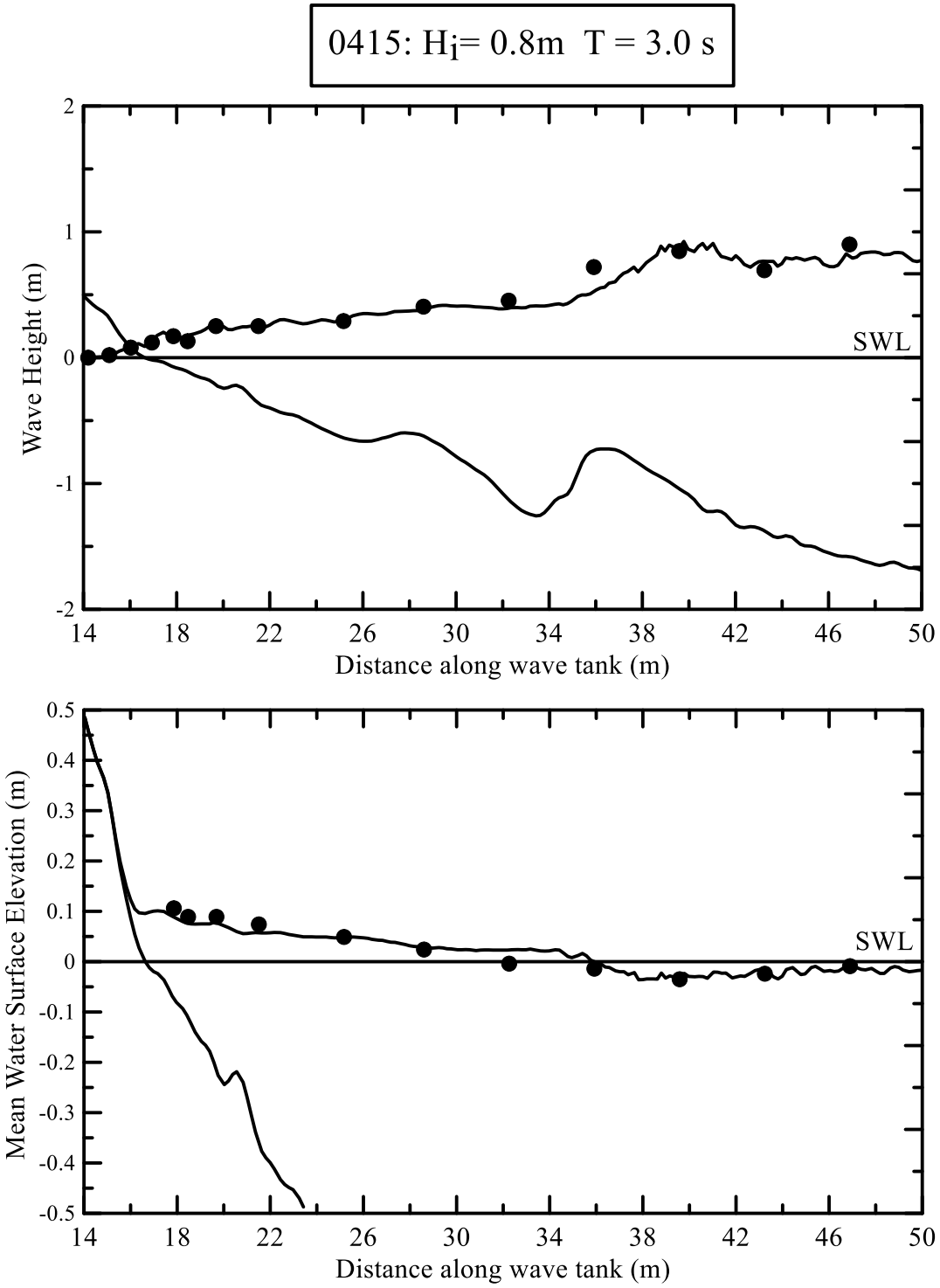

Figure 8.2: Comparison of measured lab data from Supertank test ST_G0, run 0415 to modeled COULWAVE results.

Table 8.1 summarizes the computed error statistics for the four runs and **Figure 8.3** presents a scatter plot of the measured and predicted wave heights. The table indicates good agreement by the COULWAVE model against the measured results. However, the plot shows a tendency of the model to underpredict wave heights in the outer surf zone. Additionally, the consistency of the four test cases shows that COUWLAVE can accurately replicate similar conditions with slightly varying nearshore bed geometry, which are depicted in detail in Appendix B of Kraus et al. (1993). **Figure 8.3** demonstrates the deficiency in the modeled results as the wave heights directly shoreward of the break point are underpredicted.

Table 8.1: Comparative statistical parameter for predicted (COULWAVE) versus measured (wave tank) wave heights.

Test	N	Bias (cm)	RMS error (cm)	Scatter index	Mod. index agreement
0414	13	-0.02	0.07	0.26	0.88
0415	12	-0.01	0.06	0.20	0.90
0416	12	0.00	0.07	0.22	0.88
0417	12	0.03	0.06	0.21	0.84
Average*	-	**0.00**	**0.07**	**0.22**	**0.88**

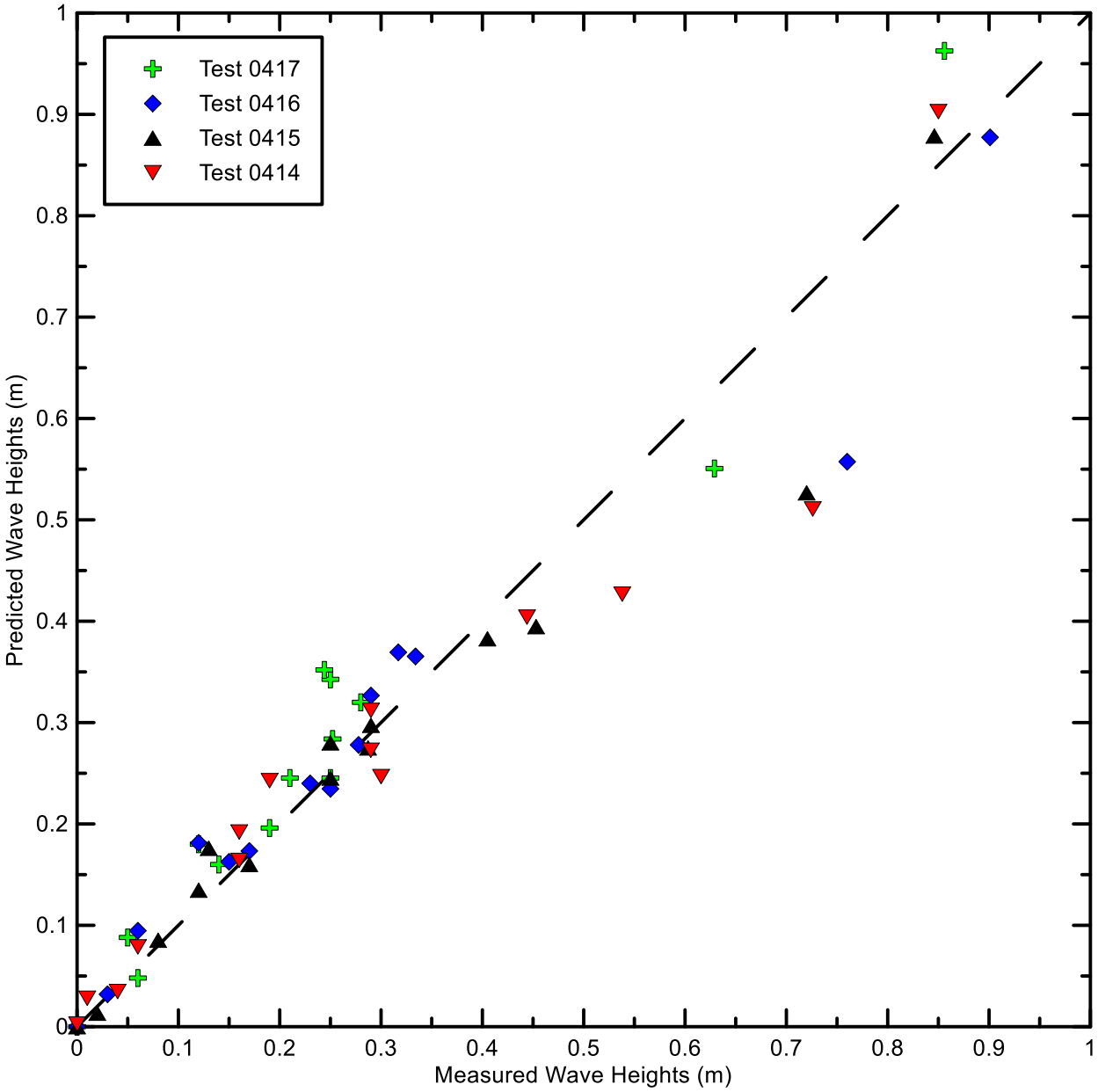

Figure 8.3: Measured v. predicted wave heights plotted to show effectiveness of the current COULWAVE model to recreate laboratory data of the Supertank mobile-bed experiment.

9 Summary and Conclusions

The COULWAVE model has been rigorously tested in comparison to laboratory measurements across a broad range of wave conditions and profile slopes and shapes, in a quest to determine if the model is suitable for use in an as-yet-to-be-developed cross-shore sediment transport model. This exercise has generated a great deal of insight into the abilities and performance of COULWAVE and provides justification for any decision made on using COULWAVE in future applications.

A review of cross-shore sediment transport concepts, along with a brief investigation of existing physics-based beach profile evolution models, demonstrated the need for a phase-resolving wave transformation algorithm that can drive a new beach profile evolution model. Reviewing three current cross-shore sediment models (Dally and Dean 1984, CSHORE, and XBEACH) it was apparent that they do not meet established criteria for a 'good' model. More specifically, it became clear that an effective cross-shore sediment transport model to be viable, the wave processes must be reliably described.

Two groups of wave models, those based on Computational Fluid Dynamics (CFD) and those based on various forms of the Boussinesq equations, demonstrate potential suitability for driving a cross-shore sediment transport model. Three CFD models (OpenFOAM, IH Foam, and STAR CCM+) and three Boussinesq type models (FUNWAVE, COULWAVE, and Celeris) were reviewed to determine which should be investigated further to determine its suitability for driving

a cross-shore sediment transport model. The COULWAVE model was determined to be the most promising.

The background and description of the COULWAVE model provides insight that is crucial to understanding the results of testing the model against various measured data sets from the literature. The wave breaking algorithm internal to COULWAVE is important as it will drive many of the wave characteristics that are critical to modeling cross-shore sediment motion.

Initial testing of COULWAVE was conducted to verify effective operation. The five calibration tests presented in Lynett et al. (2008) come from a single planar beach experiment conducted by Hansen and Svendsen (1979). The results of those tests were crucial in establishing the breaking wave algorithm. Those five tests were recreated with suggested default settings and it was shown that the operation of COULWAVE was consistent with the approach prescribed by the authors and further testing was warranted.

From a review of the literature, nine experimental wave tests were found that are suitable for recreation with the COULWAVE model. These nine tests, with varying planar sloped beaches, provide a means of testing whether the COULWAVE breaking algorithm is suitable for slopes beyond the singular case used in calibration. The results of those additional nine tests provided mixed results but demonstrated that the COULWAVE model can be effective on planar slopes beyond the slope used in calibration. Moving beyond planar slope test conditions, thirty-four tests drawn from Smith and Kraus (1990), which include artificial bars on fixed beds, were modeled.

These tests also produced results with inconsistent agreement between the predicted and measured data. Overall, the COULWAVE model was able to recreate the wave conditions but failed to capture many important details including the wave height at incipient breaking and the initial phase of wave decay towards the shoreline. Those results generated a need to determine if the scope of this work, that is operating COULWAVE with limited computational demand at lower spatial and temporal resolution, was the cause of the poor results.

Varying the spatial and temporal resolution of COULWAVE for three of the previously run test cases demonstrated a limit for effective results. Finally, the COULWAVE model was tested both qualitatively and quantitatively on mobile beds with natural bar features. These tests showed again that COULWAVE produces acceptable results, but is limited in its ability to capture all the details of a wave decay after breaking.

In total, sixty wave cases from experimental setups were built in COULWAVE with the results providing a more complete picture of the effectiveness of the model. Ultimately, these tests demonstrate that COULWAVE is not an effective candidate for use as the foundation for a future cross-shore sediment transport model. The consistency of the results does not provide confidence that the model will capture key features in a wide array of breaking wave cases. Additionally, the investigation of the models spatial and temporal resolution demonstrated that the computational commitments needed to capture wave conditions on an evolving bed would be too great for an effective engineering solution.

Although this investigation resulted in the rejection of COULWAVE for the stated purpose it has provided a great deal of insight and can be the foundation of future work that will expand the understanding of this field. Testing of FUNWAVE in a similarly robust manner as COULWAVE was would provide an effective comparison of the two models, something that does not exist in the literature to date. Deeper investigation and possible manipulation of the breaking wave approach in COULWAVE would also be a worthwhile endeavor. It may be possible to prescribe a more generic approach that ensures the model operates on a wider array of conditions.

10 References

Battjes, J.A., 1974. Surf similarity. Proc. 14th Int. Conf. Coast. Eng. ASCE 466–480. https://doi.org/10.1007/978-1-61779-361-5

Battjes, J.A., Janssen, J.P.F.M., 1978. Energy Loss and Set-Up Due to Breaking of Random Waves. Coast. Eng. 1978 569–587. https://doi.org/10.1061/9780872621909.034

Bolle, A., Mercelis, P., Roelvink, D., Haerens, P., Rtouw, K., 2011. Application and validation of XBEACH for three different field sites. Coast. Eng. Proc. 40.

Brocchini, M., 2013. A reasoned overview on Boussinesq-type models : the interplay between physics , mathematics and numerics, in: Proceedings of the Royal Society A: Mathematical, Physical and Engineering Sciences. p. 469.

Dally, W.R., 1980. A numerical model for beach profile evolution. University of Delaware.

Dally, W.R., Dean, R.G., 1984. Suspended Sediment Transport and Beach Profile Evolution. J. Waterw. Port, Coastal, Ocean Eng. 110, 15–33. https://doi.org/10.1061/(ASCE)0733-950X(1984)110:1(15)

Dally, W.R., Dean, R.G., Dalrymple, R.A., 1985. A Model for Breaker Decay on Beaches, in: Coastal Engineering 1984. American Society of Civil Engineers, New York, NY, pp. 82–98. https://doi.org/10.1061/9780872624382.007

Dalrymple, R.A., 1992. Prediction of Storm/Normal Beach Profiles. J. Waterw. Port, Coastal, Ocean Eng. 118, 193–200. https://doi.org/10.1061/(ASCE)0733-950X(1992)118:2(193)

Dean, R.G., 1973. Heuristic Models of Sand Transport in the Surf Zone, in: Engineering Dynamics of the Coastal Zone. Sydney, pp. 208–214.

Dean, R.G., 1972. Evaluation and development of water wave theories for engineering application. Vicksburg, MS.

Gourlay, M.R., Meulen, T., 1968. Beach and dune erosion tests (I).

Hansen, J.B., Svendsen, I.A., 1984. A theoretical and experimental study of undertow. Coast. Eng. Proc. 1, 2246–2262. https://doi.org/10.9753/icce.v19.%25p

Hansen, J.B., Svendsen, I.A., 1979. Regular waves in shoaling water, experimental data, 21.

Harter, C., Figlus, J., 2017. Numerical modeling of the morphodynamic response of a low-lying barrier island beach and foredune system inundated during Hurricane Ike using XBeach and CSHORE. Coast. Eng. 120, 64–74. https://doi.org/10.1016/j.coastaleng.2016.11.005

Higuera, P., Lara, J.L., Losada, I.J., 2013. Simulating coastal engineering processes with OpenFOAM®. Coast. Eng. 71, 119–134. https://doi.org/10.1016/j.coastaleng.2012.06.002

Horikawa, K., Kuo, C., 1966. A study on wave transformation inside surf zone. Coast. Eng. Japan 9, 69–81.

Johnson, B.D., Kobayashi, N., Gravens, M.B., 2012. Cross-Shore Numerical Model CSHORE for Waves, Currents, Sediment Transport and Beach Profile Evolution" Vicksburg, MS.

Kennedy, A.B., Chen, Q., Kirby, J.T., Dalrymple, R.A., 2000. Boussinesq Modeling of Wave Transformation, Breaking, and Runup. I: 1D. J. Waterw. Port, Coastal, Ocean Eng. 126, 39–47. https://doi.org/10.1061/(ASCE)0733-950X(2000)126:1(39)

Kim, D., Lynett, P., Socolofsky, S.A., 2009. A depth-integrated model for weakly dispersive , turbulent , and rotational fluid flows. Ocean Model. 27, 198–214. https://doi.org/10.1016/j.ocemod.2009.01.005

Kobayashi, N., Johnson, B., 1998. Computer program CSHORE for predicting cross-shore transformation of irregular breaking waves. Newark, DE.

Kraus, N., Larson, M., 1988. Beach Profile Change Measured in the Tank for Large Waves 1956-1957 and 1962.

Kraus, N., Smith, J.M., Sollitt, C.K., 1993. Supertank Laboratory Data Collection Project, in: Coastal Engineering 1992. American Society of Civil Engineers, New York, NY, pp. 2191–2204. https://doi.org/10.1061/9780872629332.167

Kriebel, D.L., Dally, W.R., Dean, R.G., 1987. Undistorted Froude Model for Surf Zone Sediment Transport, in: Coastal Engineering 1986. American Society of Civil Engineers, New York, NY, pp. 1296–1310. https://doi.org/10.1061/9780872626003.095

Kriebel, D.L., Dean, R.G., 1984. Beach and Dune Response to Severe Storms. Coast. Eng. 1584–1599. https://doi.org/10.1061/9780872624382.109

Lynett, P., Liu, P.L.F., 2004. A two-layer approach to wave modelling. Proc. R. Soc. A Math. Phys. Eng. Sci. 460, 2637–2669. https://doi.org/10.1098/rspa.2004.1305

Lynett, P., Liu, P.L.F., Sitanggang, K.I., Kim, D., 2008. Modeling wave weneration, evolution, and interaction with depth-integrated, dispersive wave equations, COULWAVE code manual, Cornell University Long and Intermediate Wave Modeling Package.

Lynett, P., Wu, T.R., Liu, P.L.F., 2002. Modeling wave runup with depth-integrated equations. Coast. Eng. 46, 89–107. https://doi.org/10.1016/S0378-3839(02)00043-1

Madsen, P.A., Murray, R., Sørensen, O.R., 1991. A new form of the Boussinesq equations with improved linear dispersion characteristics. Coast. Eng. 15, 371–388.

https://doi.org/10.1016/0378-3839(91)90017-B

Nwogu, O., 1993. Alternative Form of Boussinesq Equations for Nearshore Wave Propagation. J. Waterw. Port, Coastal, Ocean Eng. 119, 618–638. https://doi.org/10.1061/(ASCE)0733-950X(1993)119:6(618)

Okayasu, A., Shibayama, T., Horikawa, K., 1988. Vertical Variation of Undertow in the Surf Zone, in: Coastal Engineering 1988. American Society of Civil Engineers, New York, NY, pp. 478–491. https://doi.org/10.1061/9780872626874.034

Okayasu, A., Shibayama, T., Mimura, N., 1986. Velocity Field under Plunging Waves, in: Coastal Engineering 1986. American Society of Civil Engineers, New York, NY, pp. 660–674. https://doi.org/10.1061/9780872626003.050

Peregrine, D.H., 1967. Long waves on a beach. J. Fluid Mech. 27, 815–827.

Roelvink, D., Reniers, A., van Dongeren, A., van Thiel de Vries, J., McCall, R., Lescinski, J., 2009. Modelling storm impacts on beaches, dunes and barrier islands. Coast. Eng. 56, 1133–1152. https://doi.org/10.1016/j.coastaleng.2009.08.006

Saville, T., 1957. Scale Effects in Two-Dimensional Beach Studies, in: Transactions of the Seventh Meeting of the International Association of Hydraulic Research. p. A3.1-A3-10.

Schäffer, H.A., Madsen, P.A., Deigaard, R., 1993. A Boussinesq model for waves breaking in shallow water. Coast. Eng. 20, 185–202. https://doi.org/10.1016/0378-3839(93)90001-O

Shi, F., Kirby, J.T., Harris, J.C., Geiman, J.D., Grilli, S.T., 2012. A high-order adaptive time-stepping TVD solver for Boussinesq modeling of breaking waves and coastal inundation. Ocean Model. 43–44, 36–51. https://doi.org/10.1016/j.ocemod.2011.12.004

Smith, E.R., Kraus, N., 1990. Laboratory study on macro-features of wave breaking over bars and artificial reefs. Coast. Eng. Res. Cent.

Stive, M.J.F., Wind, H.G., 1986. Cross-shore mean flow in the surf zone. Coast. Eng. 10, 325–340. https://doi.org/10.1016/0378-3839(86)90019-0

Svendsen, I.A., 1984. Mass flux and undertow in a surf zone. Coast. Eng. 8, 347–365. https://doi.org/10.1016/0378-3839(84)90030-9

Tao, J., 1984. Numerical modelling of wave runup and breaking on the beach. Acta Oceanol. Sin. 6, 692–700.

Tavakkol, S., Lynett, P., 2017. Celeris: A GPU-accelerated open source software with a Boussinesq-type wave solver for real-time interactive simulation and visualization. Comput. Phys. Commun. 217, 117–127. https://doi.org/10.1016/j.cpc.2017.03.002

Tonelli, M., Petti, M., 2009. Hybrid finite volume-finite difference schem for 2DH improved Boussinesq equations. Coast. Eng. 56, 609–620.

Wei, G., Kirby, J.T., 1995. Time-Dependent Numerical Code for Extended Boussinesq Equations. J. Waterw. Port, Coastal, Ocean Eng. 121, 251–261. https://doi.org/10.1061/(ASCE)0733-950X(1995)121:5(251)

Weller, H.G., Tabor, G., Jasak, H., Fureby, C., 1998. A tensorial approach to computational continuum mechanics using object-oriented techniques. Comput. Phys. 12, 620. https://doi.org/10.1063/1.168744

Yamamoto, S., Daiguji, H., 1993. Higher-order-accurate upwind schemes for solving the compressible Euler and Navier-Stokes equations. Comput. Fluids 22, 259–270.

https://doi.org/10.1016/0045-7930(93)90058-H

11 **Appendix A**: COULWAVE sample code

The following is the sim_set.dat file for test case 031041 of the original Hansen and Svendsen (1974) dataset.

1

1

2

2

1

0

5

0.3600000

4.3000001E-02

0.3600000

10.00000

0.000000

0.000000

0.000000

0.000000

0.000000

0

0.000000

0.000000

0.000000

1

1.000000

0

1

50

20.00000

2

15

0.5000000

1

1

1

1

1

0

0

0

1

3

0.000000

0.3600000

20.00000

0.3600000

44.66720

-0.3600000

0.000000

0.000000

0.000000

0.000000

0.000000

0.000000

0.000000

0.000000

0.000000

0.000000

0.000000

0.000000

0.000000

101.0000

1.000000

150

0.3500000

0

6.121500

0.000000

0.000000

1.250000

10.00000

9.9999998E-03

0

0

0.000000

0.000000

0.000000

0.000000

0.000000

0.000000

0.000000

1

0.000000

1

9.9999997E-05

1

4.9999999E-06

4.9999999E-06

0.000000

1

1

0

0

0.000000

0.000000

0.000000

0.000000

0.000000

60

0

0.000000

0.000000

0

500.0000

1

1.000000

0

0.000000

0.2000000

1

0

1

1

1

10

1

0

0

0

6.6670001E-02

0

30.00000

0.000000

0

0.1000000

0.000000

0.000000

0.000000

0.000000

0.000000

0.000000

0.000000

0.000000

0.000000

0.000000

0.000000

0.000000

0.000000

0.000000

0.000000

0.000000

0.000000

0.000000

0.000000

12 **Appendix B**: Complete plotted data for Hansen and Svensen tests

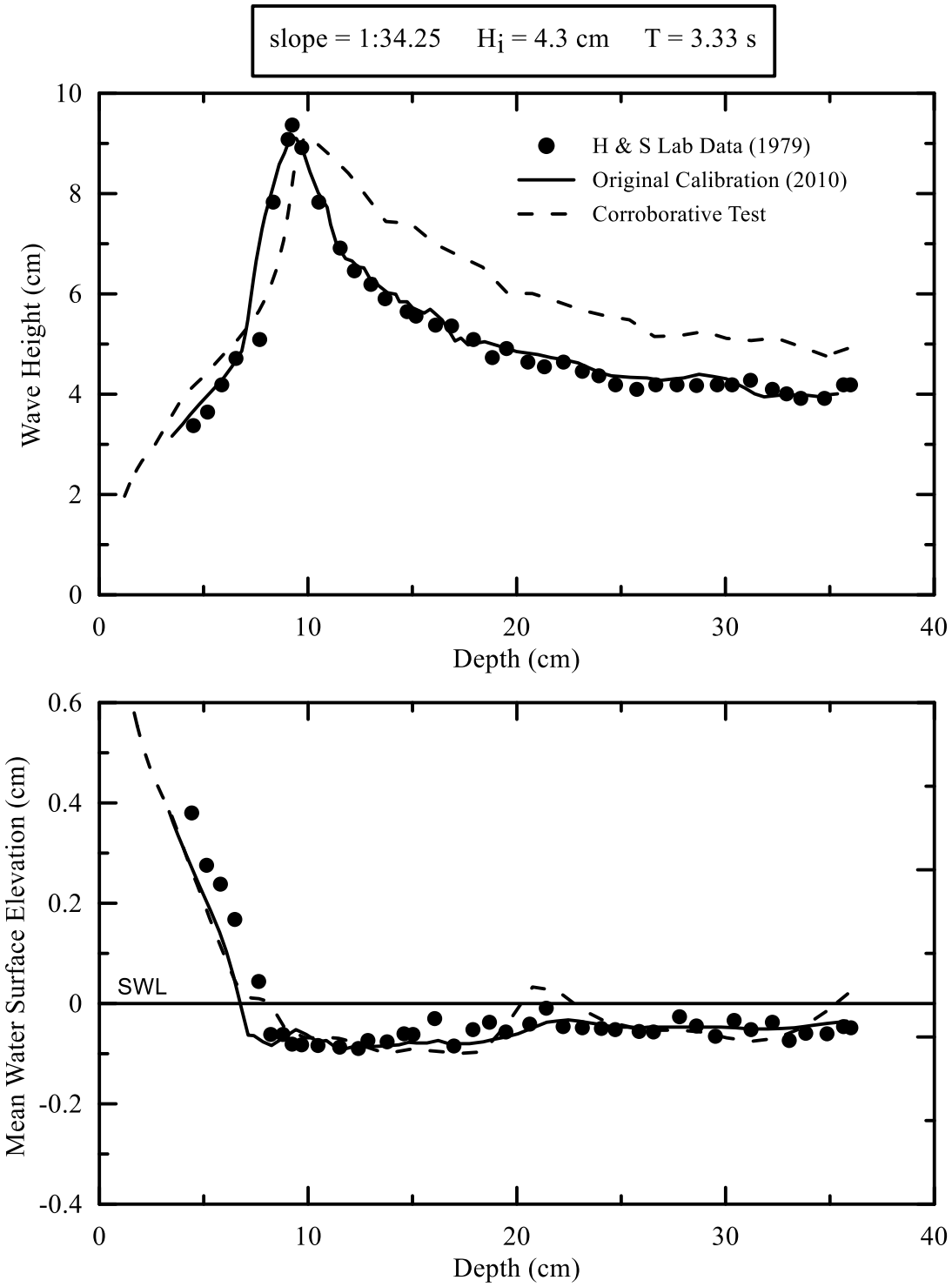

Figure 12.1: Comparison of Hansen and Svendsen (1979) measured wave data for case 031041 with predicted results from Lynett et al. (2008) and current results for this investigation.

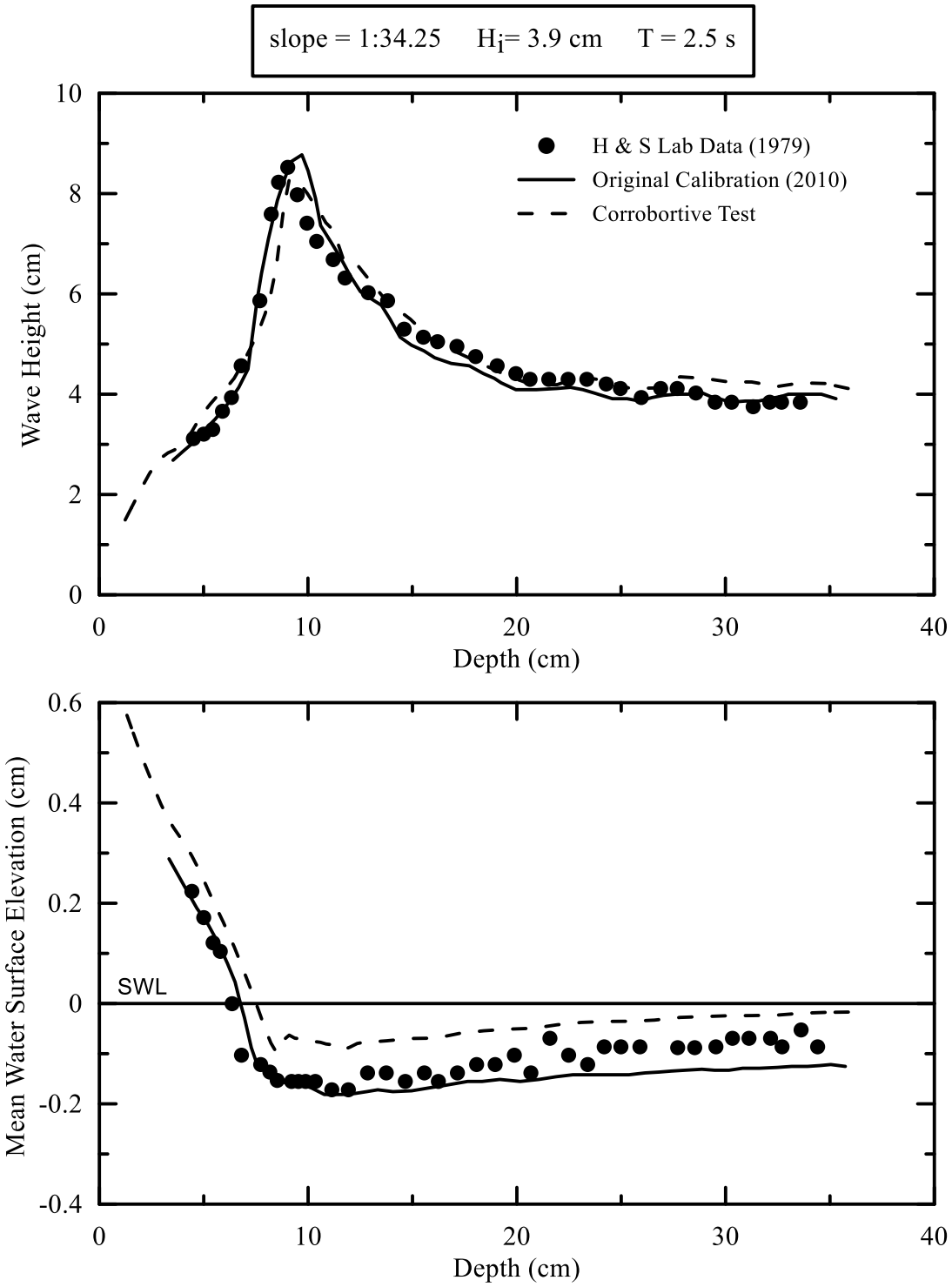

Figure 12.2: Comparison of Hansen and Svendsen (1979) measured wave data for case 041041 with predicted results from Lynett et al. (2008) and current results for this investigation.

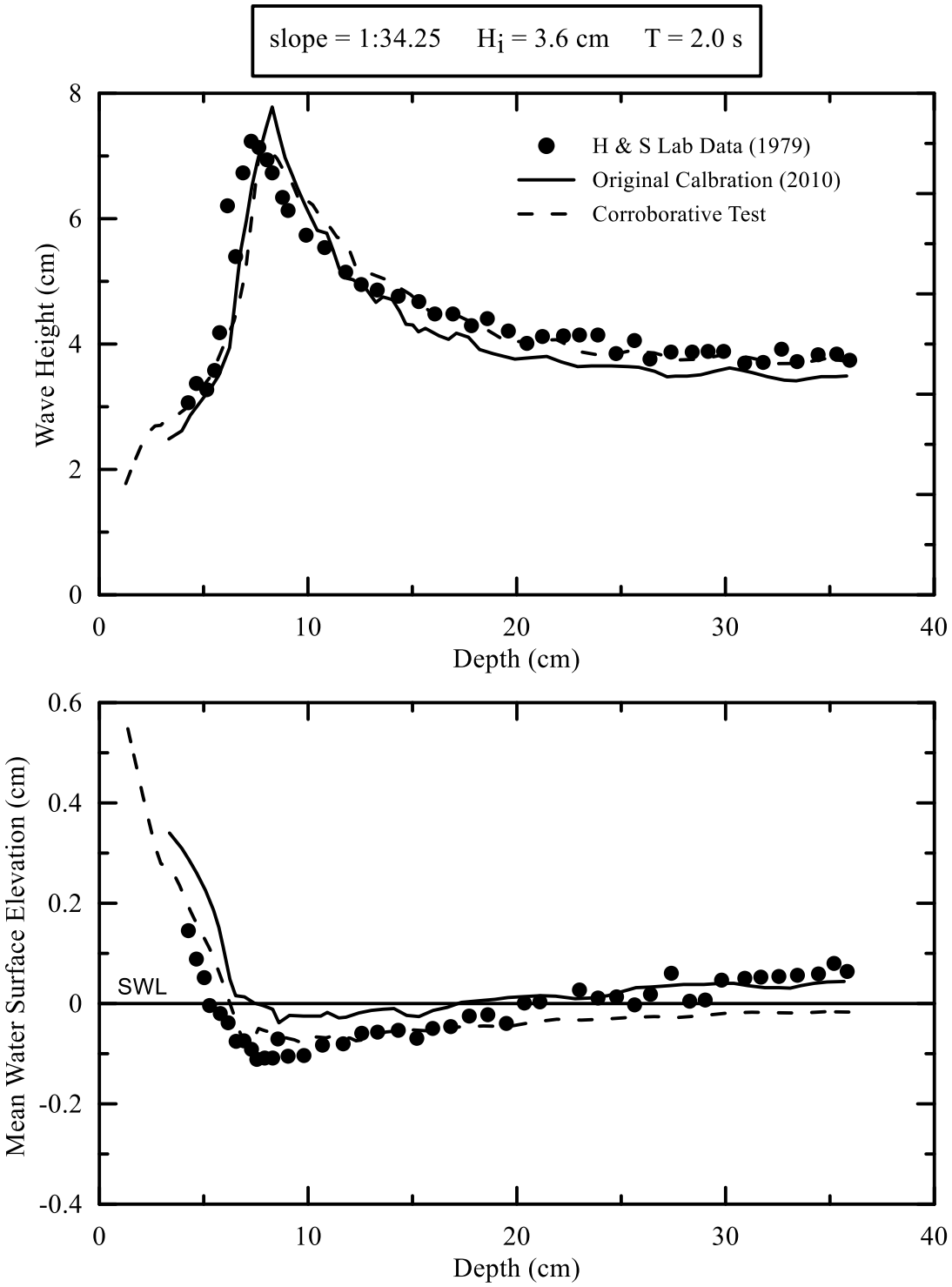

Figure 12.3: Comparison of Hansen and Svendsen (1979) measured wave data for case 051041 with predicted results from Lynett et al. (2008) and current results for this investigation.

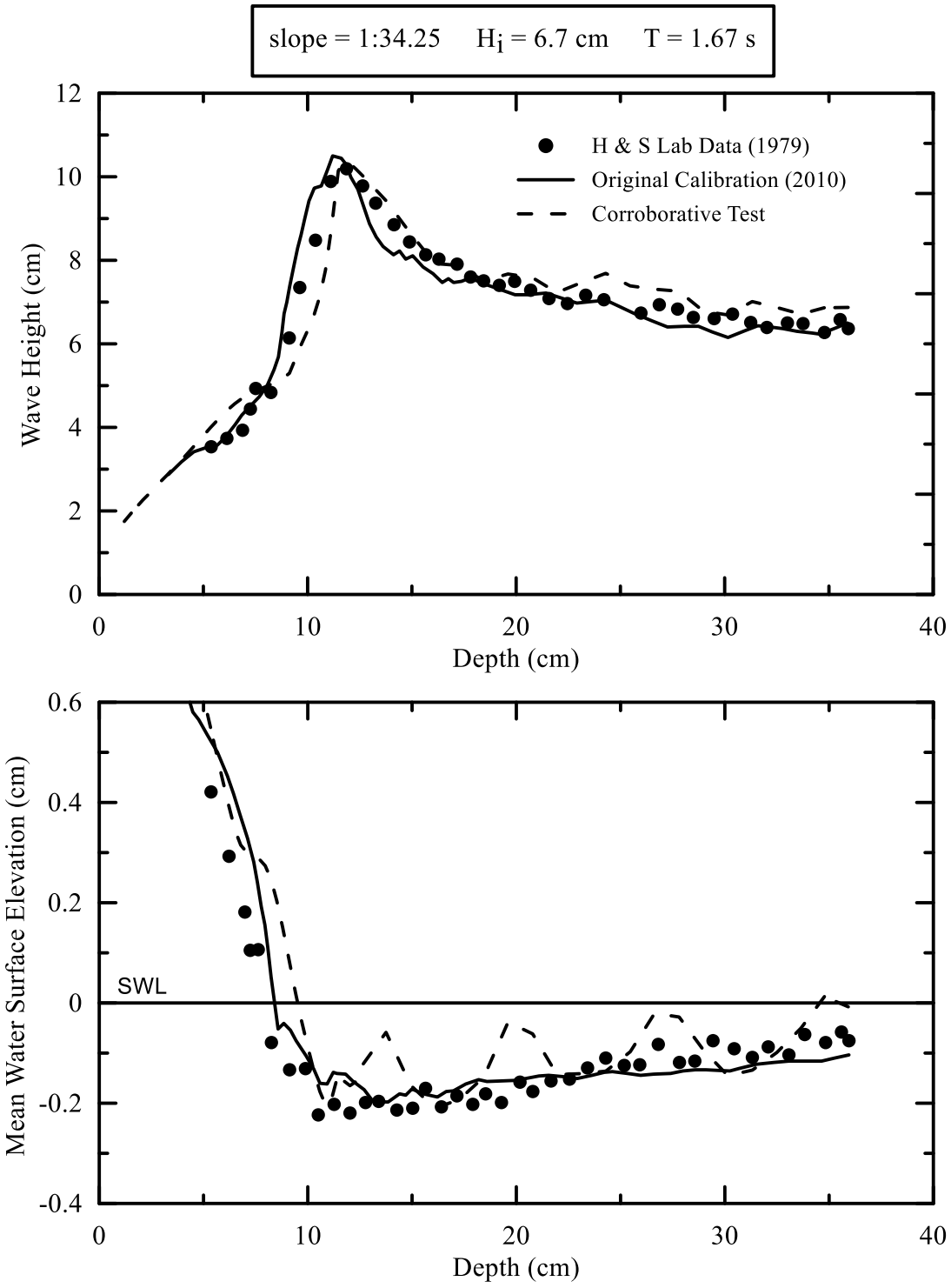

Figure 12.4: Comparison of Hansen and Svendsen (1979) measured wave data for case 061041 with predicted results from Lynett et al. (2008) and current results for this investigation.

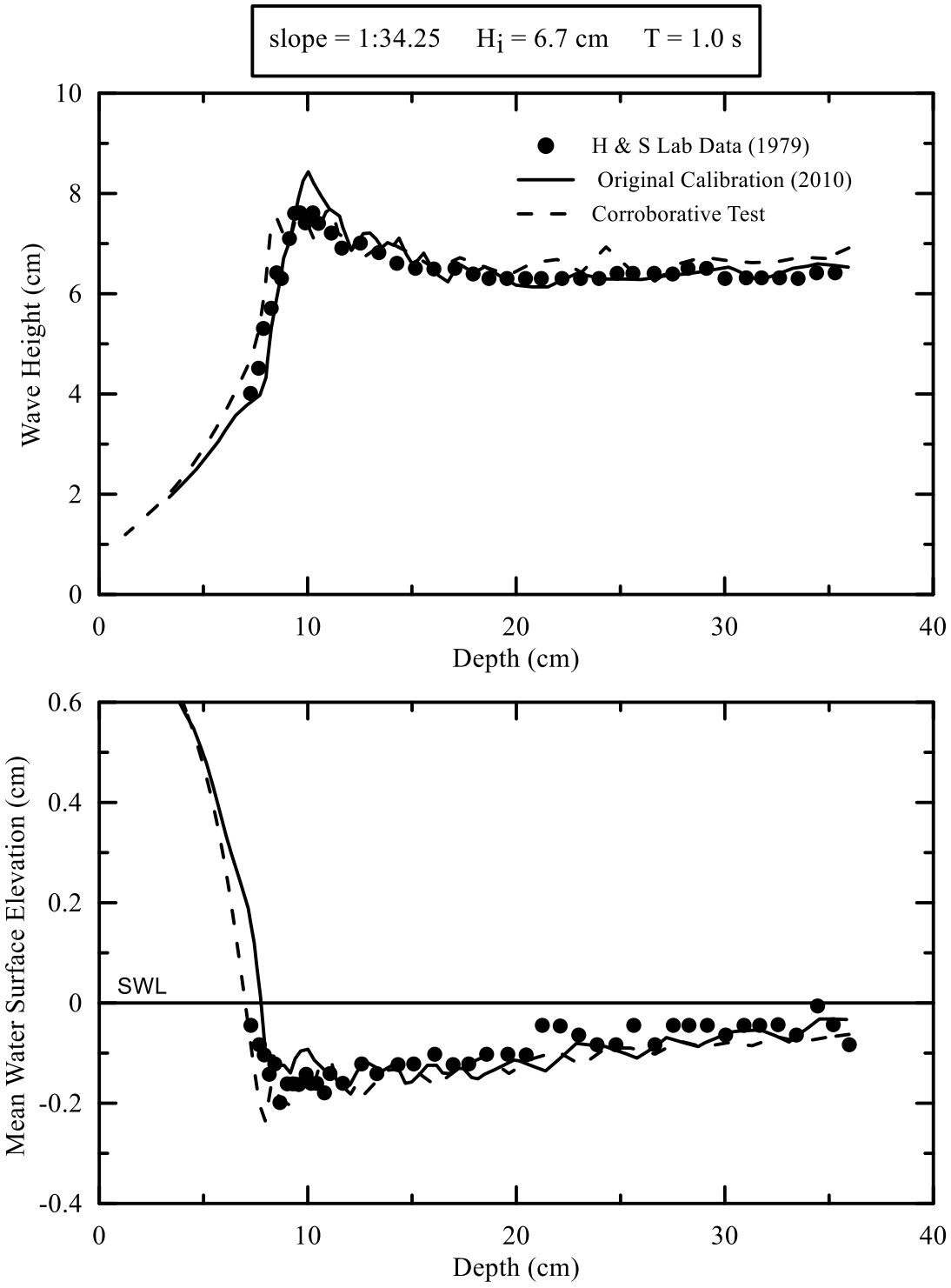

Figure 12.5: Comparison of Hansen and Svendsen (1979) measured wave data for case A10112 with predicted results from Lynett et al. (2008) and current results for this investigation.

13 Appendix B: Results of COULWAVE tests on artificial bar-trough formations.

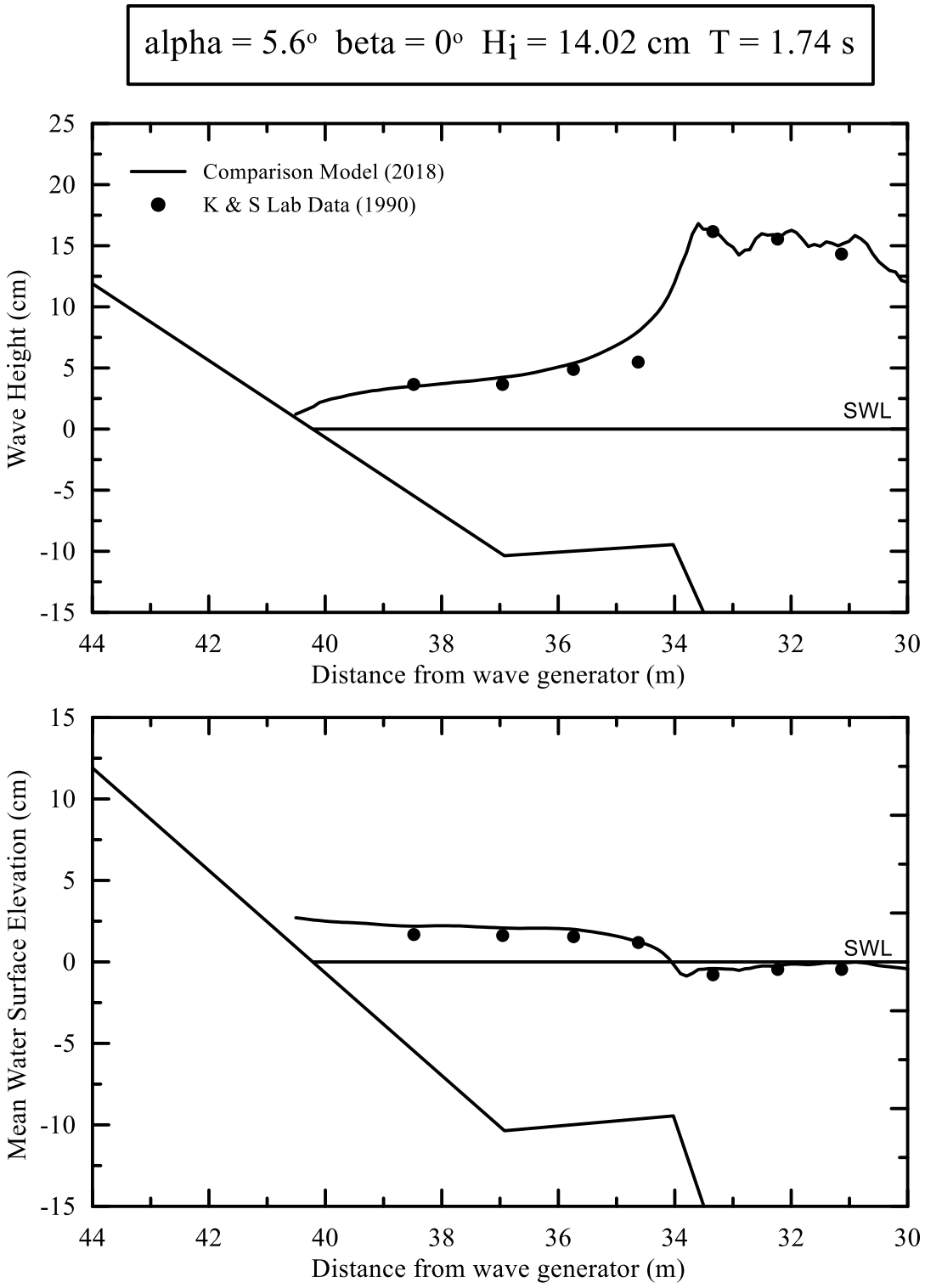

Figure 13.1: Test 8110.

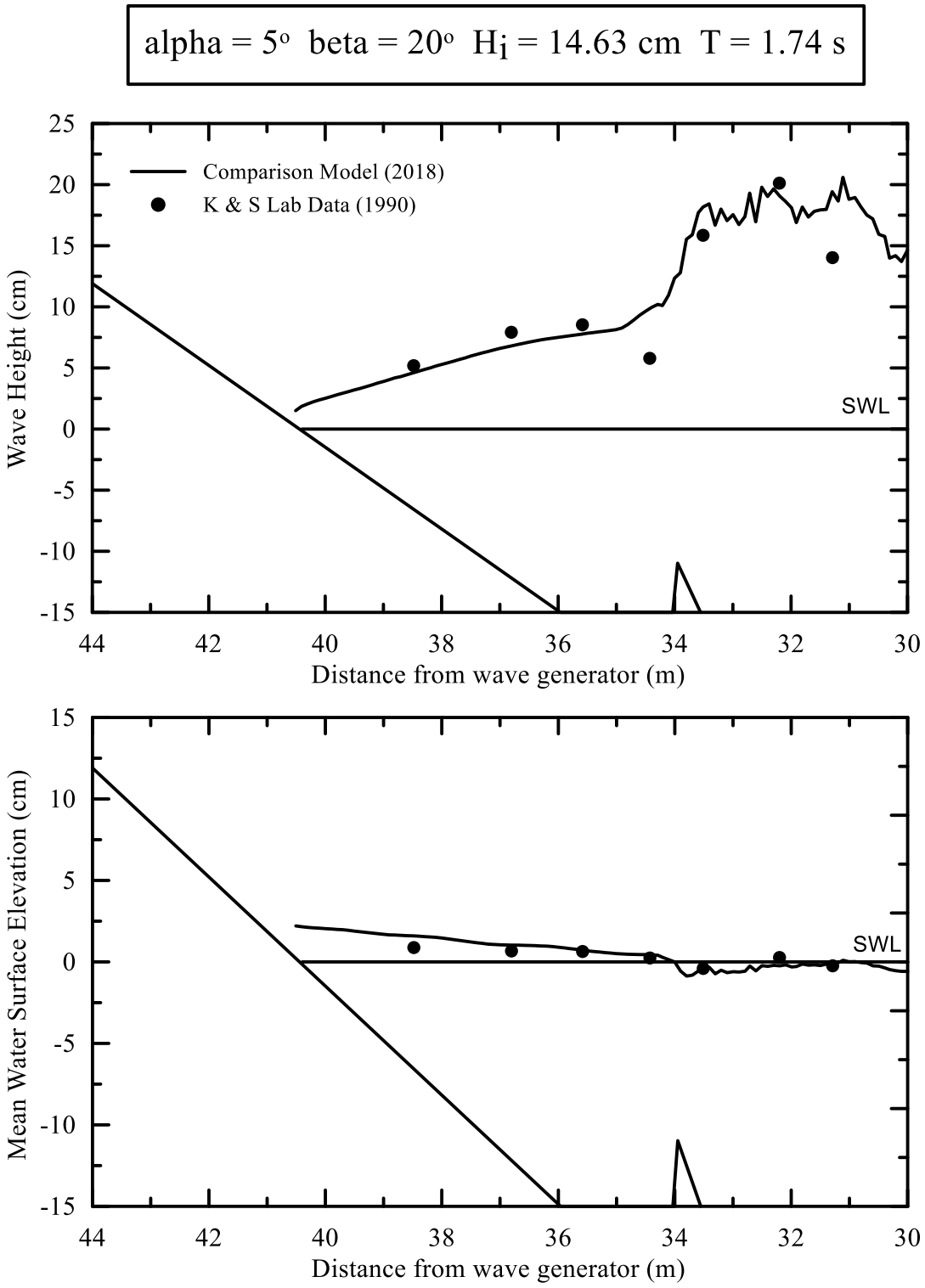

Figure 13.2: Test 8210.

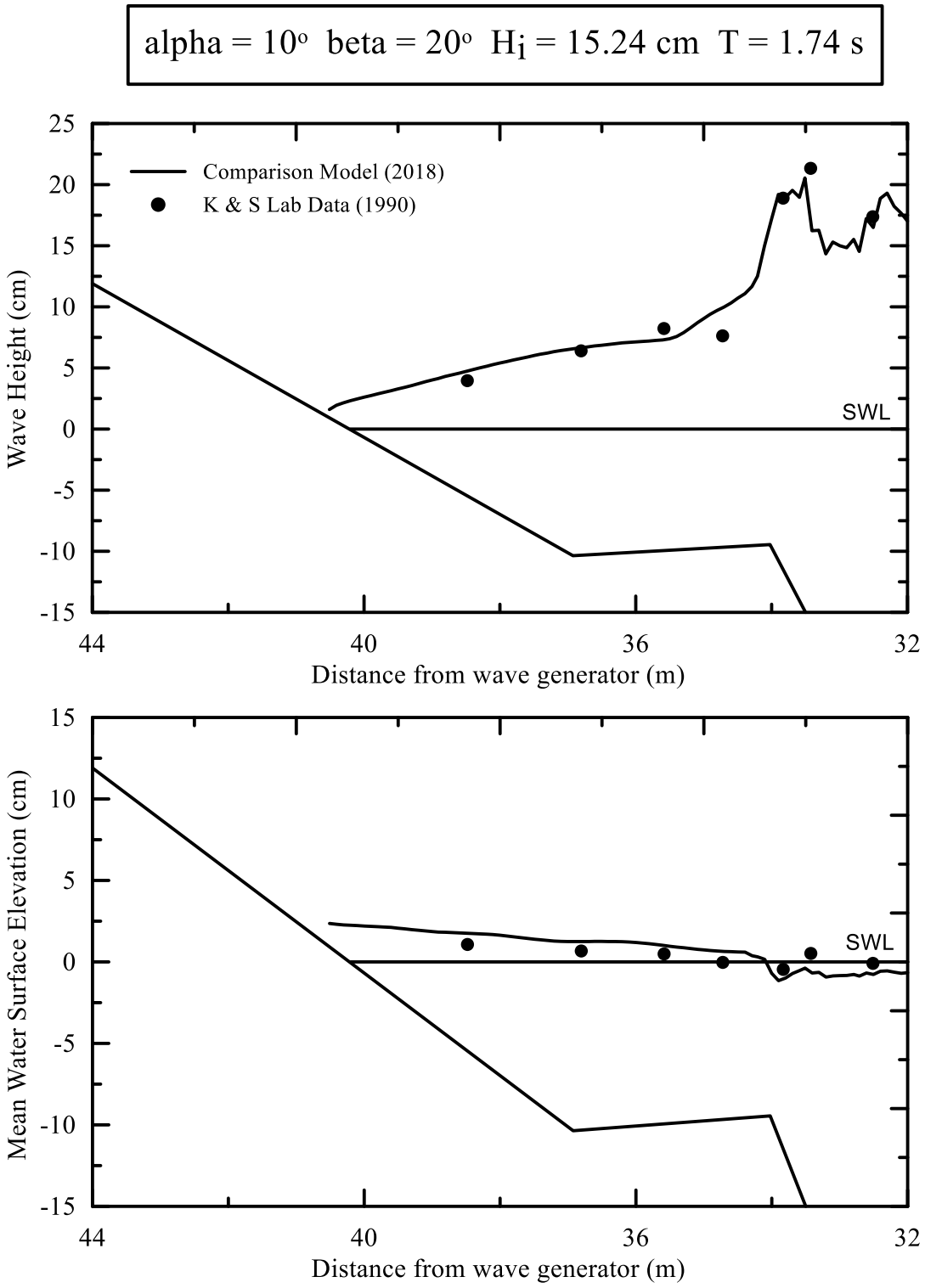

Figure 13.3: Test 8220.

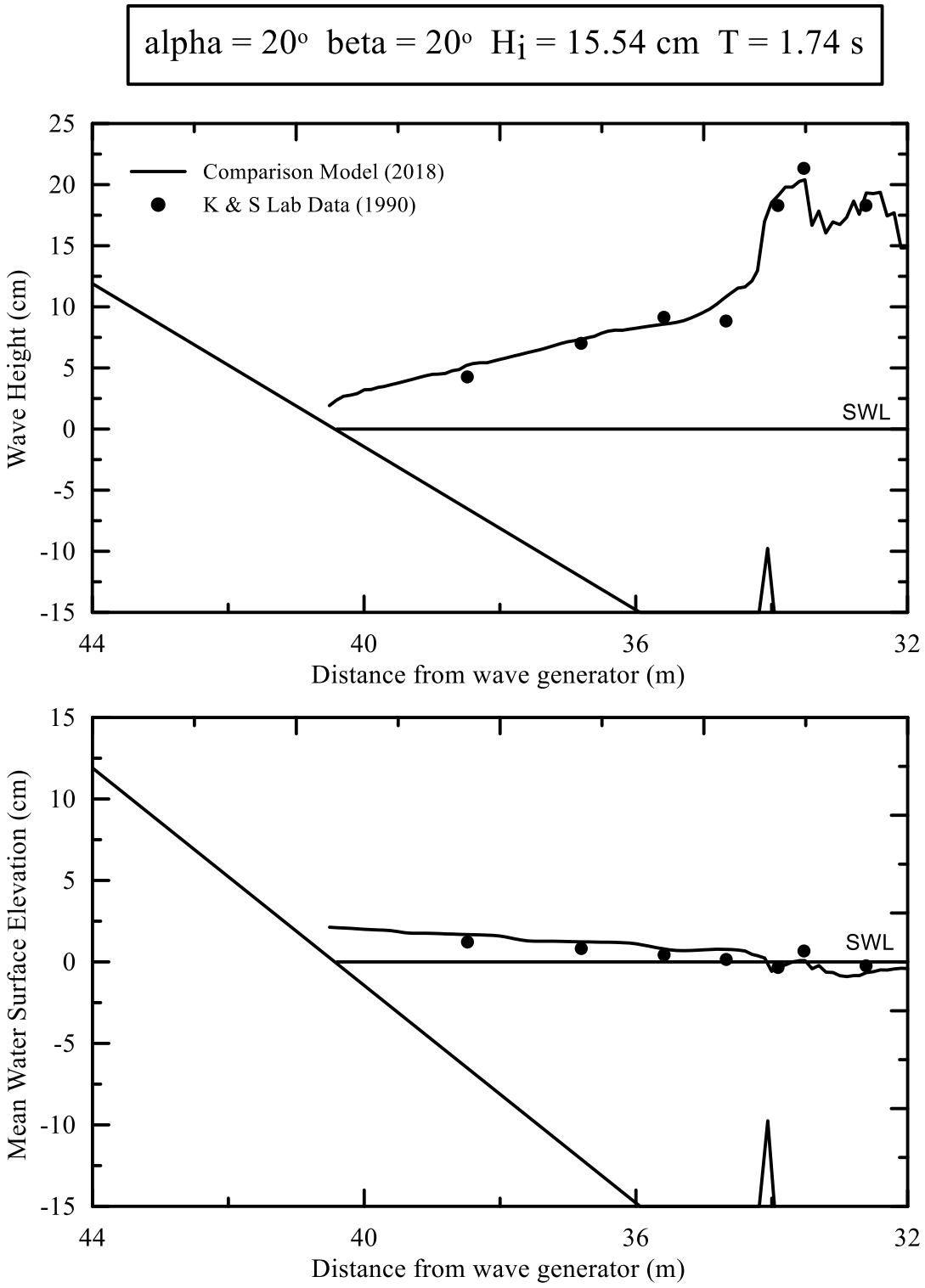

Figure 13.4: Test 8240.

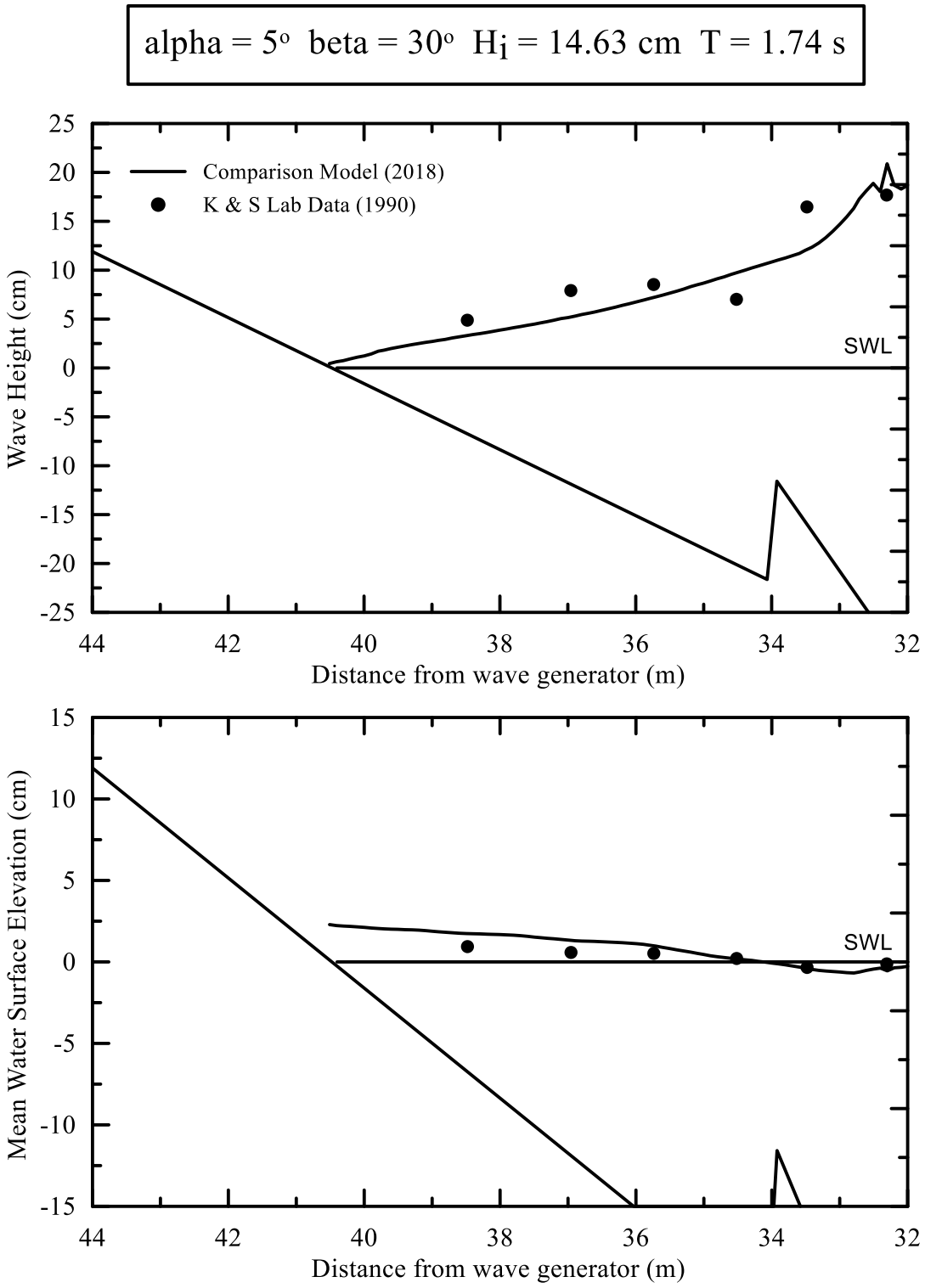

Figure 13.5: Test 8310.

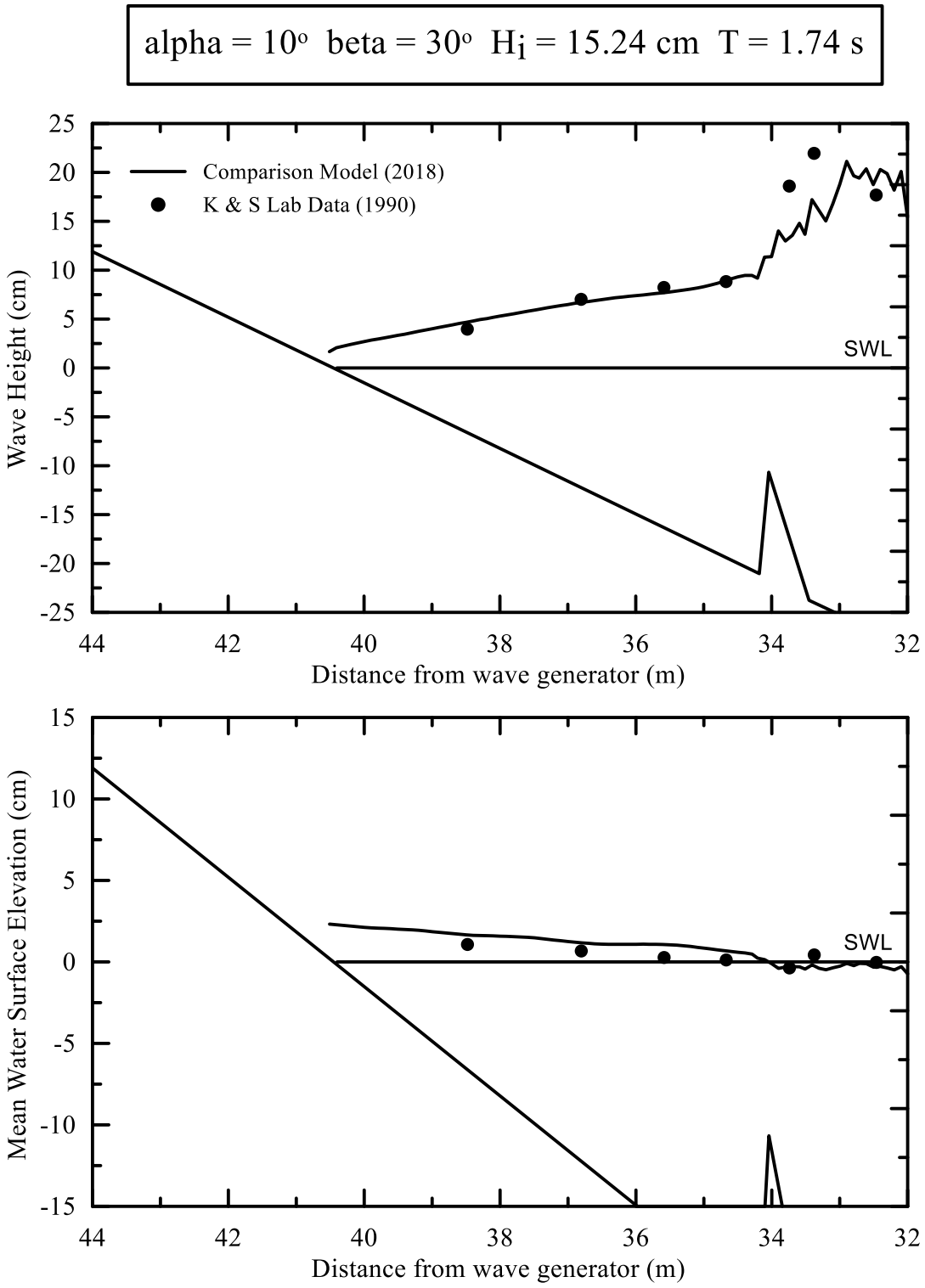

Figure 13.6: Test 8320.

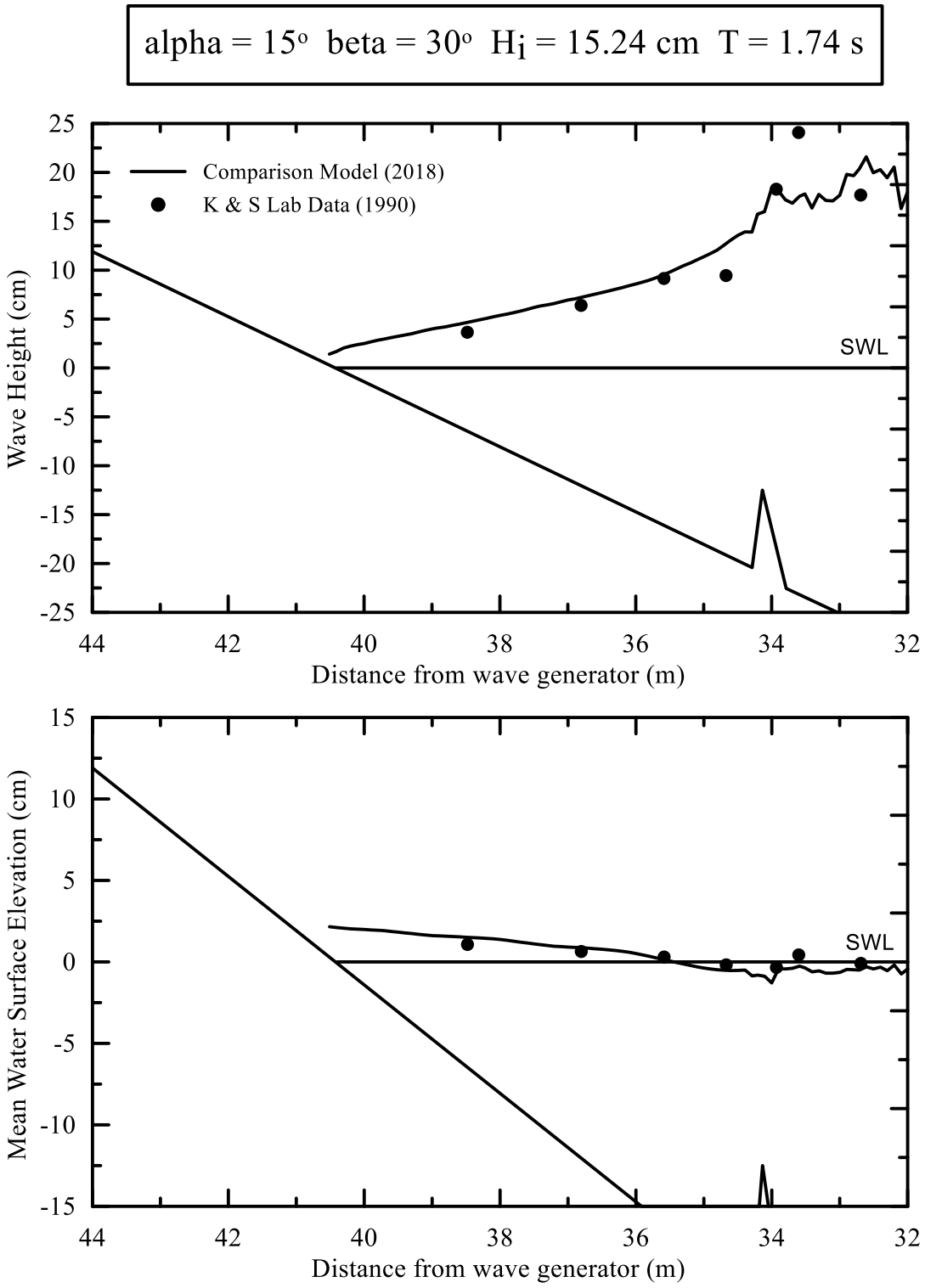

Figure 13.7: Test 8330.

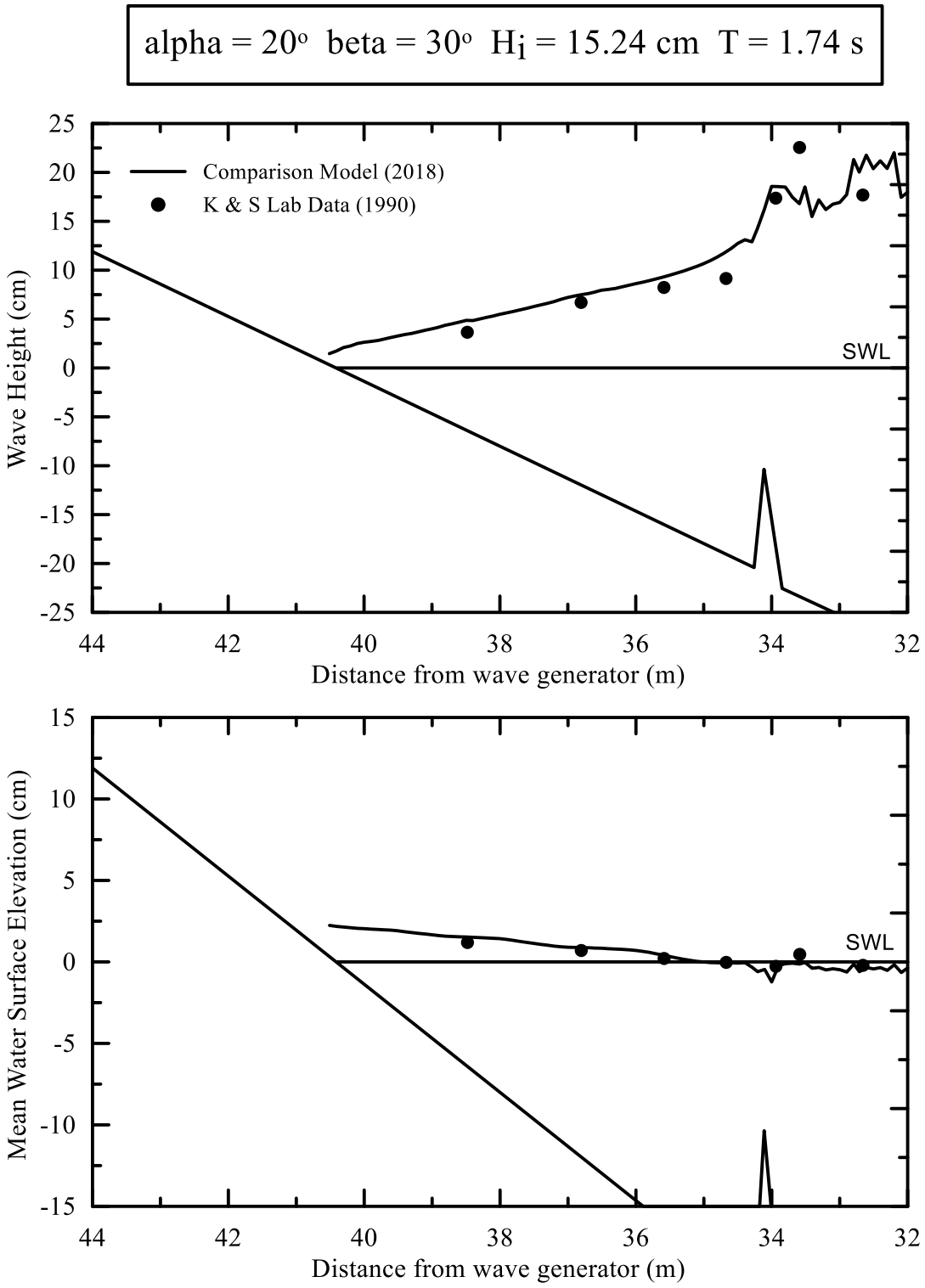

Figure 13.8: Test 8340.

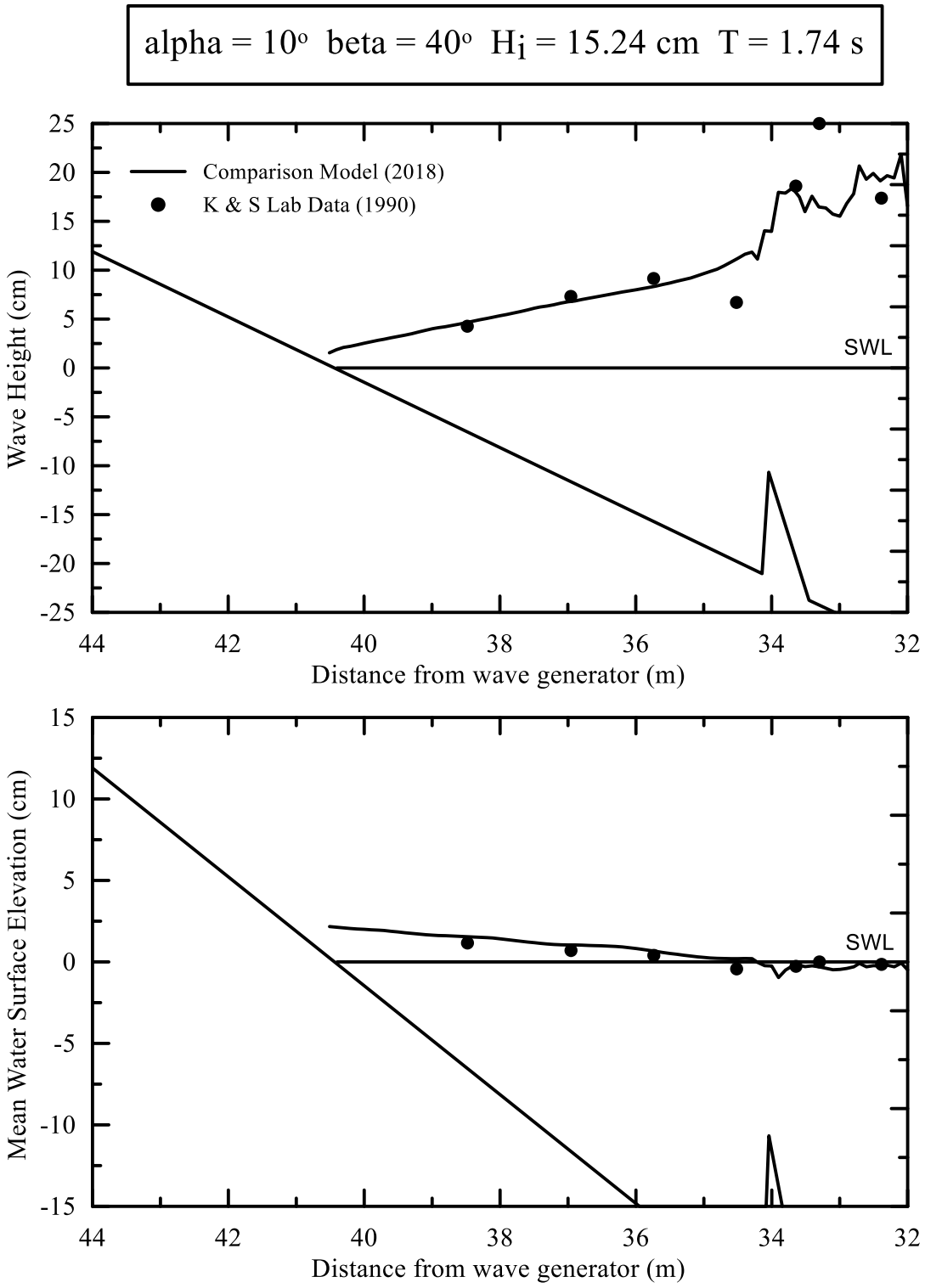

Figure 13.9: Test 8420.

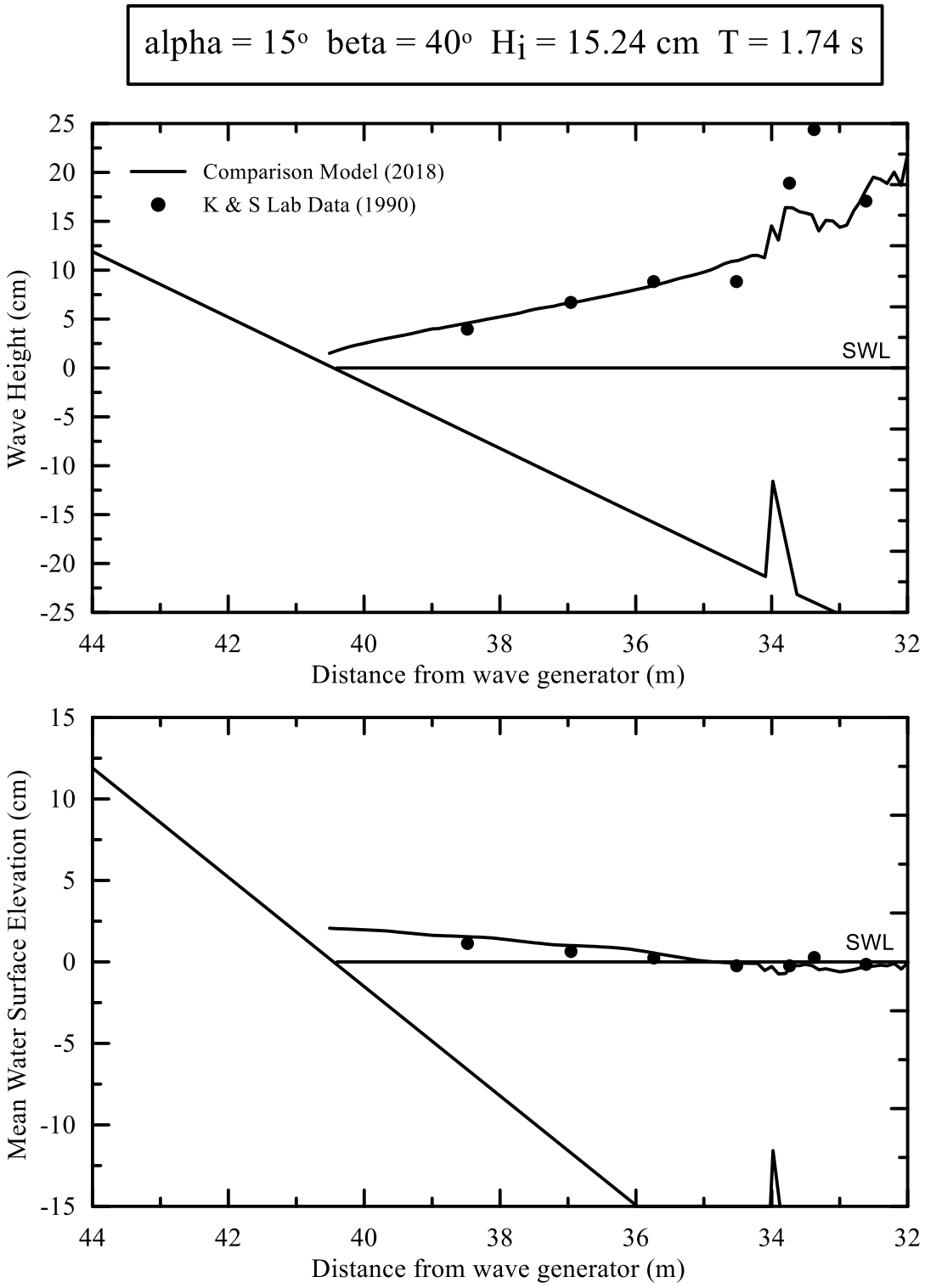

Figure 13.10: Test 8430.

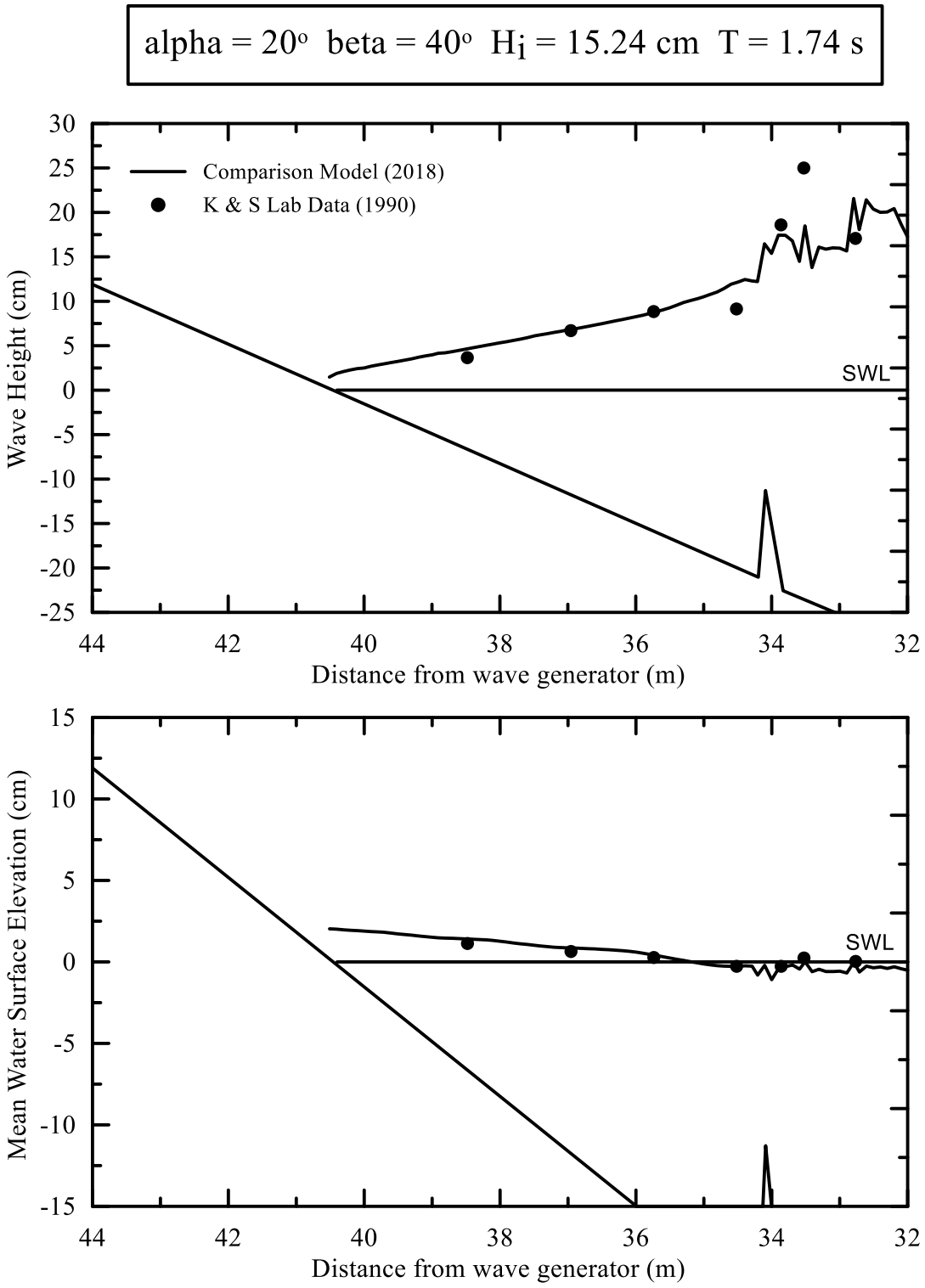

Figure 13.11: Test 8440.

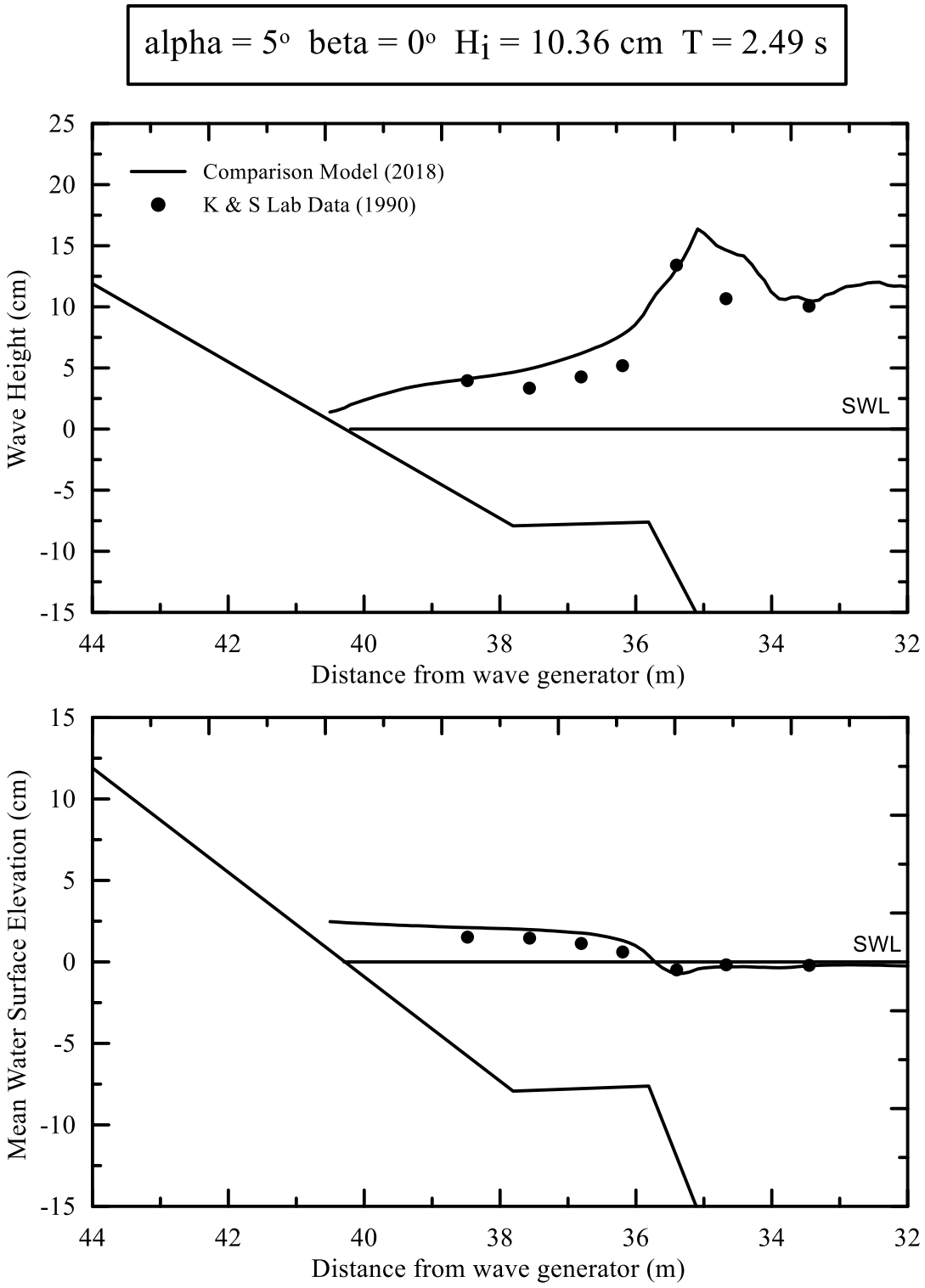

Figure 13.12: Test 10110.

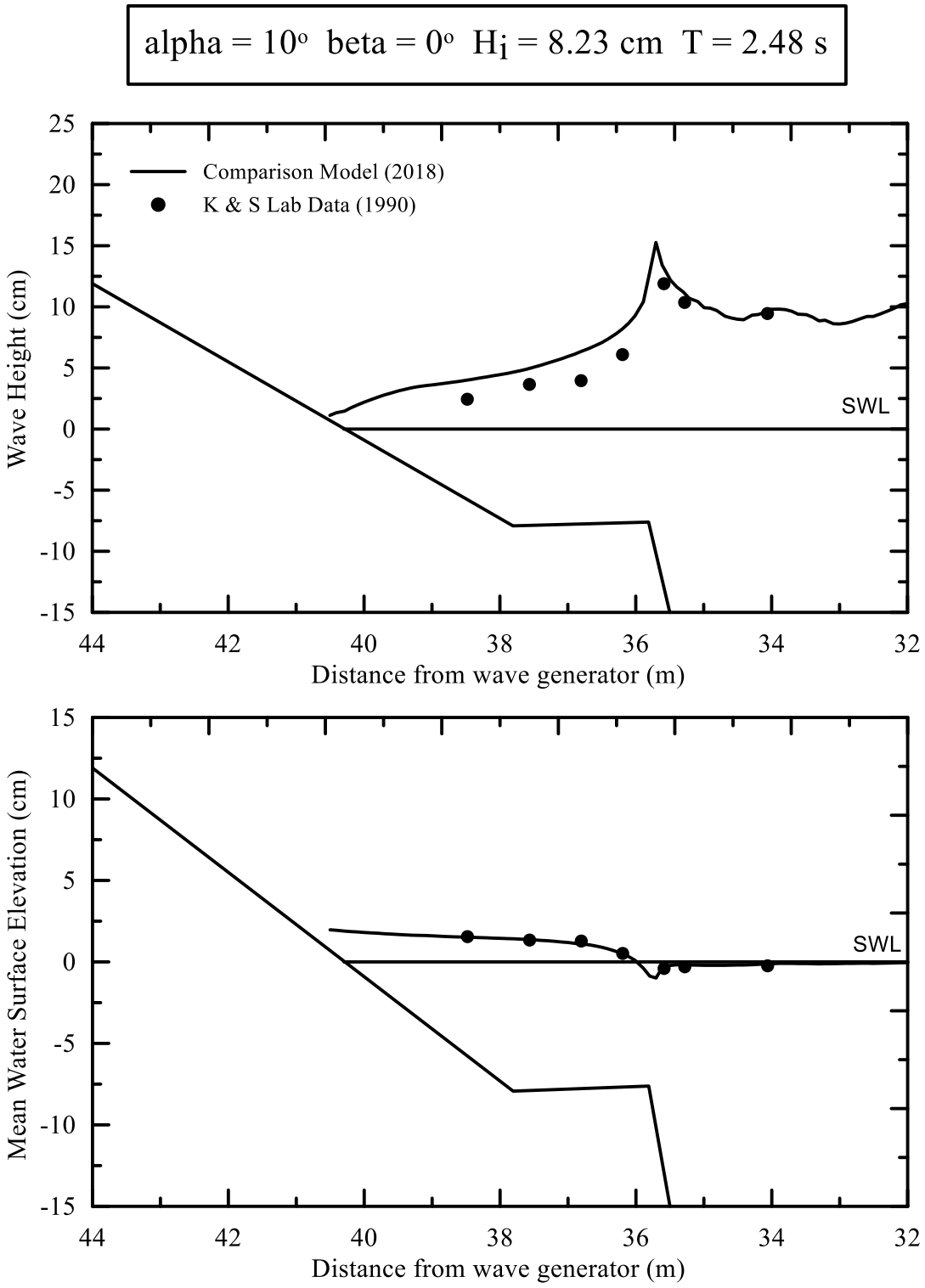

Figure 13.13: Test 10120.

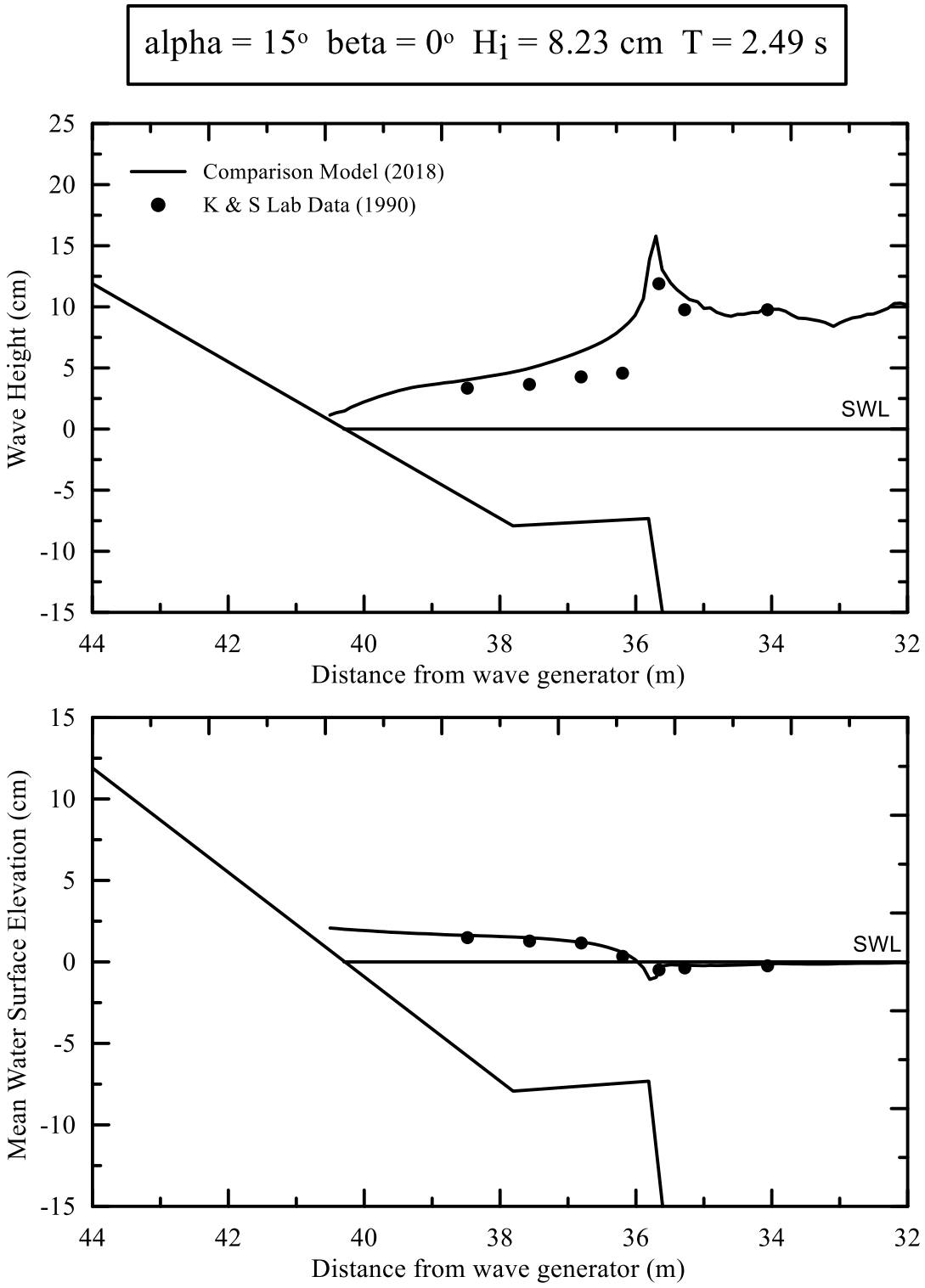

Figure 13.14: Test 10130.

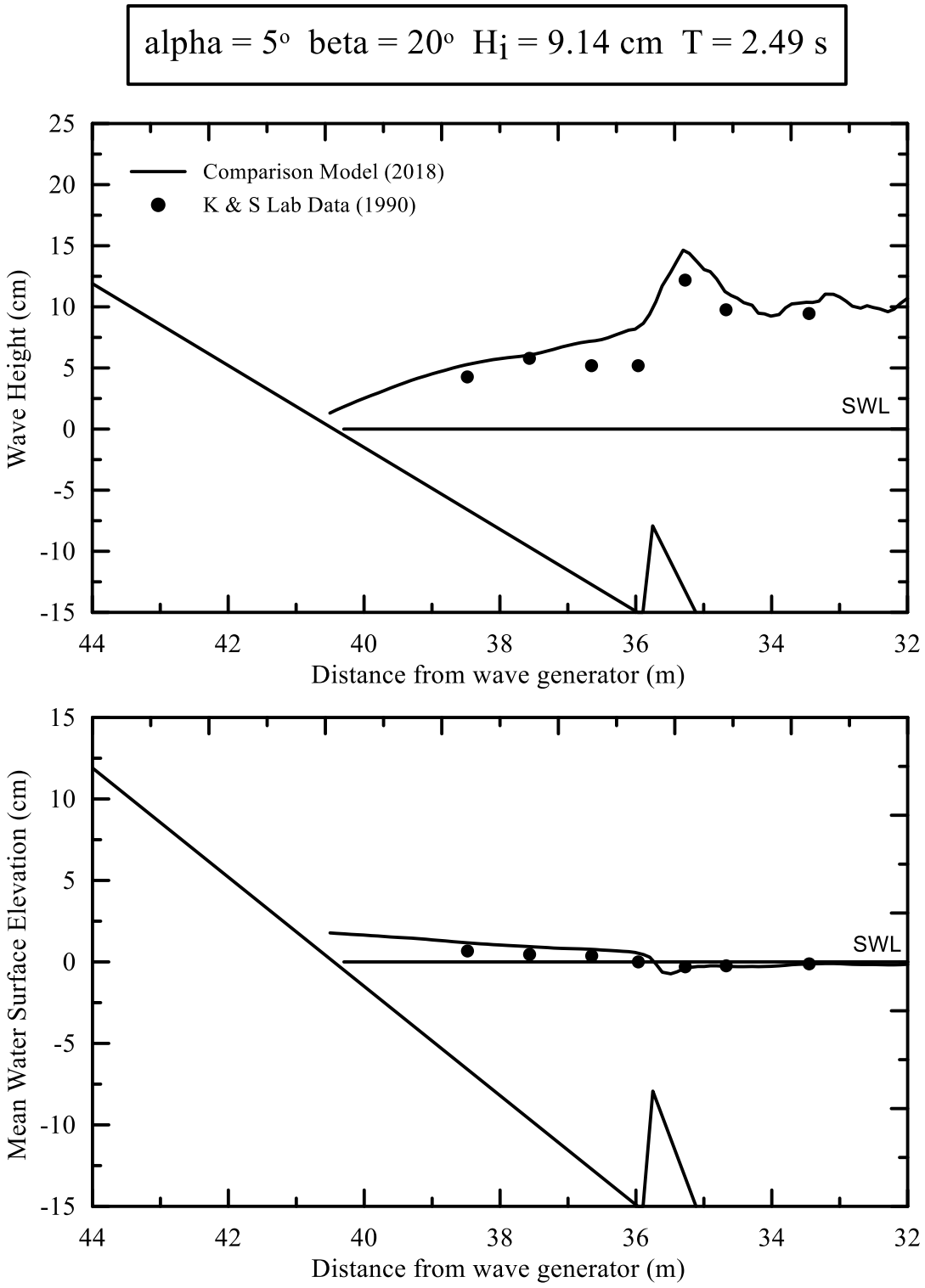

Figure 13.15: Test 10210.

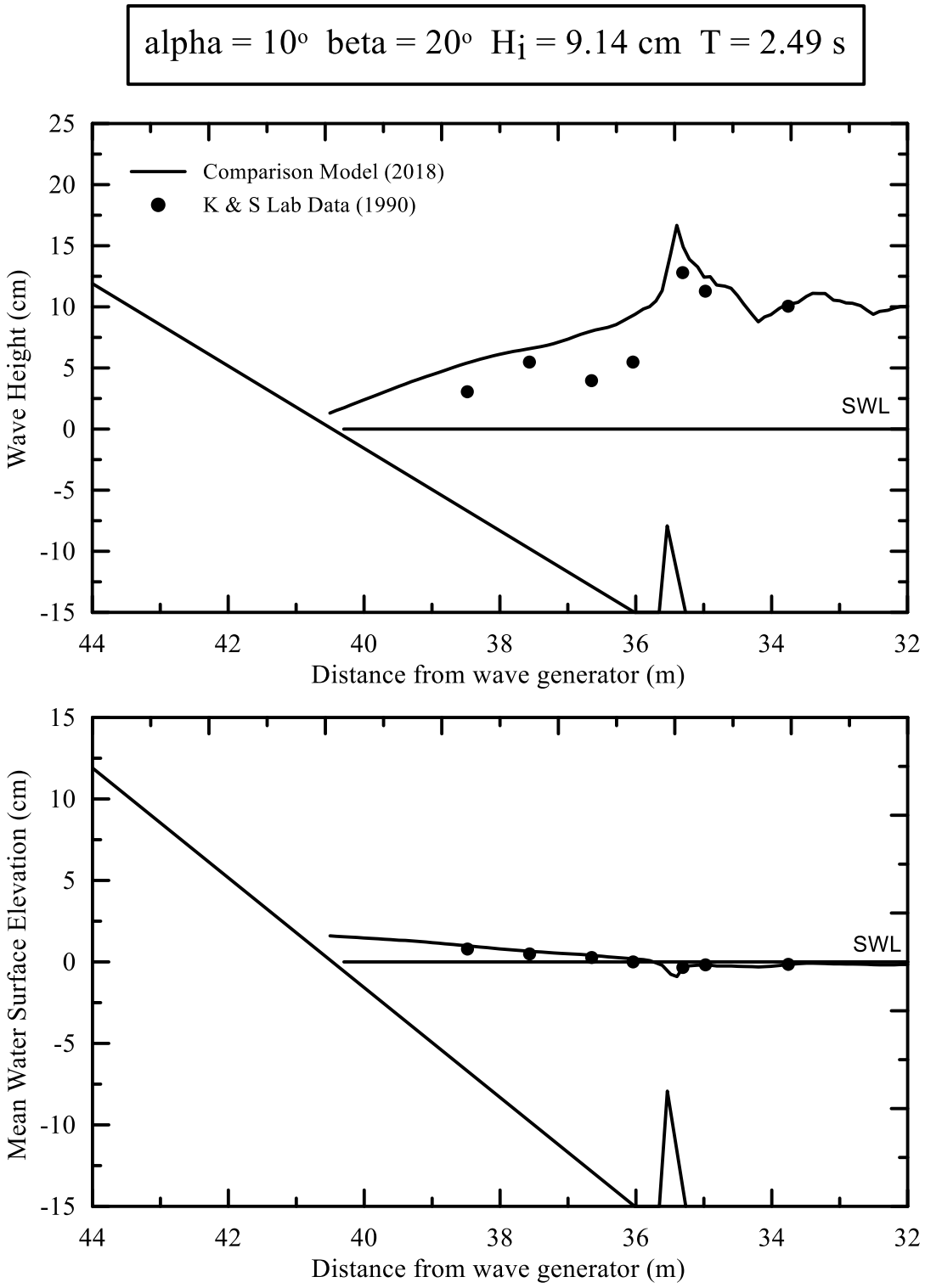

Figure 13.16: Test 10220.

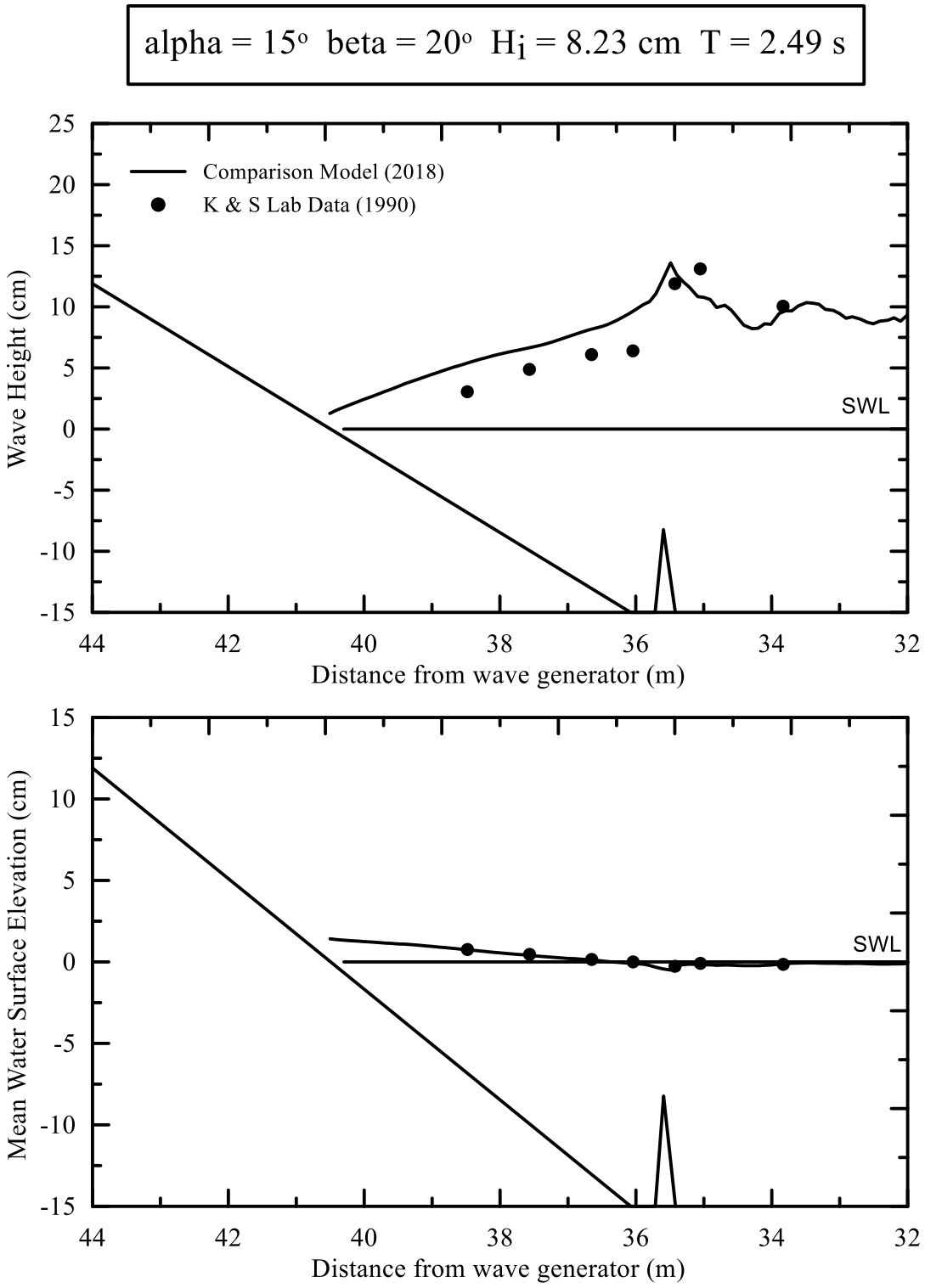

Figure 13.17: Test 10230.

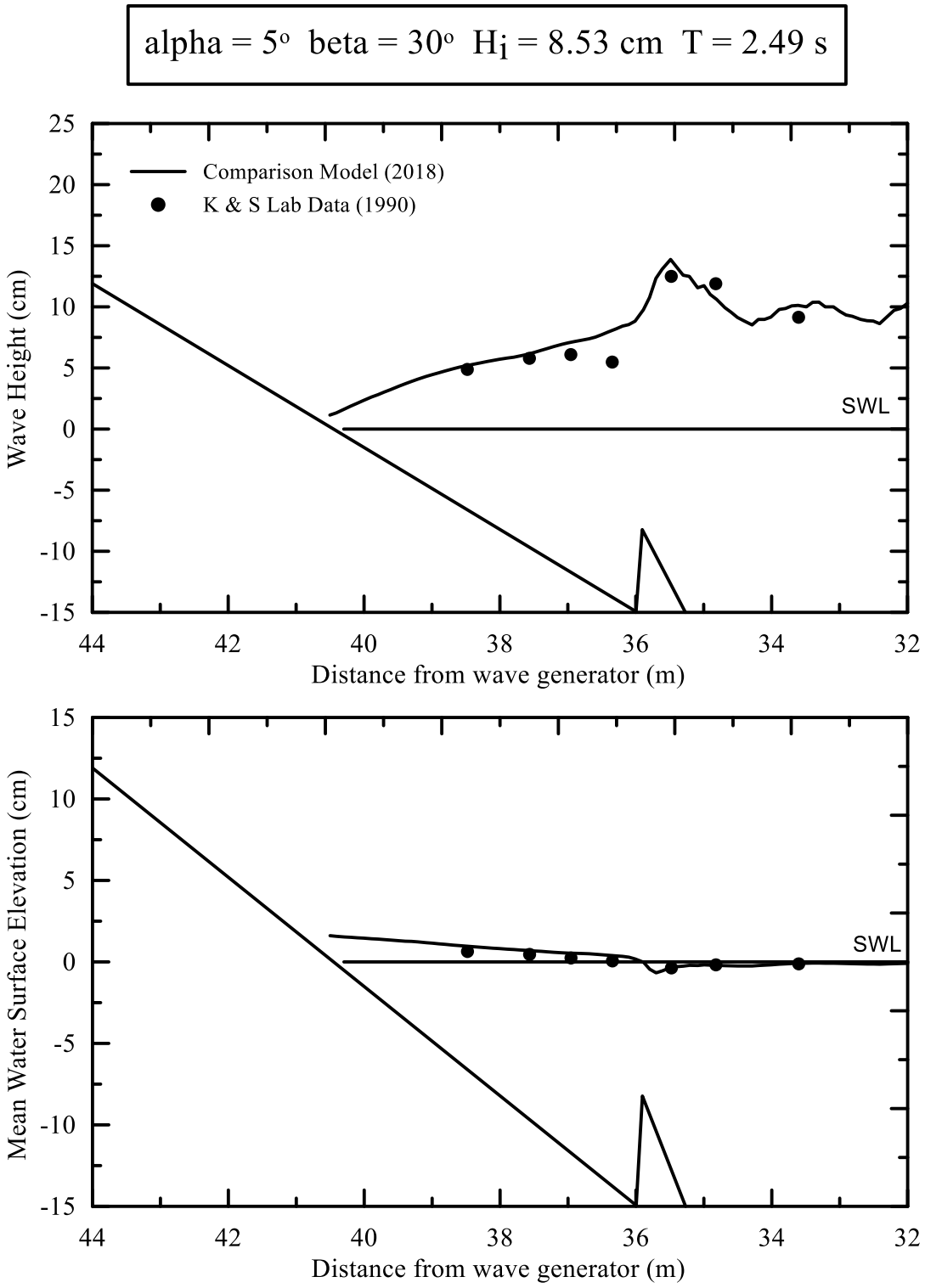

Figure 13.18: Test 10310.

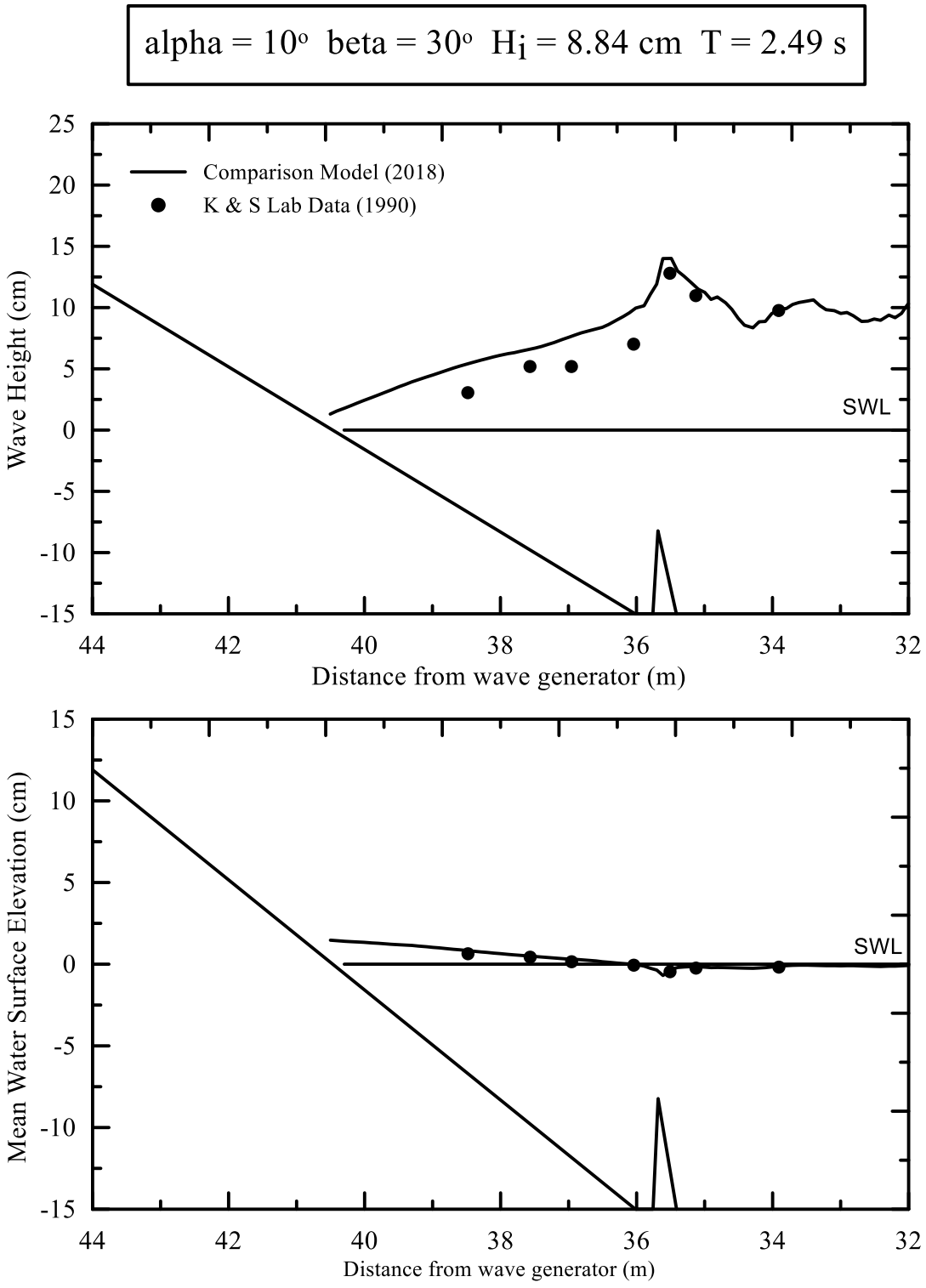

Figure 13.19: Test 10320.

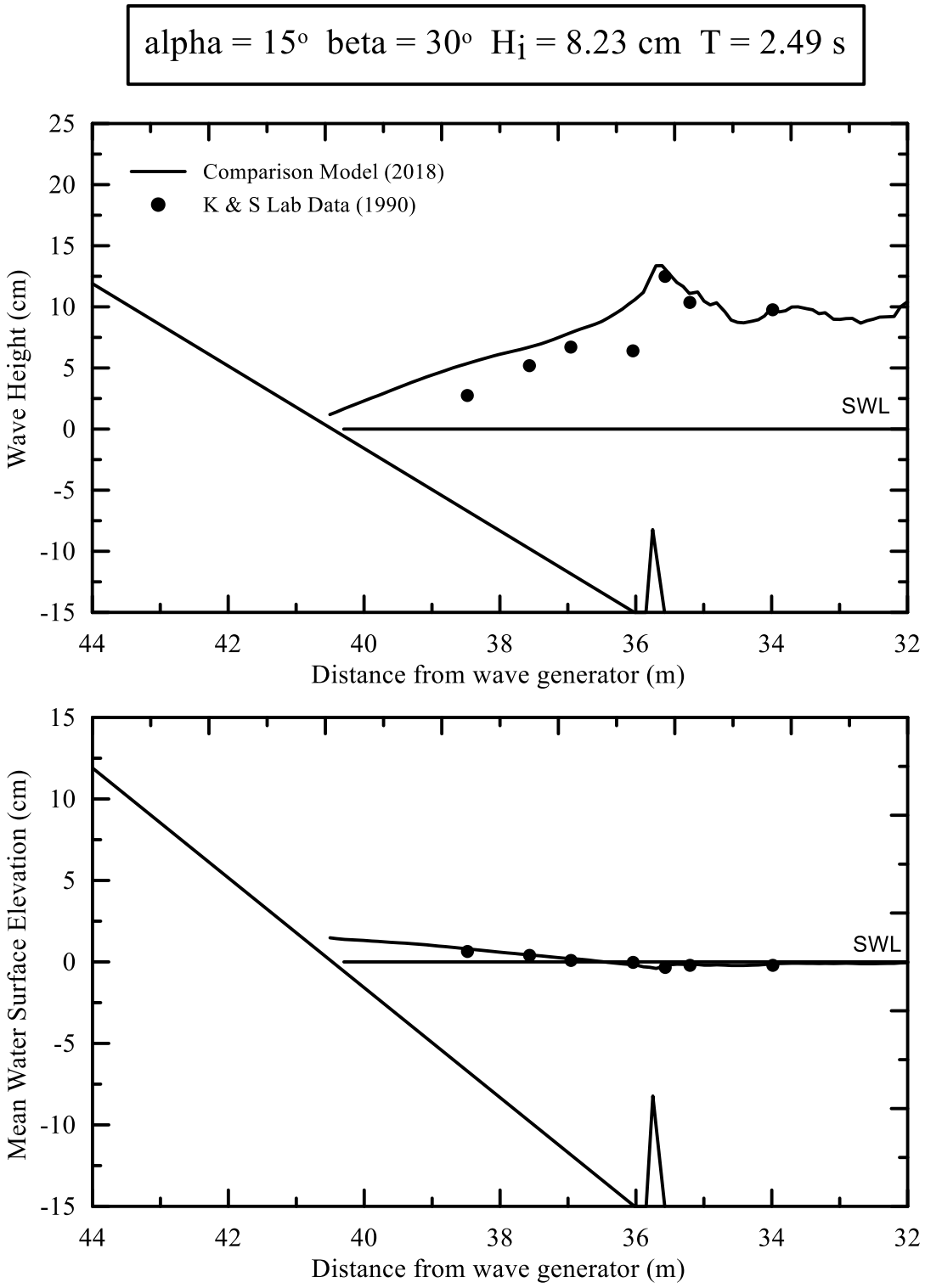

Figure 13.20: Test 10330.

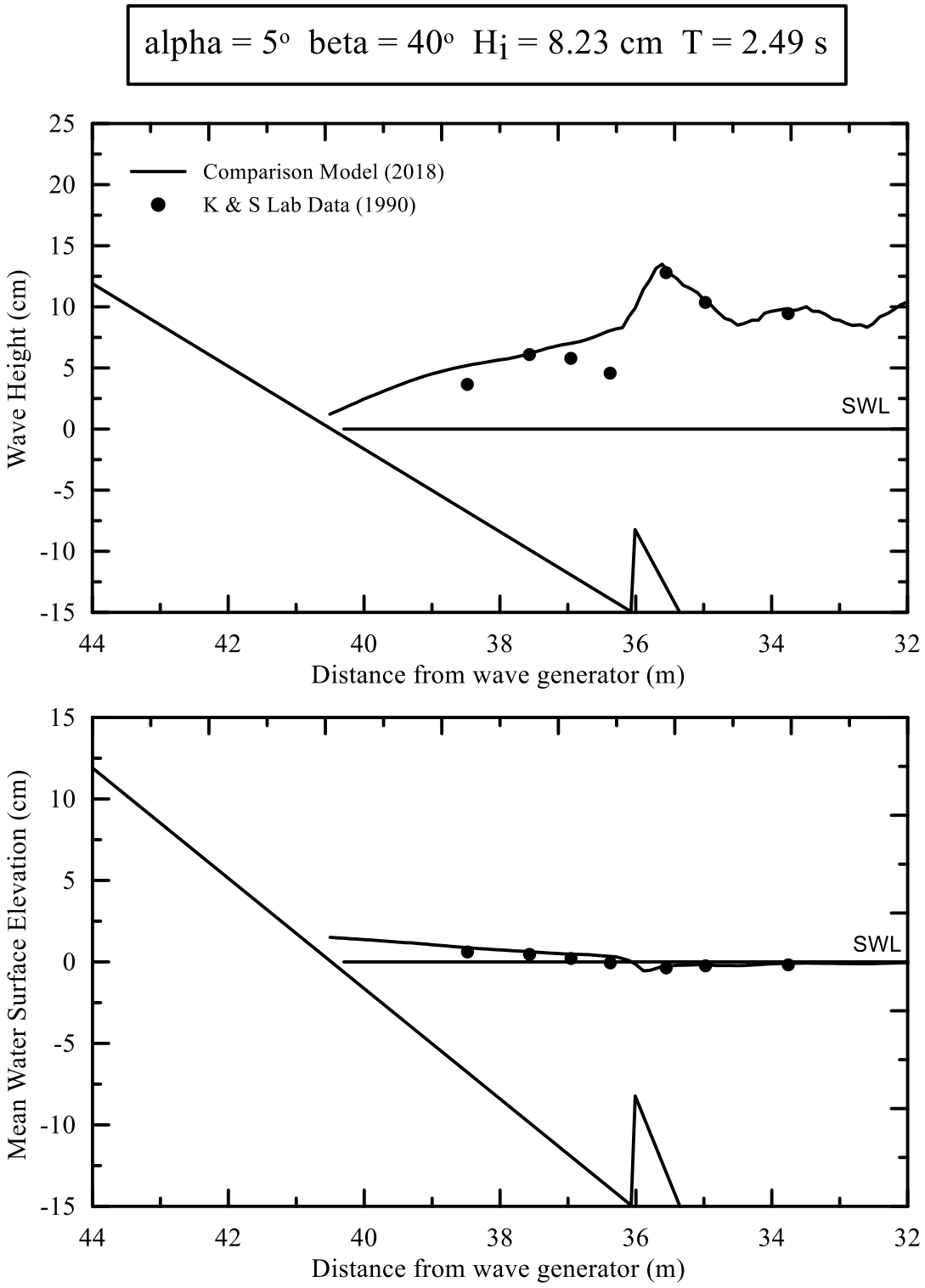

Figure 13.21: Test 10410.

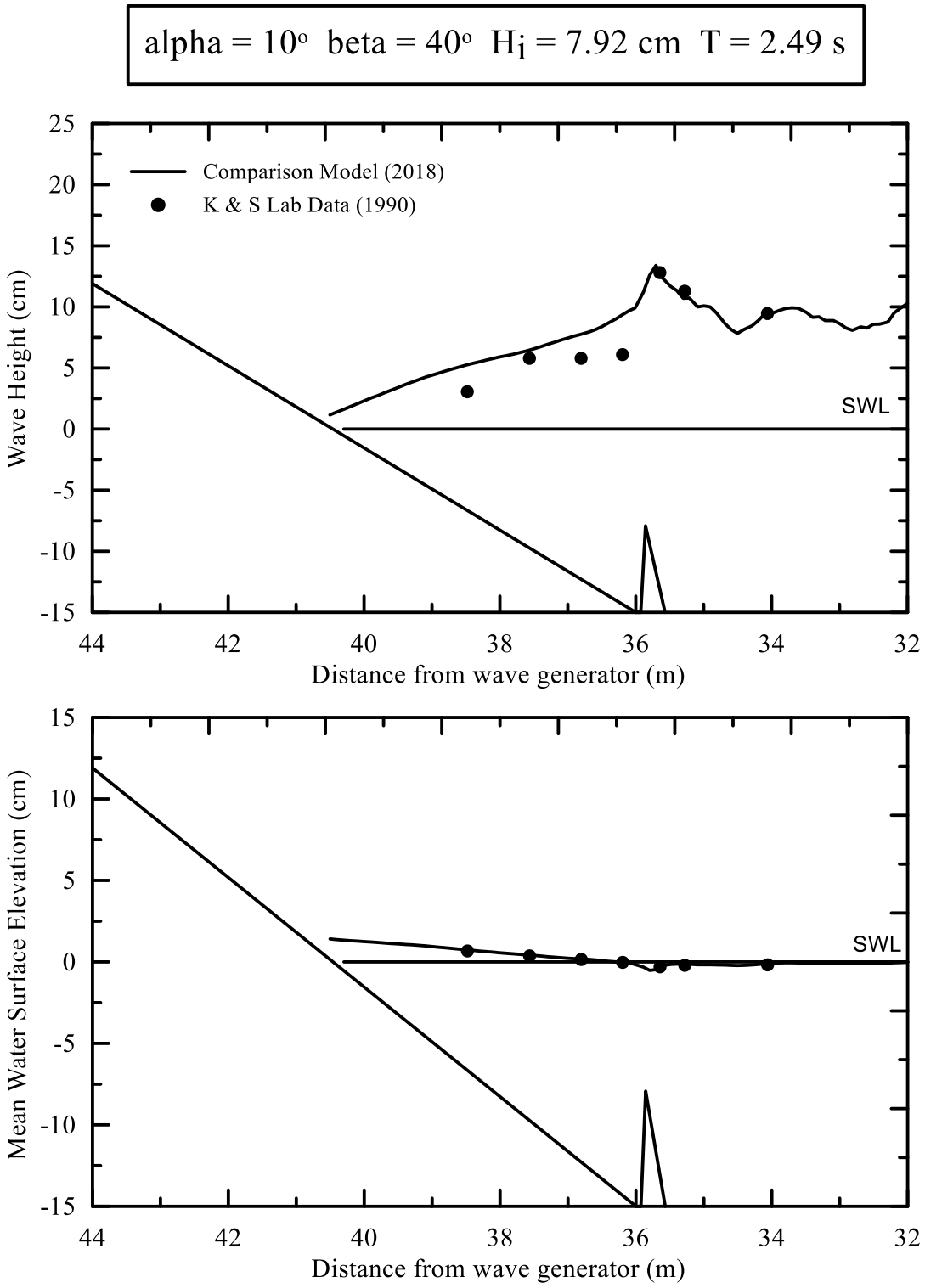

Figure 13.22: Test 10420.

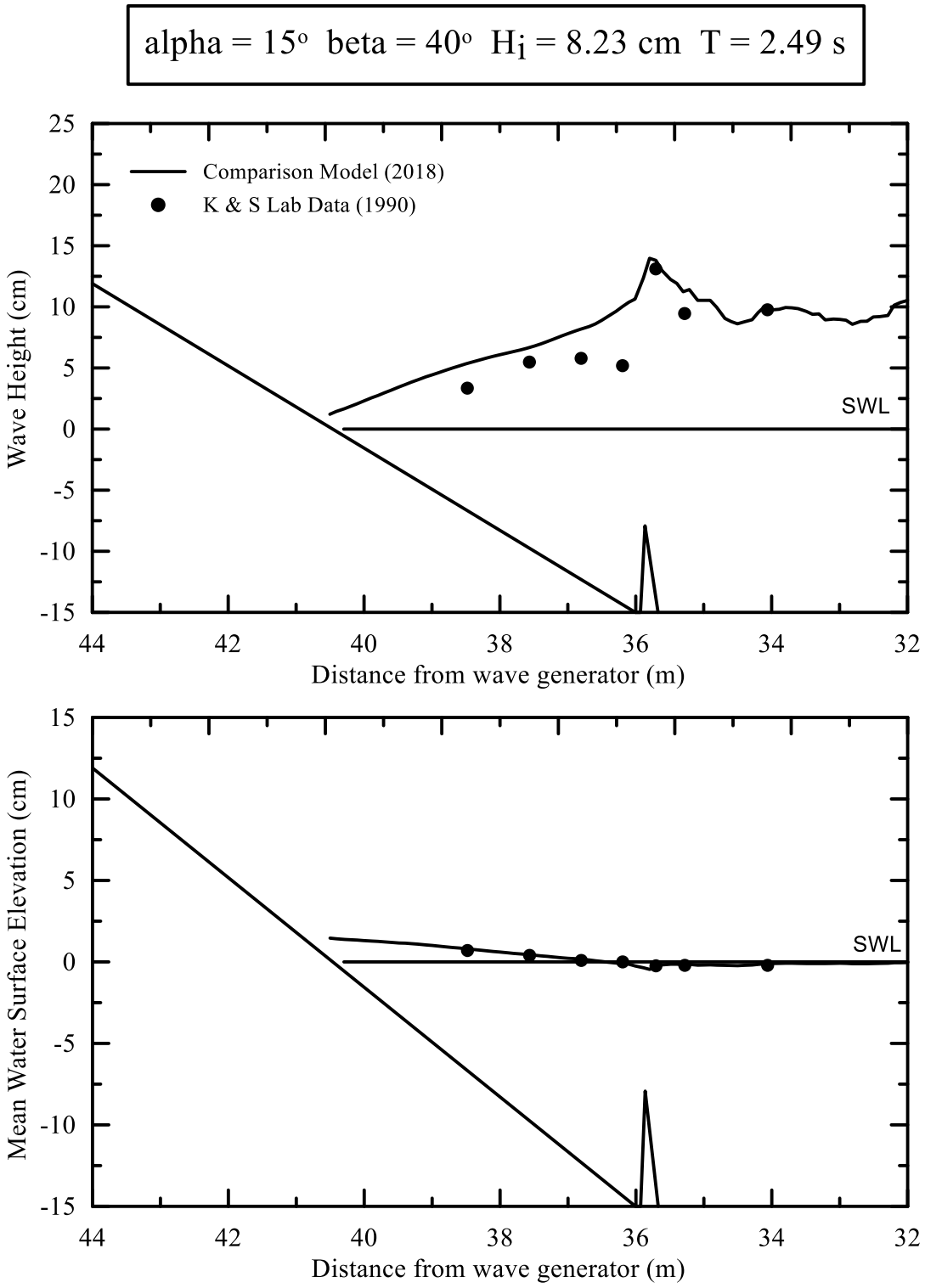

Figure 13.23: Test 10430.